Argonne NATIONAL LABORATORY

ANL/ESD/13-1

Computer Modeling and Analysis of Truck Generated Salt Spray Transport Near Bridges

May 2013

About Argonne National Laboratory

Argonne is a U.S. Department of Energy laboratory managed by UChicago Argonne, LLC under contract DE-AC02-06CH11357. The Laboratory's main facility is outside Chicago, at 9700 South Cass Avenue, Argonne, Illinois 60439. For information about Argonne and its pioneering science and technology programs, see www.anl.gov.

Availability of This Report

This report is available, at no cost, at http://www.osti.gov/bridge. It is also available on paper to the U.S. Department of Energy and its contractors, for a processing fee, from:
U.S. Department of Energy
Office of Scientific and Technical Information
P.O. Box 62
Oak Ridge, TN 37831-0062
phone (865) 576-8401
fax (865) 576-5728
reports@adonis.osti.gov

Computer Modeling and Analysis of Truck Generated Salt Spray Transport at Bridges

by
S.A. Lottes and C. Bojanowski
Transportation Research and Analysis Computing Center (TRACC)
Energy Systems Division, Argonne National Laboratory

submitted to
Kornel Kerenyi and Justin Ocel
Turner-Fairbank Highway Research Center

May 2013

Table of Contents

List of Figures

List of Tables

1. Introduction and Objectives

Bridge painting is very expensive. Over the lifetime of a bridge, painting to protect the steel from the elements can cost a large fraction of the original construction cost. In addition to monetary costs, maintenance workers face health risks if strict procedures are not in place to avoid exposure to hazardous dust when old paint is removed and the fumes of hazardous chemicals when new paint is applied.

Use of weathering steel in bridge construction avoids the large cost of periodic painting and the hazards of paint removal and repainting because this type of steel is never painted. When exposed to weather, the initial corrosion of weathering steel forms a natural corrosion resistant layer that prevents further corrosion under a wide variety of conditions. Given the advantages of using weathering steel, the choice might appear to be obvious. However, the large potential savings in bridge maintenance costs in using weathering steel are not always realized because the protective patina layer fails to adhere when the steel is exposed to excessively salt-laden and moisture-laden environments.

A multi-year study is underway by the FHWA to better quantify the conditions that lead to excessive corrosion in weathering steel bridges. This report documents work using computational fluid dynamics (CFD) analysis to study the conditions and mechanisms that lead from the salt spray thrown from truck tires to salt water droplets reaching bridge girders. Computer simulations use the advanced motion modeling capability called a “sliding mesh” in the CFD software to move one or more large trucks under bridges at 60 mph. The computations include multiphase spray droplet tracking of salt-laden water droplets coming off the tires.

Safety concerns over salt generated from large trucks and other vehicles have led to several studies of salt sprays coming from trucks that included multiphase analytical studies using CFD in the past. Salt spray reaching the windshield level of passenger cars is a particular hazard during snow storms because the salt in the spray deposited on the windshields of cars following or passing trucks during snow events can quickly obscure and even totally block the driver’s vision. The earlier analytical studies involved solving a much simpler problem because the fluid domain did not contain three dimensional solid objects moving with respect to each other. In that case, the problem could be modeled by creating a truck geometry in the computational domain and setting up an analysis with the observer stationary on the truck. The effect of a truck moving through the air could be created by defining a large external flow domain where the truck is stationary and the air enters in the direction of the truck with the truck velocity. The two dimensional road boundary can also be assigned a tangential velocity equal to the

truck velocity, a moving wall boundary condition. For the problem of interest in this study, this simple earlier approach is not possible because two three-dimensional objects are moving with respect to each other in the fluid domain. This type of problem required advanced motion modeling capabilities with either moving meshes or a mesh free volume analysis with the relative motion of the objects. Two approaches to solving the problem were planned for testing. One used the structural analysis software LS-DYNA, which could easily handle moving the truck under the bridge, and LSTC was in the process of adding CFD analysis capabilities to LS-DYNA. The other approach was to apply a relatively new capability in the STAR-CCM+ CFD software to have meshed domains that could slide past each other with free exchange of flow and energy across the shared domain interfaces that were open and sliding with respect to each other.

The objectives of the study were to build a model with a truck moving relative to a bridge in which the flow field could be solved by existing CFD software and available computational resources. Although this requirement entailed one of the major challenges of the study, it was accomplished using the sliding mesh capabilities of STAR-CCM+. The CFD capabilities of LS-DYNA, after extensive testing, were found not to be sufficiently well developed and benchmarked to be applied to this problem. The other modeling requirement was to model a two phase flow that included air and droplets. Nearly all modern CFD software includes several options for modeling multiphase flow with a combination of a continuous or carrier phase and a dispersed phase that could be droplets, particles, or bubbles. These options include an Eulerian approach, where the dispersed phase is modeled as a distributed continuum of, for example, the number density of droplets, and partial differential equations are solved for the distribution, velocity, and other properties. The other primary option for modeling a dispersed phase is a Lagrangian approach where ordinary differential equations are used to track the dispersed phase objects, droplets for example, through the continuous phase, air in this case. The Lagrangian approach is preferred in problems where droplets enter the domain from multiple points and their paths may cross because in the Eulerian approach the droplets in a droplet size group can have only a single velocity in a computational cell and droplet paths or stream lines cannot cross. The limitation of the Lagrangian approach is that large numbers of droplets must often be tracked. The number of droplets in a system can easily be millions to hundreds of millions or more. Tracking such a large number of droplets is far beyond the available computational resources. This computational capacity limitation is handled by tracking a statistical significant number of droplets through the flow field so that the behavior of the much larger, by orders of magnitude, number droplets in the system can be inferred with a high degree of confidence. When using the Lagrangian model in this way the tracked droplets are referred to as parcels because each represents a statistical sample of a much larger number. Due to its capability to track multiple crossing paths of droplets rebounding from walls in wheel wells with droplet breakup, in addition to droplets entering the flow from multiple points on tire surfaces from multiple tires, the Lagrangian model was chosen for use in the modeling.

The study included the goals of modeling three things that are related to the physics of droplet transport that were considered to be potentially significantly related to the amount of salt laden droplet spray that could reach the girder level of bridges when thrown from approaching truck tires when the trucks passed underneath the bridge. These three conditions were geometry effects, the effects of traffic, and

the effect of the wind. The primary geometry differences were sloped bridge abutments compared to bridges that are in confined spaces where the abutments are vertical with wing walls and the approach may also be a vertical wall or steep berm. Another geometry condition considered was a depressed grade approach. In the cases with vertical abutments and approach walls that confine the truck wake to the area of the roadway the effect on the amount of salt spray transported to bridge girder level is of interest. Traffic is of interest, especially large following truck traffic, because the following object acts as a bluff body diverting the salt plume wake flow of the lead vehicle around and up and over it. Finally, the effects of wind are of interest because wind changes the paths of droplets suspended in air, and the smaller the droplet, the faster its velocity (magnitude and direction) relaxes to that of the surrounding air.

Given the potential complexity of the multiphase flow field and interacting physics, a major objective of the study was to use the visualization capabilities of analysis software to show what is happening visually in the test cases that are significantly different in the amount of salt spray transported to bridge girder level in addition to the usual data processing that yields graphs to show relations between parameters.

This report documents the results of the test cases that could be completed within the budget and time available for this study and also to document the model for future use. The goals for the test cases were to identify the primary mechanisms that contribute to de-icing salt transport from road surfaces up to weathering steel bridge girders that span over roads, and to test to the extent possible the relative importance of the mechanisms.

2. Background

2.1 Weathering Steel Use in Bridges and the 1989 Technical Advisory

The use of weathering steel in infrastructure grew into a large market with its application in electrical transmission towers in the 1960s (McDad, et al., 2000). Application in bridge structures began in 1964 with Michigan taking the lead and grew through the 1970s with the potential advantage of much lower maintenance and life cycle costs compared to using steel in bridges that requires periodic painting. Between 1964 and 1980, Michigan built 513 weathering steel bridges (Schmitt, 1989). One of these was the Eight Mile Road Bridge in Detroit, Michigan. A portion of this bridge interchange was a depressed roadway with a low, 14'7" clearance and vertical retaining walls very near the shoulder (AISI, 1982). This structural geometry created what later became referred to as a "tunnel effect" where the overhead spanning structure formed the ceiling of the "tunnel". After an eight-year exposure study, it was found the corrosion rate never tapered off and in general their overall experience with weathering steel was poor. This led the Michigan DOT to issue a total moratorium on weathering steel in 1980, leading other states to also question their use of weathering steel. In October, 1989 the Federal Highway Administration issued a Technical Advisory (TA) 5140.22, (FHWA, 1989), to provide guidance to bridge owners and designers on conditions and locations that appeared to be associated with increased corrosion risk for existing bridges and identify situations in which the use of weathering steel should be avoided. In particular, the TA advised against using weathering steel in grade separations, "produced by the combination of narrow depressed roadway sections between vertical retaining walls, narrow shoulders, bridges with minimum vertical clearances and deep abutments adjacent to the shoulders."

Weathering steel remains a popular choice due to significantly lower life cycle costs when it performs as intended, avoiding health risks to workers repainting bridges, and avoiding traffic problems when lane closures are required during maintenance. Over two decades have passed, since the 1989 Technical Advisory was issued, providing an additional 24 years of experience with these bridges. The FHWA has undertaken a multi-year project to update the 1989 advisory that includes collection of new data on the corrosion performance of these bridges, analysis of accumulated experience, and some computational fluid dynamics (CFD) analysis. The CFD analysis is focused on salt sprays from vehicle traffic using large trucks as the vehicles most likely to produce significant salt spray plumes to further investigate the geometric parameters defining the so-called "tunnel effects".

2.2 Previous Truck Spray Studies

2.2.1 Truck Aerodynamics Studies

A large number of truck aerodynamics studies have been carried out in the past to, among other things, help improve fuel economy by reducing the drag coefficients of large vehicles with rectangular cargo containment volumes. The Department of Energy (DOE) sponsored a project on Heavy Vehicle Aerodynamic Drag with the goals of improving understanding of drag on large trucks and identifying new methods to achieve economic drag reduction. The project was a collaborative effort between a number of national laboratories and universities and included extensive use of CFD analysis. The 2006 project report (McCallen, et al., 2007) covers both CFD analysis and experimental tests with references. This effort and many others demonstrated that CFD is a useful engineering tool that can be applied to the study of the aerodynamics of vehicles.

2.2.2 Experimental and Computational Studies of Spray Generation by Trucks

Salt sprays generated from trucks during and after snow events in regions where road salt is applied during winter storms are a potential safety hazard when the spray rapidly covers the windshield of vehicles traveling in the truck wake. Paschkewitz, (Paschkewitz, 2006) used STAR-CD CFD software to study the spray distribution pattern from a tandem dual slick wheel model. He observed in the simulation results that wheel housing structures prevented ballistic transport of droplets greater in size than about 100 µm, but that a fine mist of smaller droplets is transported out of such confining structures. A second study by Paschkewitz, (Paschkewitz, 2006), of spray dispersion in a truck wake also used STAR-CD CFD software. The goals of the study were to investigate the feasibility of using CFD to study spray dispersion from trucks and in particular to characterize the effects of base flaps. The results indicated that the use of base flaps can decrease visibility in the passing lane to the side of the truck because the flaps block the rearward transport of droplets and consequently the primary unblocked route to escape from beneath the truck is to the sides.

A third study by Paschkewitz, (Paschkewitz, 2006), focused on comparing the degree of spray dispersion using large eddy simulation (LES) versus unsteady Reynolds averaged Navier-Stokes with a two equation turbulence model (URANS). This study indicated that small particle dispersion could be under predicted by as much as forty percent when using URANS. Small, low inertia droplets are most affected by the details of eddy structures and flow patterns that are not well captured by URANS simulations. Droplet tracking models in URANS do incorporate random kicks to droplets to model interactions with eddies, however, apparently those dispersion models either do not capture enough of the physics or need to be better tuned using experimental data. While LES may be preferred for accuracy, it remains too computationally intensive to be applied to routine analysis in a wide range of problems that are constrained by budget and time. URANS is currently the best available option for multiphase turbulent flow studies that are time and budget limited. It can yield results that correctly show the relative importance of design options or mechanisms of flow behavior that provide needed insights as long as its limitations are kept in mind.

2.2.3 Aerosol Concentration Studies

A deicing salt dispersion study (Williams, et al., 2000) concluded that a large portion of deicing salt is entrained into the air by vehicle traffic after an initial snow event as dry particulates. It also concluded that 90% of the particles aerosolized were greater than 2.5 μm in diameter and noted that a dry salt film thickness of 10 μm remaining on the road is consistent with observed application amounts per mile of road. A study was done of data collected from 1980 through 1998 (Williams & Stensland, 2004) at an Illinois site in the National Atmospheric Deposition Program, known as Location IL19, located within Argonne National Laboratory in a field 1.9 km south east of I-55 and 0.8 km from Lemont Road. The IL19 site is unique in being located in a suburban area near a major highway with a record of dry deposition records extending over a period of two decades when a large amount of deicing salt was applied during the winter. The authors note that vehicle traffic on I-55 is about 145,000 vehicles per day and 15,000 vehicles per day on Lemont Road. The only comparable site is located in suburban Boston where atmospheric chemical deposition data was collected over a long period of time, and that site is not well suited for road salt dispersion analysis due to the additional presence of sea salt aerosol in the atmosphere resulting from its proximity to the ocean.

The study defines wet emission of salt from vehicles to refer to droplets thrown from tires during wet or slushy road conditions, typically during and immediately after snow events and dry emission to refer to dry salt particles thrown from tires, typically a day or more after snow events when the roads are clear and dry with a remaining salt film. On the other hand, wet deposition refers to the removal of the substance from the atmosphere with precipitation, while dry deposition refers to gravitational settling of either droplets or particles. A splash deposition zone is somewhat arbitrarily defined as the region within 15 meters of the road where large droplets or salt particles will rapidly settle under the force of gravity. The study showed that about 78% of the salt mass deposited was particles with diameter greater than 10 μm, about 18% of the mass was from particles in the 2.5 to 10 μm range, with 4% being smaller than 2.5 μm. Amounts recorded over an eight week dry sampling period correlated well with the amount of salt applied to the roadways over the course of each year. Dry side sample collections were about 7 times wet side sample amounts in mg/m^3. Wet deposition did not correlate well with snow events, indicating that wet deposition was more an indicator of background salt concentrations in the atmosphere. The significant amount of coarser particles collected 1.5 km or more from the road is an indication that wind plays a significant role in the particle or droplet transport.

A final report on deicing salt dispersion at the Chicago suburban sites (Williams & Stensland, 2006) includes a dispersion model based on exponentially decaying road salt source emission functions and exponential decaying salt deposition functions that drop off with in inverse proportion with the distance from the source road section. The time constant that best fits the data was 48 hours, indicating that for the data sets used in the model about 63% of the aerosolized salt deposited on measurement devices was entrained into the air in the first two days, and about 37% was entrained in the period greater than two days after a snow event. The salt emission source strength also included a vehicle use density factor.

A study of particulate re-entrainment from roads in the Lake Tahoe basin (Gertler, et al., 2006) included sand and salt. This study roadside sampling equipment mounted at 0.5, 1, 2, and 3 m above the road surface, 1 m from the side of the road. In addition to road side sampling, this study employed a van instrumented with particulate sampling equipment and pipe intakes behind the rear tires and a third pipe sampling air at the centerline of the front bumper to correct for the ambient particulates and determine the amount re-suspended from the road surface by the tires. The truck measurements were calibrated using the road side instruments. In this area salt was applied as a liquid deicer, and a road abrasive particulate was applied for vehicle traction. The 2.5 µm and 10 µm particulate classes measured in the air were observed to reach maximum concentrations over the winter period and then declined during the spring and summer. The road side measurements showed highest concentrations nearest the road at 0.5 and 1 m decreasing by about half at the 3 m height. Local protocols called for street sweeping to remove particulates from roads four days after roads are clear of ice and dry after a snow event to try to reduce the amount of re-suspended dust. The street sweeping itself resulted in a slight increase in dust concentrations and near term reductions in dust concentrations after street sweeping were not observed. Because street sweeping occurred four days after roads were clear of ice and dry, and the Chicago salt dispersion found exponential entrainment source decay with a time constant of two days, it appears likely that the street sweeping would at best remove the small tail of the distribution of the particulate re-suspension source due to vehicle traffic.

3. Modeling of Truck Generated Salt Spray under Bridge with Sliding Mesh

3.1 Stages in Salt Spray Transport Analysis

Based on a review of the literature and initial studies that were conducted, the whole process from creating the salt-spray, through its transport, to the contact with the bridge girders was divided into several stages as listed in Figure 3.1. Splash and spray generation on the tire thread and road interface is a very complex process and not many studies have been done on it so far that are publicly available. The amount of droplets injected from the tires into the system depends on many factors including tread shape and tire condition, water film thickness on the road surface, which is related to the amount and rate of rainfall, condition of the road surface, and other factors. Such data, if obtained by tire manufacturing companies in the tire design cycle, is never made available to the public. Unfortunately this stage cannot yet be modeled directly in commercial CFD software. Measurement and characterization of sprays coming off tires requires intricate experiments and is a topic for bigger projects than the current one; see for example (Radovich, 2010).

For the purpose of this study, the amount of water injected by the truck tires to the computational domain and the mean initial droplet size was assumed based on studies conducted at LLNL (Paschkewitz, 2006). The current study focuses primarily on the stages that follow the salt-spray generation process. A set of simulations was done to study droplet breakup in the wheel well, to determine size range of the particles of interest, and to further simplify the calculations. To conserve computer resources and make these simulations feasible, they were restricted to a single tire and wheel-well. The breakup models implemented in STAR-CCM+ are very computationally intensive, and each particle breakup generates at least two particles out of one, significantly increasing the computation time. For this reason, that stage was separated from the following ones, and its results were treated as a droplet injection condition in the following stages of these studies, where droplet breakup was no longer active in the model.

In the main set of simulations, constant mono-size droplets were chosen from the range established in the breakup study. The simulations were, however, repeated for several sizes of the particles to cover the whole range of interest.

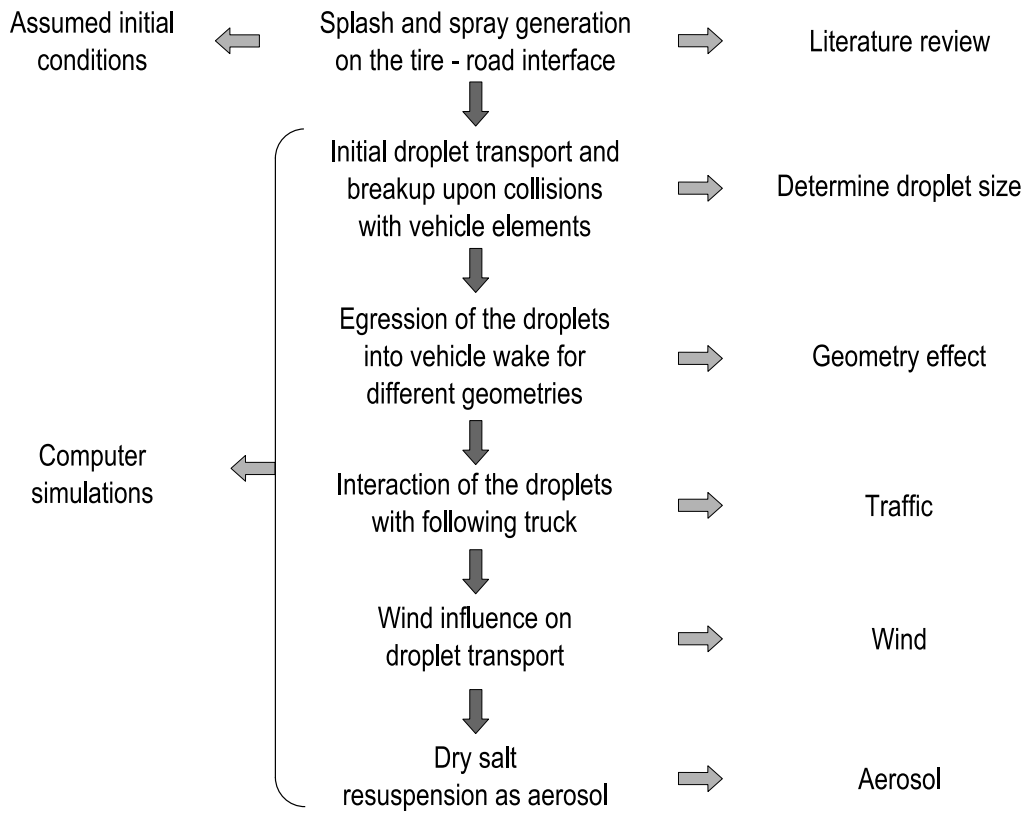

Figure 3.1: Stages in the salt spray transport analysis

3.2 Development of Geometry for the Base CFD Model

The geometry modeling started with obtaining the plans for several bridges affected by excessive corrosion of weathering steel girders. One of these was the highway bridge Raleigh - Tamarack Overpass (Bridge No. 4172) on the I-64/77 crossing. Its plans are shown in Figure 3.2. While this bridge does suffer from excessive corrosion, it was mostly attributed to the design of the deck joints, and not necessarily the geometry of the bridge and surroundings. However, when sending inquiries to bridge owners asking for bridge plans, this set of plans was the first received, and it serves as reasonably good base case from which to make geometry changes for other cases of interest. It is a two span composite bridge with a concrete deck supported by eight steel girders. The minimum vertical clearance under the bridge is 16 ft 6 in. In the CFD analysis half of the bridge with the East abutment was modeled (see Figure 3.3) to save computer resources.

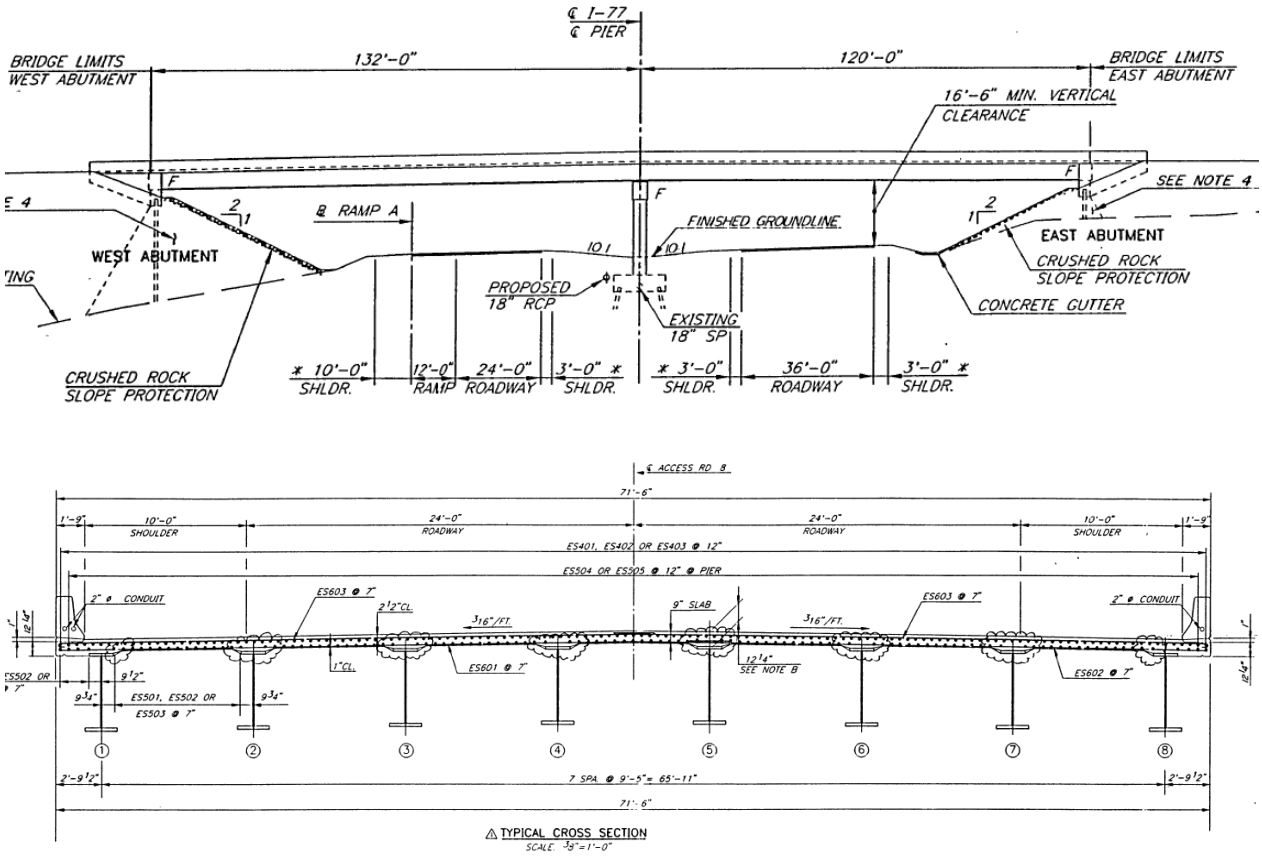

Figure 3.2: Bridge No. 4172 plans used for the CFD model geometry

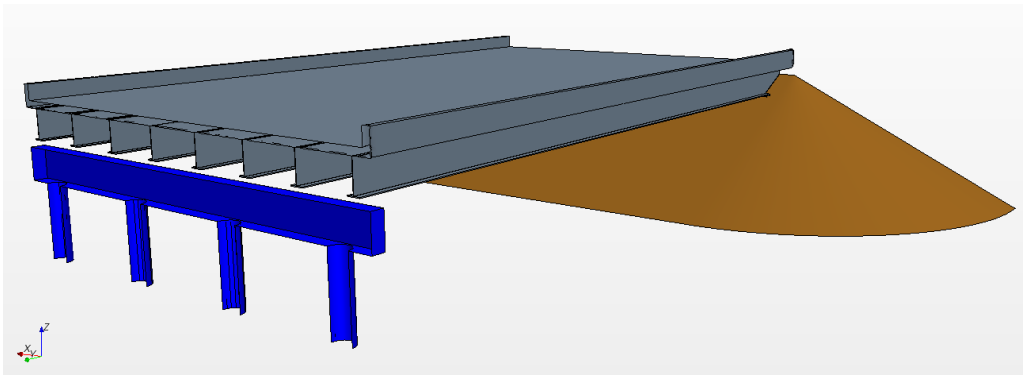

Figure 3.3: Geometry of half of the Bridge No. 4172 in the CFD model

It was assumed that the worst cases of salt spray from vehicle tires reaching the girders would be caused by the passage of large 18-wheel trucks with trailers. The model of a truck tractor was built based on the geometry of the Mack CH 613 tractor. The sleeper and the dry freight van type trailer were also modeled. The biggest allowed (16.16 m long and 2.89 m wide) trailer was modeled. Figure 3.4 shows the geometry of the Truck used in the CFD model.

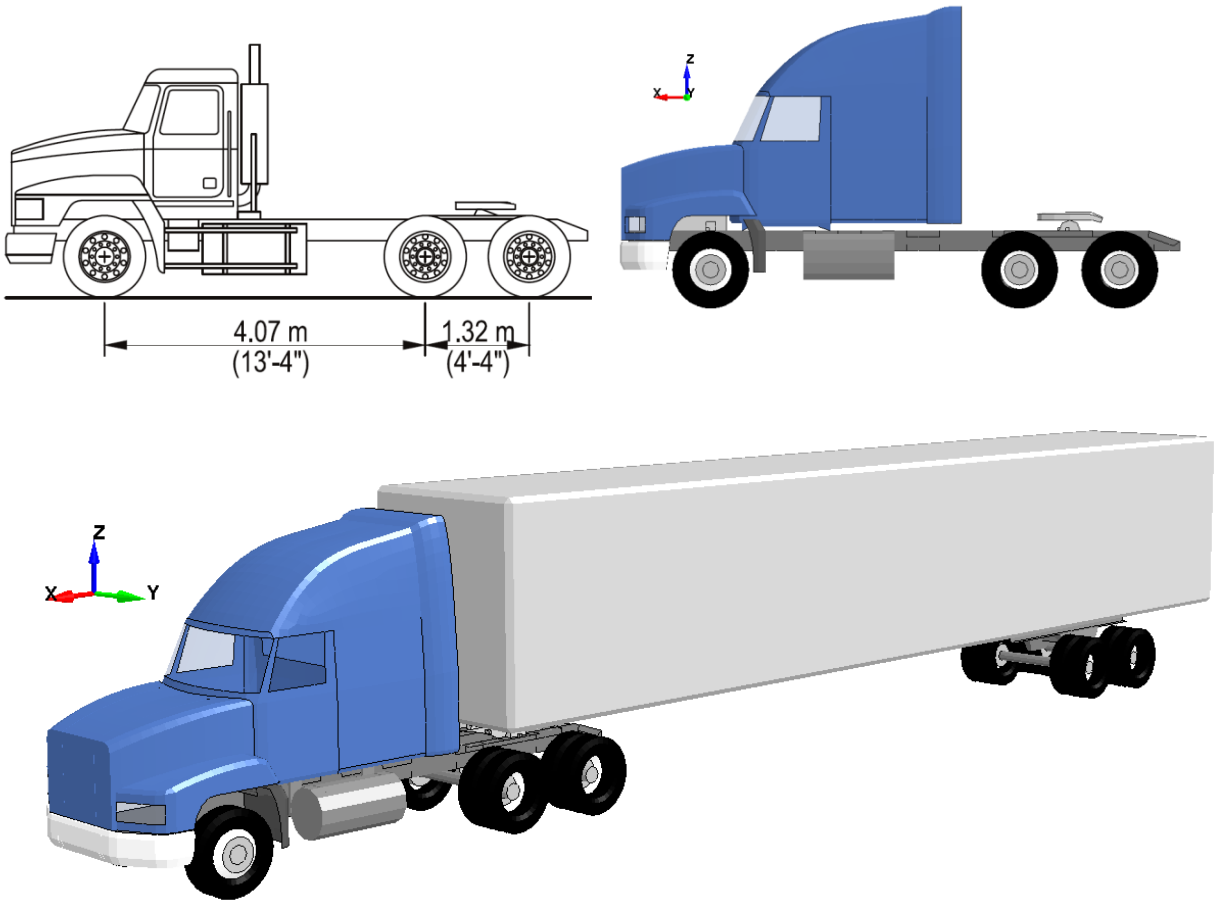

Figure 3.4: Truck geometry model based on Mack CH 613 tractor and 53 ft long trailer

The wake behind the truck can extend for several trailer lengths. To allow the wake to develop before the truck reaches the bridge, an air domain 186 m long, 42.8 m wide and 11.6 m high was used in the CFD model. Computational cell size in the areas distant from the bridge deck and the truck was set to maximum value of 1 m. In the vicinity of the vehicle and the bridge girders computational cells have been defined with a cell size of 30 mm close to the tires, 60 mm next to the other details of the truck and 120 mm near the bridge girders. The mesh settings and extent of the model resulted in an overall computational cell count of 4,500,000 to 5,400,000 cells depending on the geometry of the case studied. Figure 3.5 shows the geometry of the base model at an intermediate stage of the analysis.

The truck was placed in a separate sub-domain separate from the bridge, a 300 m long box. Initially the box with the truck was placed about 85 m in the front of the bridge. That distance was assumed enough for the flow around the vehicle to fully develop. Openings in the air domain with exact size of the truck box were created. The sliding mesh with the vehicle perfectly fills that volume once the vehicle is set in motion. Common interfaces between the domain with the truck and the surrounding boundaries were defined so the flow can be exchanged between the sub-domains without any loses or deflections. A cross wind passing through the stationary mesh and an empty sliding mesh box goes right through yielding a flow field solution equal within computational accuracy to that of an empty stationary box in the domain. This test confirmed the functioning of the sliding mesh model.

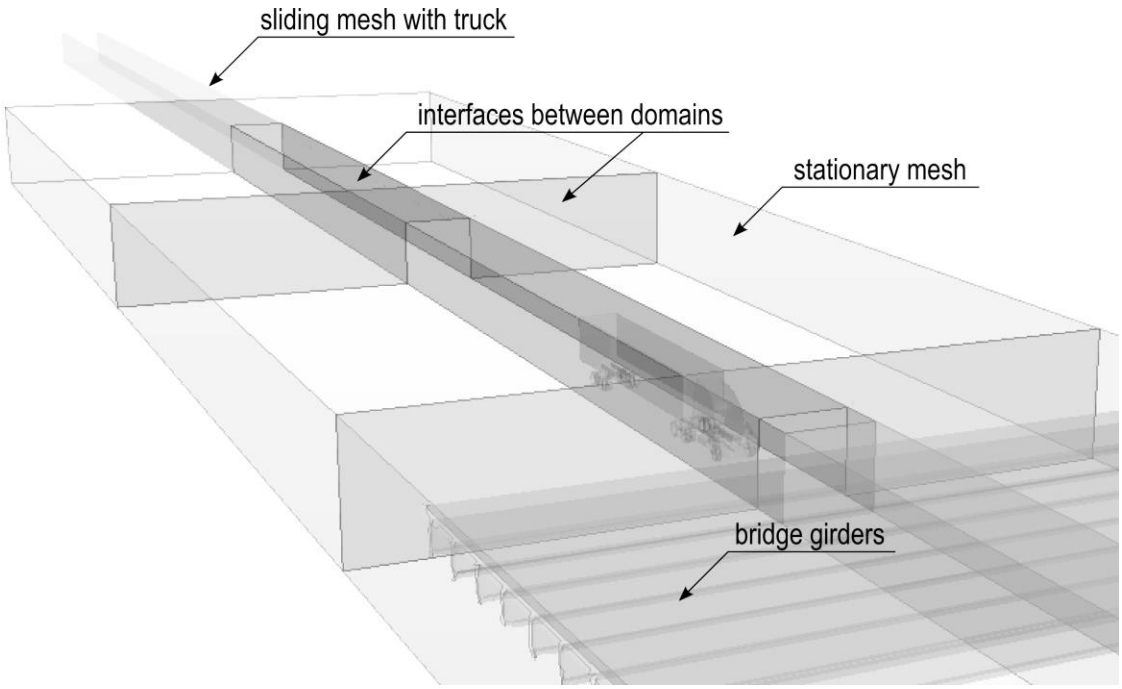

Figure 3.5: Geometry of the STAR-CCM+ model for analysis of truck generated salt spray

The flow field was solved using implicit unsteady analysis with a time step of 0.015 s. The number of inner iterations of the solver was set to 20 to converge each time step. Motion of the box with the vehicle was prescribed in the forward X-direction with a velocity of 26.8 m/s (60 mph). In each time step interfaces between the adjacent domains are recomputed and flow between them is calculated.

While the most important locations of droplet injectors are the tire treads, a few cases were run initially with the injectors attached to the cabin's edges. Figure 3.6 shows the location of the injector surfaces with surfaces at the rear side surfaces of the cabin. In reality all the edges of the truck and trailer can introduce salt spray particles assuming that the truck has intercepted spray from vehicles in front of it, that the intercepted spray forms a film on the truck surfaces and that the film flows under the action of shear stress downwind where it can be shed as filaments and new spray forms from downwind edges of the truck and trailer. In the absence of wind, large droplets (greater than about 1 mm) and filaments settle quickly back to the road surface. Because droplets coming from these surfaces were not observed to contribute significantly to the droplet distribution in the truck wake, the rest of the study limits droplet injection to the major source of the truck generated spray, the tires.

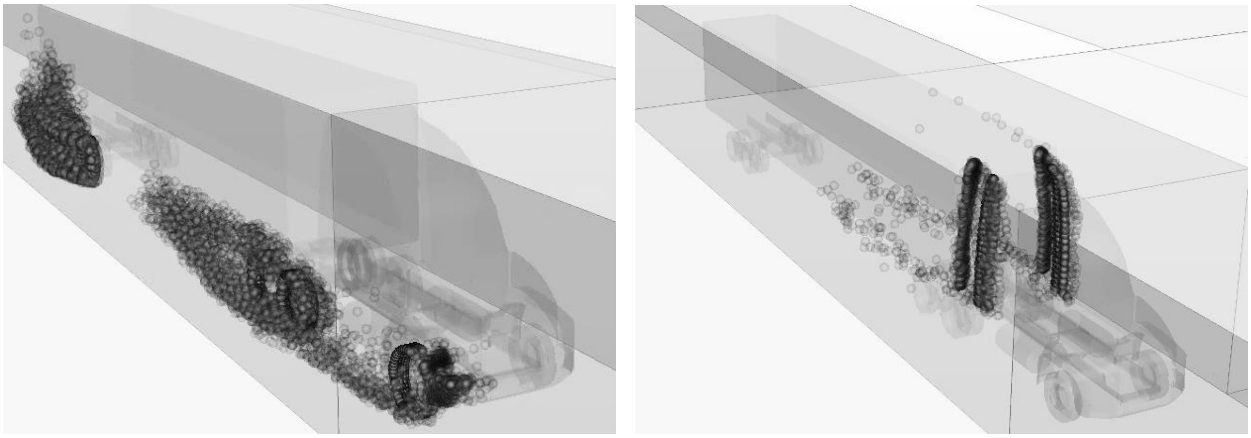

Figure 3.6: Droplets generated on the injector surfaces

3.3 Boundary Conditions

All the external boundaries of the domain were modeled as pressure outlets. Care has been taken to set the domain boundaries far enough away from the truck and other surfaces of interest on the bridge so that the far field conditions at these boundaries do not influence the flow around the truck or the truck bridge interaction. Spray droplets were modeled as Lagrangian particles and were set to escape through pressure boundaries. To reduce computation time the particles were also set to escape through most of the wall boundaries. This setting assumes that droplets that hit a wall will stick to the wall (don't rebound), possibly forming a film that will either evaporate or flow back down to the roadway. In either case, modeling the physics of that process was excluded from the analysis because the process of interest was transport of droplets to the bridge girder level. Since the breakup of droplets was deactivated in the model, the droplets were set to rebound from the tire treads and the mud flaps. Note that the injected size of the droplets has already been set within the size range of droplets after the process of breakup on truck undercarriage surfaces and wheel wells. That way the number of particles in the system was not reduced at early stages of their transport and the size is in the correct range. In reality the particles that hit the truck can either stick to it or rebound from it with breakup. In the model the particles hitting parts of the vehicle other than the tires and mud flaps were set to leave the computational domain. Another boundary type was set for the bridge girders and the deck. The particles that hit the bridge were set to stick to it so their number was then tracked and they could be visualized through all the stages of computation. These simplifying assumptions were made to reduce the computation time as much as possible. With the chosen time step for unsteady calculations of 0.015 sec and 8 seconds of real time simulated in each case, the simulations were already taking about one week of computation time. Ideally all the wall boundaries would have had breakup conditions defined for all the particles hitting them. However, these assumptions are considered to still provide engineering accuracy within the range of other uncertainties in the analysis, and they made it feasible to run the number of cases that are reported.

3.4 Case Geometries

The domain was subdivided into two main subdomains: the approach box and the bridge box. The bridge box was separately meshed for different geometrical conditions at the bridge's approach. In order to better understand the influence of different bridge approaches on amount of salt spray transported to the girders, four different geometry conditions were built: no abutment, a 2:1 sloped embankment, a close vertical abutment with a wing wall, and a close continuous wall. The models with these conditions are shown in Figure 3.7. In addition to the basic cases, several others have been built with variable distance between the truck and the bridge abutment wall boundary.

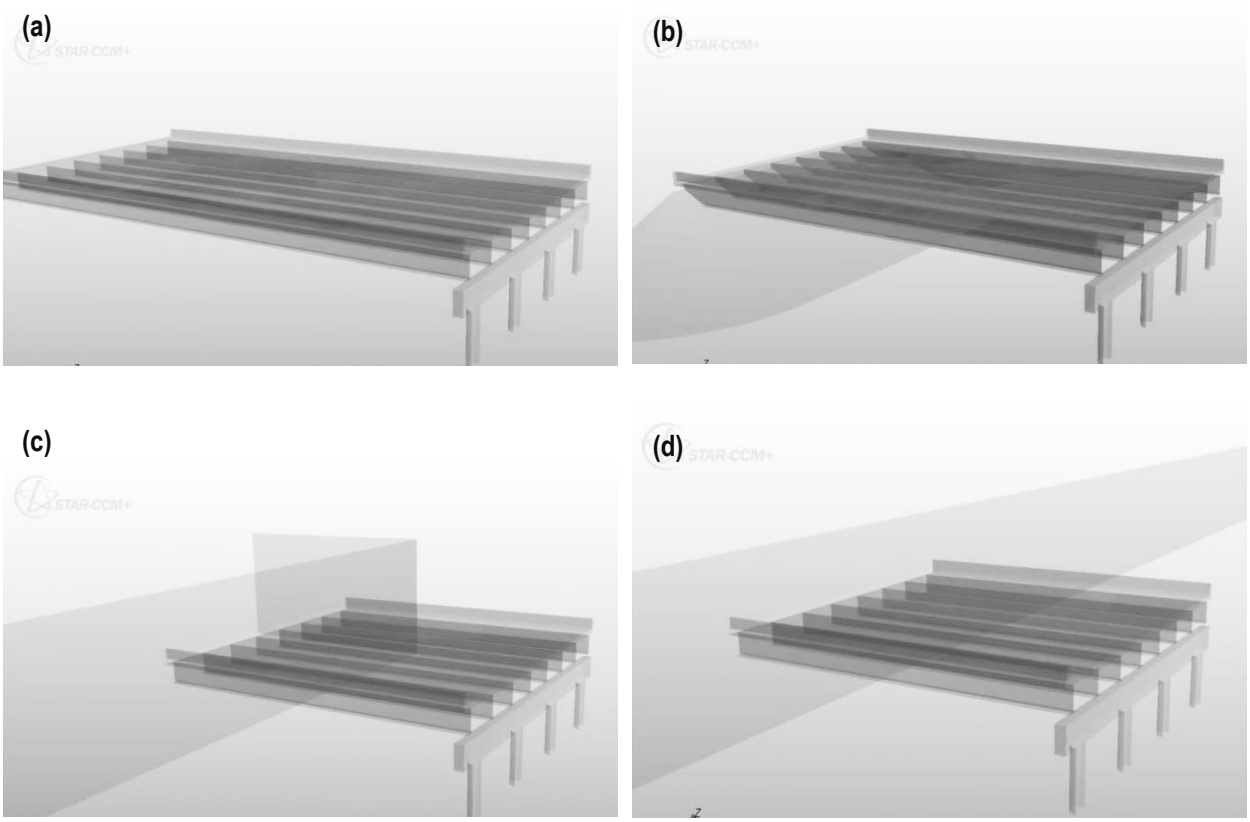

Figure 3.7: Different geometry conditions under the bridge

3.5 Particle Size Distribution

The Lagrangian particle model was used to track the transport of liquid particles released from the truck tires through the domain. STAR-CCM+ has several types of particle injectors built-in that can be introduced in the model for the Lagrangian particles:

- Part injector,
- Point injector,
- Cone injector (particles with mass only),

- Surface injector, and
- Pressure swirl injector.

While the cone injectors are most sophisticated (CD-adapco, 2012) their use in our case would require redefinition of their locations for each time step of the calculation. These injectors cannot be easily attached to the moving mesh. Surface injectors do not require re-specification of their location each time the vehicle moves between time steps. Contrary to the cone and point injectors, the surface injector is always attached to the underlying geometry. Velocity magnitude and direction are specified for droplets along with mass released by the surface injectors. The drawback of surface injectors is the lack of easy definition of number of injection points per surface. It depends on the number of cell faces on a boundary used as a surface injector, and therefore careful control of mesh parameters for tire surfaces is required. Specifying the mass flow rate ensures that the mass of injected phase is approximately right in the simulations. This rate was taken to be the rate used in the (Paschkewitz, 2006) study of 4.5 kg/s per tire. At 4.5 kg/s, with a chosen time step of 0.015 sec a tire is throwing off around 18,000 parcels/s. An ordinary differential equation is solved in each time step for each parcel to track the droplet paths through the domain. Even large cluster computers are far from capable of solving the equations for the number of droplets actually entering the system. This problem is resolved in STAR-CCM+ by using a parcel approach to represent a number of water droplets with averaged properties that all follow approximately the same path. One parcel per time step is injected from a cell face. The number parcels injected and tracked through the system is set to be a statistically significant sample of the water droplets. The name parcel will be used instead of water droplets or Lagrangian particles to mean this averaged representation.

One of the most difficult parts of this analysis was determination of initial conditions for the generated sprays. Particle size distribution, particle velocity magnitude, its direction, and particle breakup properties are the key factors in the analysis. The literature on this topic is very limited since experiments determining generation of a spray by rolling tires are difficult to conduct. In (Radovich, 2010), tests with an original Tire Spray Simulator are presented as a source of information on the creation of a spray from tires. In the experiments an apparatus like the one shown in Figure 3.8 was used. Two tires were pressed against each other. One of them had a greatly simplified tread in the form of a single circumferential groove, and the other one had no tread to simulate a smooth road surface. With the tires spinning, water was injected between the rolling tires and the spray generated behind them was analyzed using the digital particle imaging velocimetry technique (DPIV). The particle size distribution, the mean diameter, and the breakup length were shown to depend on the Weber number (We). Measurements for the breakup length of the liquid sheet showed a dependence on Weber number proportional to $We^{-1/6}$. The range of droplet sizes and the mean diameter were found to decrease with Weber number by approximately $We^{-1/2}$ (Radovich, 2010).

The Weber number characterizes the ratio of internal to surface tension forces and is defined as:

$$We = \frac{\rho V^2 D}{\sigma} \qquad \textbf{3.1}$$

Where: ρ is the carrier fluid density, V is the slip velocity between the droplet and the carrier fluid, D is the droplet diameter, and σ is the droplet surface tension.

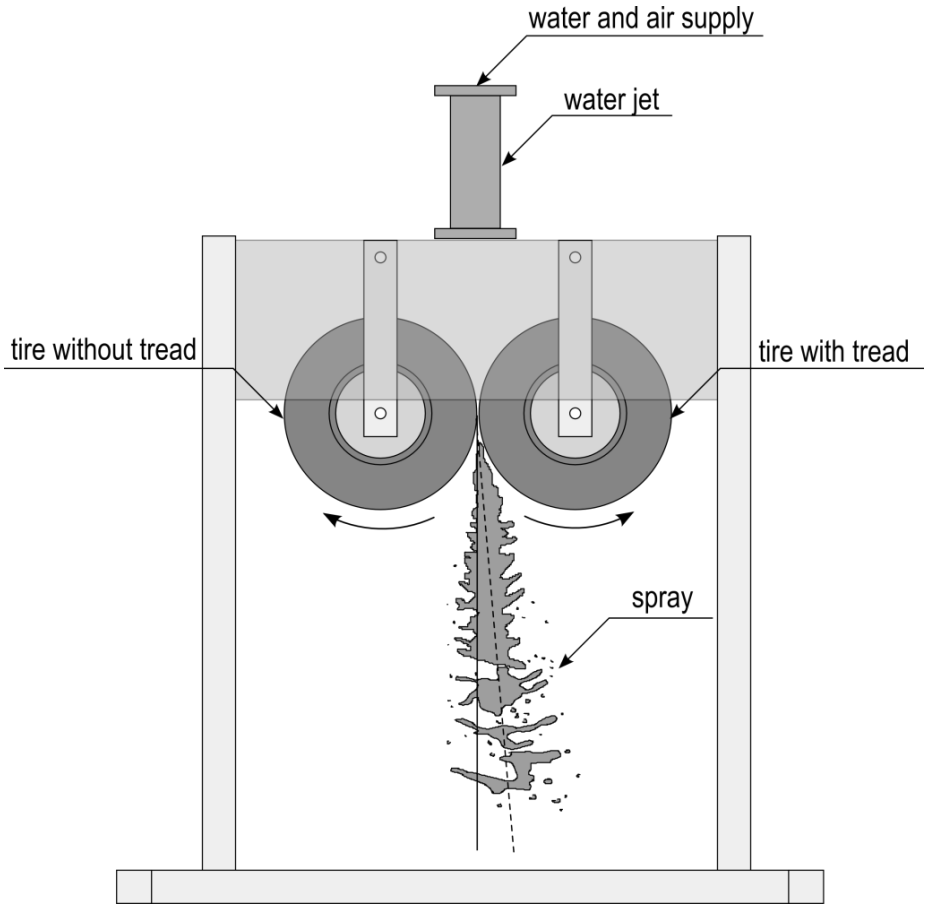

Figure 3.8: Schematic drawing of the Tire Spray Generator, based on (McCallen, et al., 2005)

The Weber number in the test depends on properties of the water, tire speed, and the tire groove width. For different Weber numbers, different particle distributions were obtained at several locations behind the tires. In all tested cases the distribution of particles can be described by a log-normal distribution. One of these distributions is shown in Figure 3.9. The following approximate mean particle sizes were observed in the spray coming off the tire at a distance of 1.5 tire diameters from the end of the contact patch:

- For the lowest *We* = 2,700, distributions had a mean particle size of approximately 750 μ,
- For *We* = 10,900, distributions had a mean particle size of approximately 400 μ,
- For the highest *We* = 24,400, distributions had a mean particle size of approximately 300 μ.

We = 24,400 was associated with the tire surface velocity of 18 m/s. In this study the velocity of the tire surface is 26.8 m/s. Also the tire geometry is substantially different since commercial tires have multiple, circumferential and non-circumferential groves in a variety of tread patterns and a larger diameter than the tested tire. Thus, the results listed here cannot be directly used as an input for the analysis of spray distribution coming from large trucks. Nevertheless, the mean values of the particle diameters were

used as a basis for further study. A larger mean droplet size was measured for lower Weber numbers. For the highest tested *We*, the mean droplet size was around 300 µm. For further study, it was concluded that the mean particle diameter leaving the wheel road interface could vary from 300 µm to 700 µm.

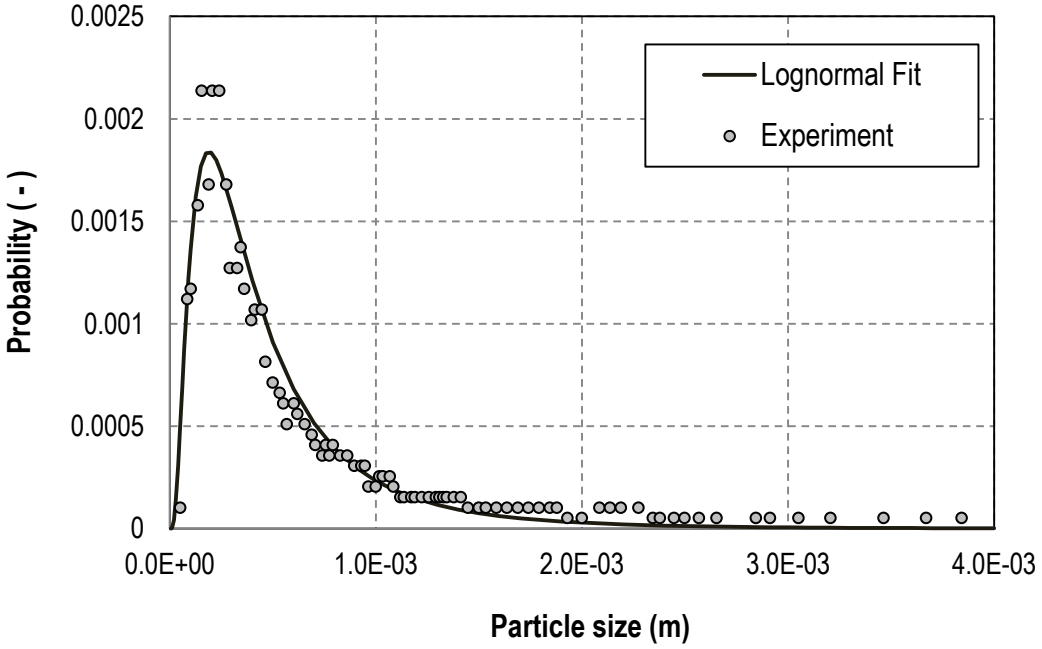

Figure 3.9: Particle size distribution in one of the Tire Spray Generator tests (Radovich, 2010)

3.6 Particle Breakup in Collisions with Walls

The spray generation experiments presented earlier were performed for a system without wheel wells and mud flaps. In the real world case, a particle, after being thrown from the tire, can impact the wheel well, break up, rebound, and collide with other elements of wheel surroundings, including a secondary impact with the tire. The mean size of particles leaving the wheel zone does appear to be much smaller than those observed in the experiment without wheel well surroundings. A set of simulations was conducted on a stationary vehicle with respect to the computational domain, but oncoming air at a velocity of 60 mph with a reduced air domain and without the bridge model in it. Of interest in these tests was just the breakup of the particles due to their impact with the front wheel well. A goal of this simulation was to determine the size range of particles that can be expected to leave the wheel well zone after the breakup. This size range is then used as a droplet injection boundary condition from the tire surfaces in the simulations of a moving vehicle and rebound without breakup conditions are used on wheel well, mud flaps, and other under truck surfaces where it is too computationally expensive to use the droplet breakup model.

The Bai-Gosman wall impingement model was activated in the simulations with droplet breakup. Depending on the Weber and Laplace numbers for the droplets, the Bai-Gosman model is simulating a

wide range of behaviors of particles impacting walls like: sticking, rebound, or break-up upon rebound (see Figure 3.10) (Bai, et al., 2002).

The Laplace number is a dimensionless ratio of the inertial force times the stabilizing surface tension force divided by the square of the viscous force and is defined as:

$$La = \frac{\rho \sigma D}{\mu^2} \qquad \textbf{3.2}$$

Where: μ is viscosity of the droplet liquid and σ is the surface tension.

The boundaries between different regimes are defined in the updated Bai-Gosman model and listed in Table 3.1. Implementation of this model in STAR-CCM+ includes the temperature dependence of these boundary values. The user also specifies number of child particles upon break-up of a particle and the angle range for possible rebound. These parameters were set to two child particles for a breakup event and a rebound angle range of 5 to 55 deg was used for the current analysis.

Table 3.1: Regime transition criteria (Bai, et al., 2002)

Wall status	Regime transition state	Critical Weber number
Dry	Adhesion to Splash	$We = 2630La^{-0.183}$
Wet	Stick to Rebound	$We = 2$
Wet	Rebound to Spread	$We = 20$
Wet	Spread to Splash	$We = 1320La^{-0.183}$

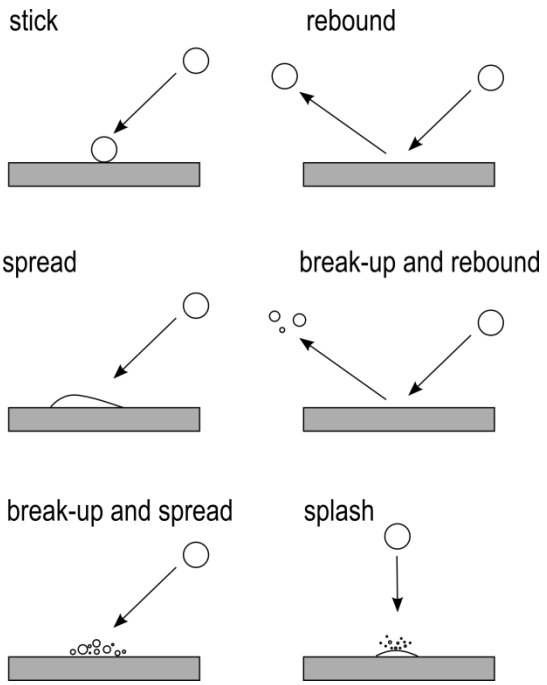

Figure 3.10: Possible particle behavior in Bai-Gosman model of wall impingement

Two separate groups of simulations were performed with different angles of injection of the droplets from the tire-street contact relative to the ground. Angles of 7.5 degrees and 15 degrees respectively were used. For both of these angles three different initial sizes of droplets were considered: 300 µm, 500 µm, and 700 µm. These were representing the mean size of droplets generated in the experiments performed at LLNL. The simulations were run for 0.5 s and the mass flow rate of the spray was set to 4.5 kg/s following the LLNL findings. The particles were injected with velocity of 26.8 m/s (60 mph). The vehicle was in a stationary reference frame but the rotation of the tire, movement of the bottom boundary (road) and movement of the air was defined to represent motion of the vehicle with a constant velocity of 26.8 m/s (60 mph) along a highway.

Figure 3.11 shows the final state of the simulations for the initial droplet size of 500 µm. In the figures on the right, droplets are colored depending on their size with blue representing the smallest and red representing the largest ones (with initial injection size). The red droplets behind the wheel didn't hit any elements of the wheel well and didn't break up. Although their trajectories look different in both cases (7.5 degrees and 15 degrees) the bulk of the smaller droplets leave the wheel well after the breakup to the side of it in a similar way for 7.5 degree and 15 degree cases.

Figure 3.12 shows the distribution of the droplet sizes in all six performed simulations. Comparing the corresponding results for injection angles 7.5 degrees and 15 degrees (left and right column) not much difference can be found. This initial angle was not relevant for the droplet size distribution and any value between 7.5 and 15 degrees used in further simulations should give similar results. For different initial size of droplets different distributions were obtained. The highest counts were noted at around sizes 60 µm, 100 µm, and 160 µm for the initial sizes 300 µm, 500 µm, and 700 µm respectively. Droplets bigger than 200 µm diameter are not influenced much by the air flow in a truck wake and move following ballistic trajectories landing back on the road. However, smaller droplets in the micron size range are very likely to be suspended in the air for extended periods of time and may significantly influence the corrosion rate of the bridge girders when they are transported up to girder height.

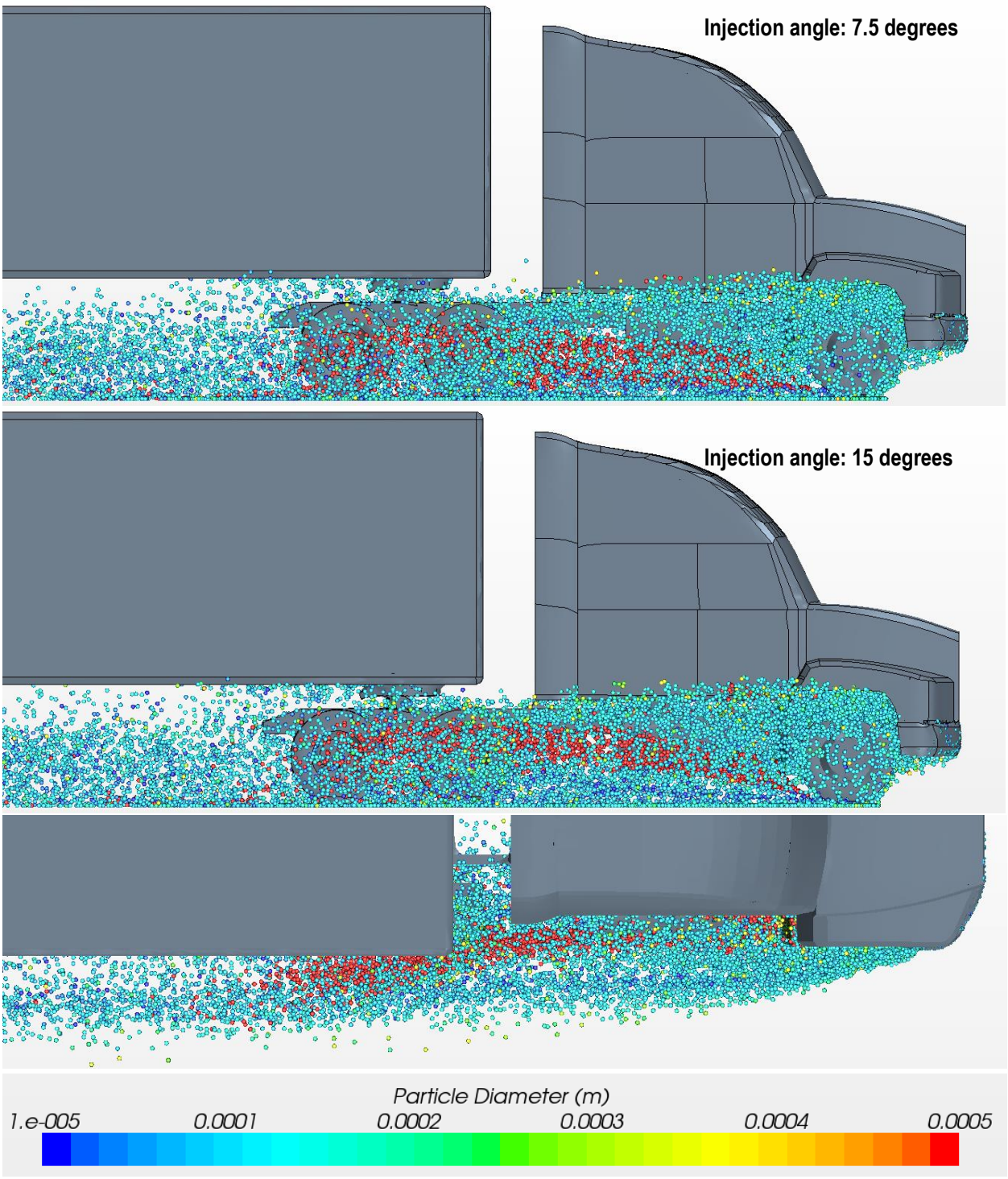

Figure 3.11: Droplet breakup in the wheel well (top) initial injection angle 7.5 degrees (bottom) initial injection angle 15 degrees

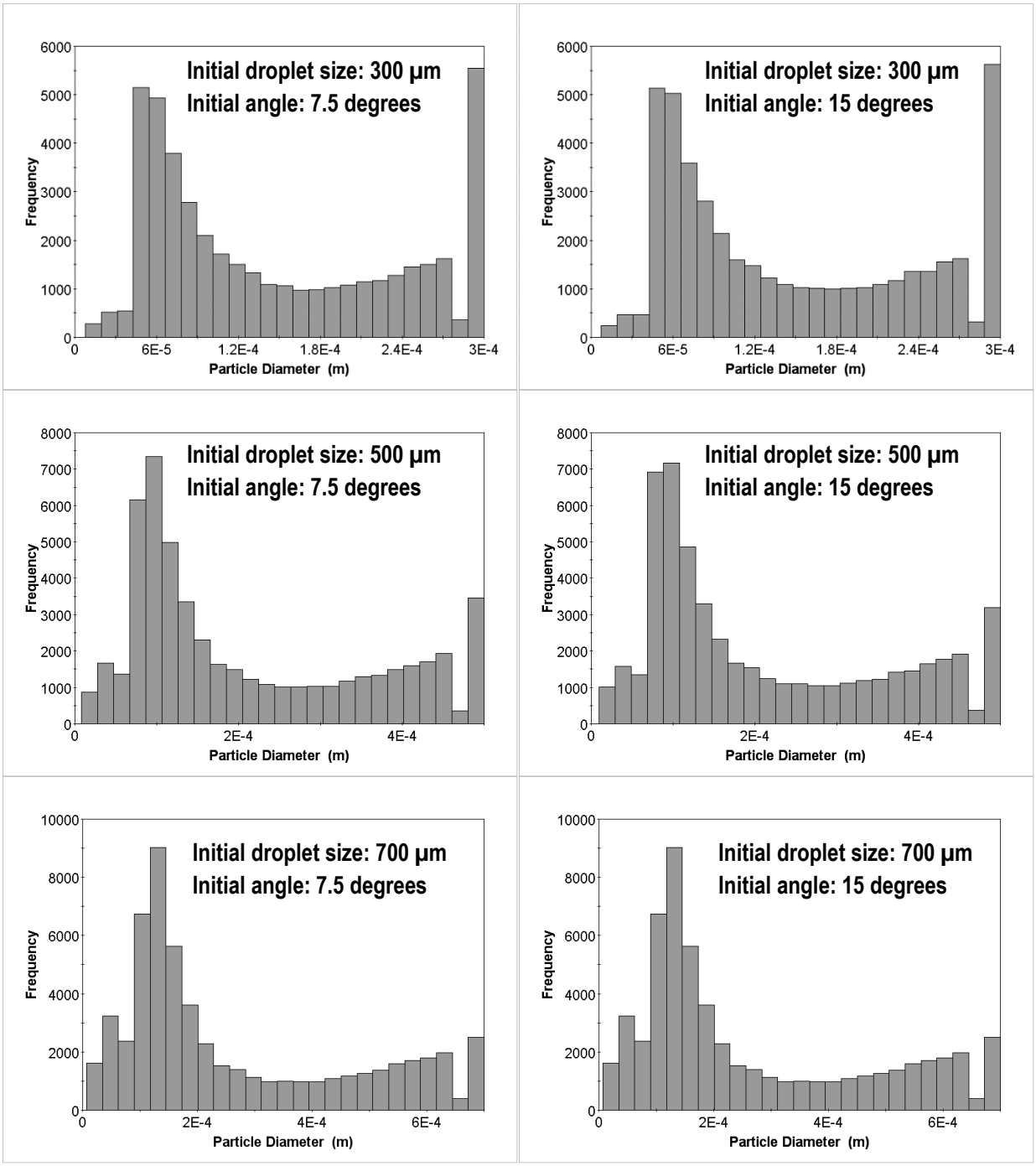

Figure 3.12: Droplet distribution after break-up in the wheel well

A range of particle sizes between 10 µm and 200 µm were investigated in the truck/bridge simulations with the majority of simulations performed for particles of 50 µm size. The Weber number of droplets in the simulations of this study is expected to be higher than the We in experiments done by (Radovich, 2010) thus smaller mean particle diameters can be also expected. It was assumed that this particle size would be more appropriate for the higher Weber numbers possible in the study cases. Figure 3.13 shows schematically the ranges of particles of interest in breakup simulations.

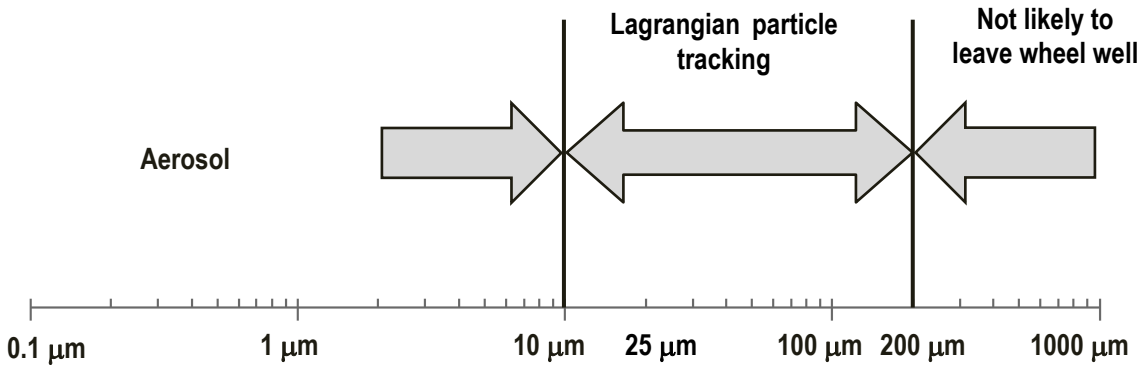

Figure 3.13: Ranges of the particle size and their treatment in the simulations

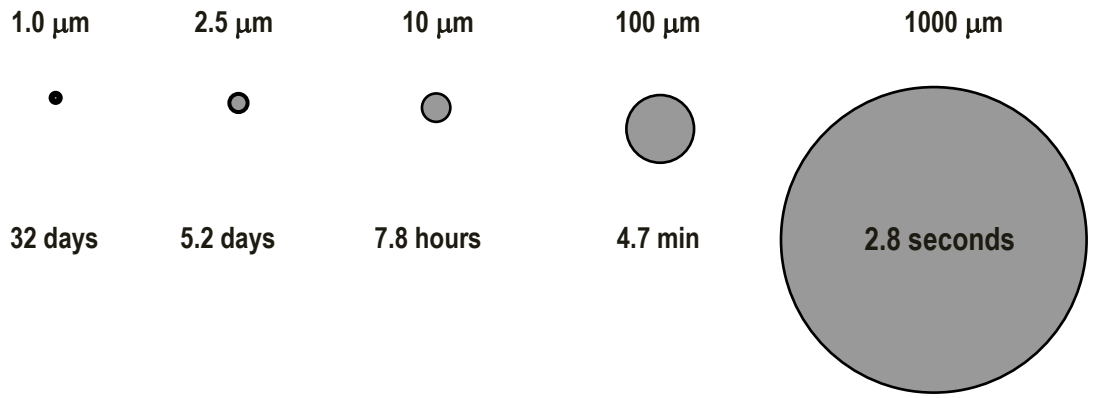

Figure 3.14: Sphere particle size and their settling time for a free fall from 5 feet

Figure 3.14 presents calculated settling time of spherical particles of different sizes in a free fall from 1.5 m (5 ft). Particles less than about 10 microns in diameter follow the fluid flow very closely and can be treated as a dissolved component of the air. Particles in the size range above 10 microns are tracked with the Lagrangian particle model, and particles of interest in this range have settling times between 5 min to 8 hours. Particles larger than about 200 microns settle back to the road surface quickly if they do not breakup on truck under side surfaces and are not likely to reach the bridge girders. The fate of droplets that remain aloft for many hours cannot be studied in one simulation even with implicit time integration because the time step of 0.015 s, which is reasonable for the mesh and Lagrangian particle tracking can take more than a week, with the currently available computing power, to compute the initial eight seconds of a truck passing event. This time is sufficient to compute the effects of multiple truck traffic by including a following truck passing under the bridge and transport of the majority of the particles to their highest position including the effects of interaction with boundary layer at surfaces and the wake of the following truck. With small droplets remaining aloft for hours, an increased simulation time may change the particle height distribution in terms of the percentage of particles from one truck that eventually reach bridge girder height. Without wind, or the passing of other vehicles that can generate upward air currents, however, droplets that have not reached girder height by the time a truck

has passed will just settle back to the roadway. Wind effects and the passage of multiple trucks are studied in separate cases, and it was assumed that the qualitative comparison of the cases is possible based on the simulated time scale that corresponds to a truck or pair of trucks passing under a bridge.

3.7 Air Flow around the Truck

Initial testing was done with passage of the truck under the bridge with massless droplets. Massless droplets are not assigned an initial velocity from the injector, and therefore, their trajectories may not be representative of droplets with mass. However, the calculations for these particles are much faster than for the particles with mass. So to understand the air flow around the truck, they were used first. Figure 3.15 shows the formation of the wake around the truck in motion. The wake boundary is very close to the truck and trailer edges as viewed in both the vertical and horizontal planes. Small particles are not likely to leave this zone easily. The wake behind the truck stretches for several lengths of the truck.

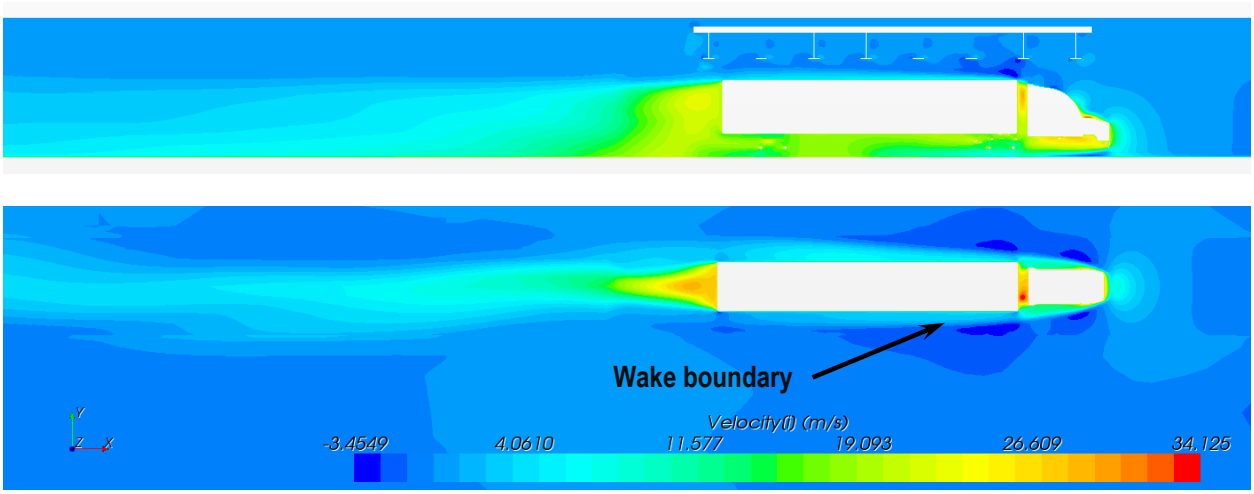

Figure 3.15: Formation of the wake around the truck in the implicit unsteady simulation

Figure 3.16 and Figure 3.17 show a comparison of the simulated parcel cloud with the photos of real spray mist behind the truck. Figure 3.17 shows how the mist is leaving the wheel well and staying within the air wake behind the truck.

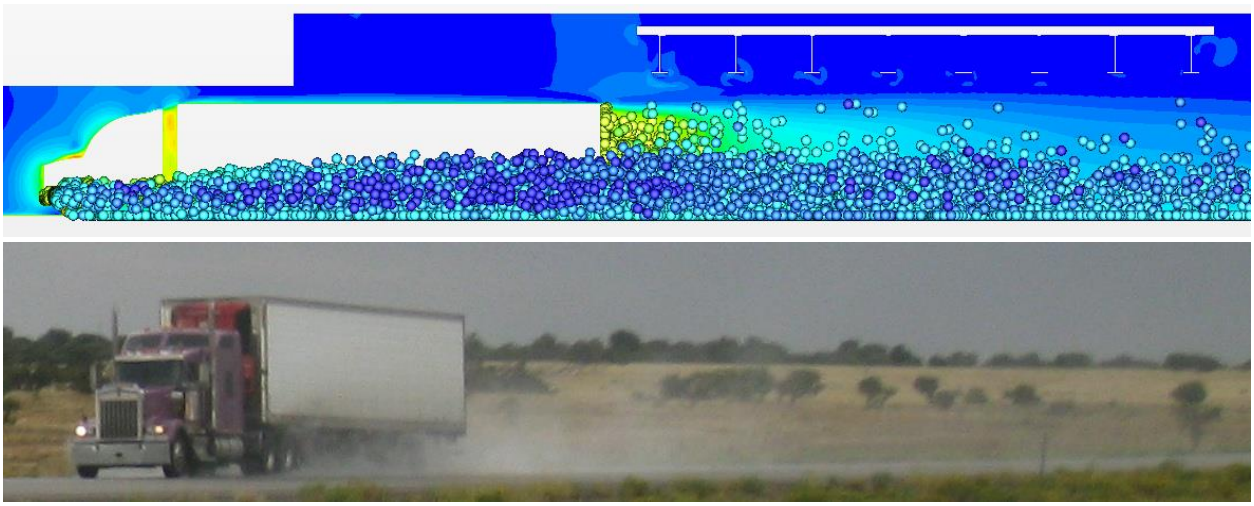

Figure 3.16: Comparison of the simulated parcel cloud with the spray mist behind the real truck

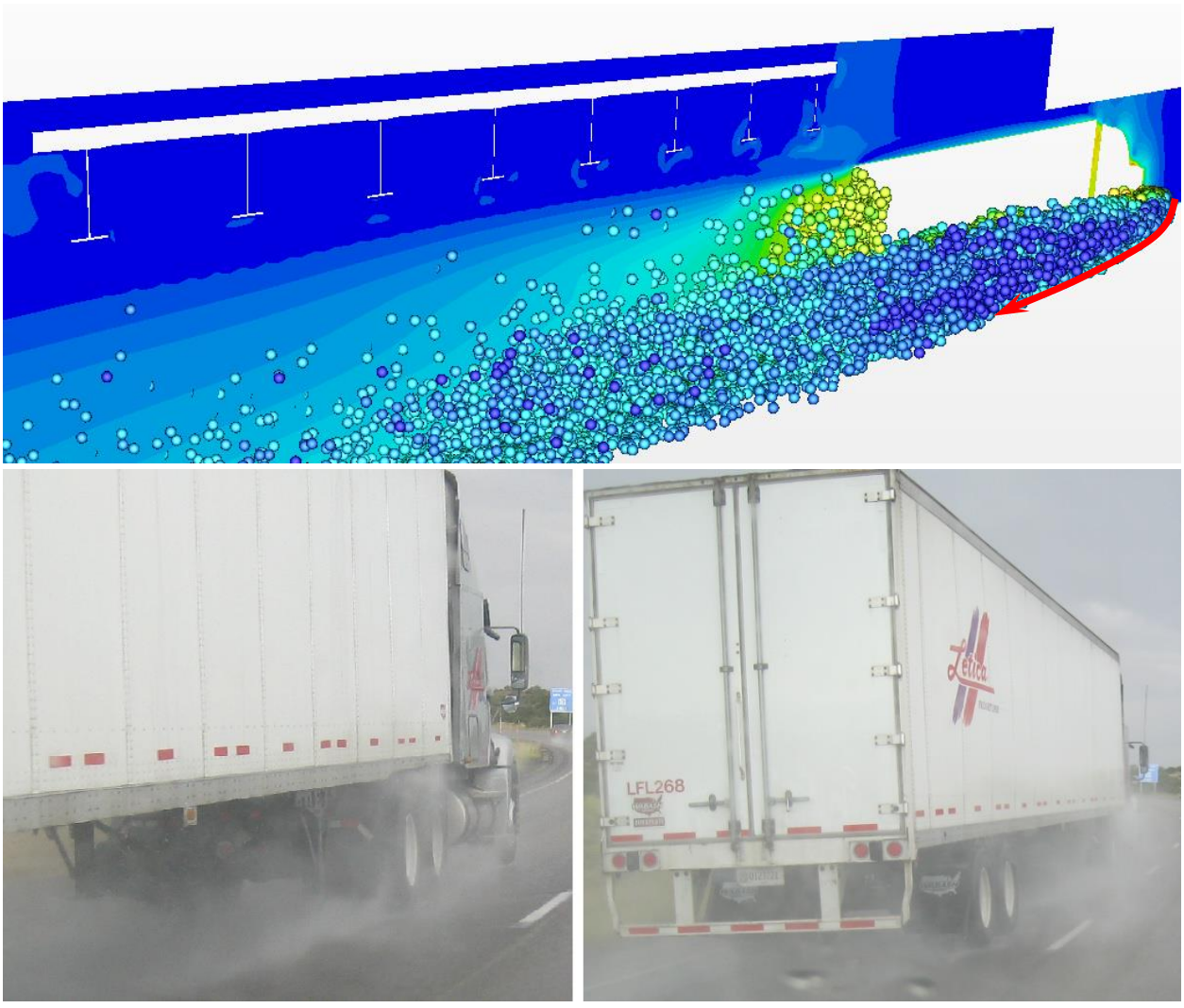

Figure 3.17: Escape of the droplets from the front wheel well

4. Case Study Results

For each of the basic cases, simulations with one and two trucks were studied. The two truck cases were added to include the effect of average daily truck traffic (ADTT) on the amount of salt transported to the bridge girders. For most of the basic cases three different particle sizes were studied: 25 μm, 50 μm, and 100 μm. For some cases, additional runs with 10 μm and 200 μm droplet diameters were also studied just to confirm the general trends. In addition to the basic cases without the wind, cases with several wind directions were studied. Cases with head and tail wind at the angle of 45 degrees were studied. Altogether about 40 simulations were scheduled for this stage of the analysis. Each of them took approximately 8 to 14 days to complete depending on the particle size, presence of the wind, and number of droplets accumulated in the system that slowed down the simulations by increasing the time to compute particle tracks. If many parcels were leaving the computational domain due to wind, then the calculation time was reduced. All the analyzed cases are listed in Table 4.1.

4.1 One Truck Studies

Initially three basic cases were considered: (1) a single passing truck, without wind, and an open space underneath the bridge, (2) a sloped embankment located close to the traffic lane and, (3) a vertical wall with wing wall (Figure 3.7c) located 5.5 ft from the wall side of the truck trailer. The cumulative number of particles in the bridge girder zone was calculated at three time instances: (i) in the wake of first truck, at 5.0 sec, (ii) in the wake of second truck for simulations with two trucks, at 6.75 sec and (iii) at the end of simulation, at 8.0 sec. The final results were plotted for the end of simulation, and the conclusions were drawn mostly based on these results. For easier interpretation of the results only the cumulative histograms for the cases with particle size of 50 μm are presented here. The influence of particle size is presented in Section 4.4. The overall tendency was that the smaller the droplets, the greater the number of them that reached the bridge girder level; the larger the droplets, the less parcels were transported to the bridge girder height.

Figure 4.1 presents number of parcels at the bridge girder level in basic cases with one and two trucks. Although the overall number of parcels transported to the girder level for the basic geometrical approaches was low, the greatest number of parcels that were transported to girder height was for the case with the close vertical wall with wing wall. The number of parcels for that case was over two times more than in the other cases. The influence of the close wall is non-negligible, but it is small for a single

truck passage when compared with other effects presented in Sections 4.2 and 4.5. In the case when the second truck was present, a similar trend was observed.

Table 4.1: Final set of analyzed cases for salt-spray generation study

cases with one truck	cases with two trucks
open 25 µm open 50 µm open 100 µm	open 25 µm open 50 µm open 100 µm
abutment with wing wall (4 ft gap) 25 µm abutment with wing wall (4 ft gap) 50 µm abutment with wing wall (4 ft gap) 100 µm	abutment with wing wall (5.5 ft gap) 25 µm abutment with wing wall (5.5 ft gap) 50 µm abutment with wing wall (5.5 ft gap) 100 µm
abutment with wing wall (5.5 ft gap) 50 µm tail wind, left side 30 mph abutment with wing wall (5.5 ft gap) 50 µm tail wind, left side 10 mph abutment with wing wall (5.5 ft gap) 50 µm abutment with wing wall (9 ft gap) 50 µm abutment with wing wall (14 ft gap) 50 µm	abutment with wing wall (5.5 ft gap) 50 µm tail wind, left side 30 mph
continuous abutment (5.5 ft gap) 50 µm continuous abutment (14 ft gap) 50 µm	
sloped embankment 25 µm sloped embankment 50 µm sloped embankment 100 µm sloped embankment 50 µm tail wind, left side sloped embankment 50 µm tail wind, right side sloped embankment 50 µm head wind, left side sloped embankment 50 µm head wind, right side	sloped embankment 25 µm sloped embankment 50 µm sloped embankment 100 µm sloped embankment 50 µm tail wind, left side
depressed approach vertical walls, 50 µm depressed approach 50 µm head wind, right side 30 mph depressed approach 50 µm head wind, right side 10 mph	

4.2 Multiple Truck Passing Studies

The results for the cases with two trucks without wind action are also shown in Figure 4.1. Comparing them with the results from the cases with one truck, the number of parcels transported to the girder level was tripled for the open and wing wall conditions under the bridge.

For the case with sloped embankment this value was nearly 15 times higher. The main conclusion that can be drawn from this comparison is the fact that presence of closely spaced truck trains, about one truck length apart, can drastically increase the droplet transport rate to girder level. The cumulative

effect of traffic after winter storm salting events may significantly increase corrosion risk at weathering steel bridges.

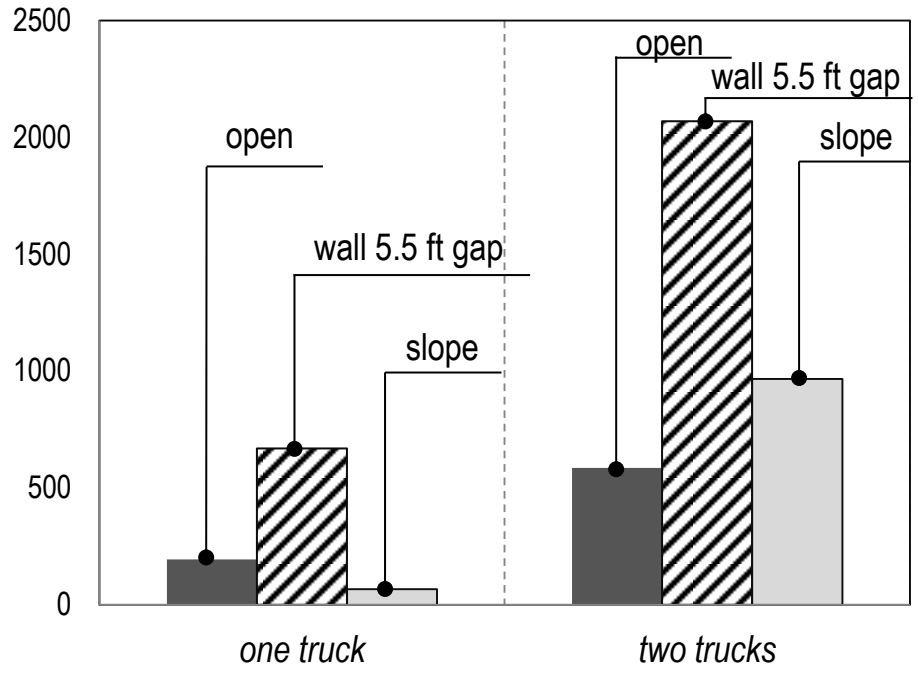

Figure 4.1: Cumulative plot presenting number of parcels at the bridge girder level in basic cases for simulations with one and two trucks

4.3 Influence of Proximity of Truck to a Vertical Wall Abutment with Wing Wall

Four different locations of the close vertical wall with a wing wall were studied with the wall located at: 4 ft, 5.5 ft, 9 ft and 14 ft from the truck. These locations are schematically shown in Figure 4.2. In addition to these cases, two cases with a close continuous wall stretching through the whole computational domain were analyzed. These were called long vertical wall cases, and the wall was located for these at 5.5 ft and 14 ft from the truck.

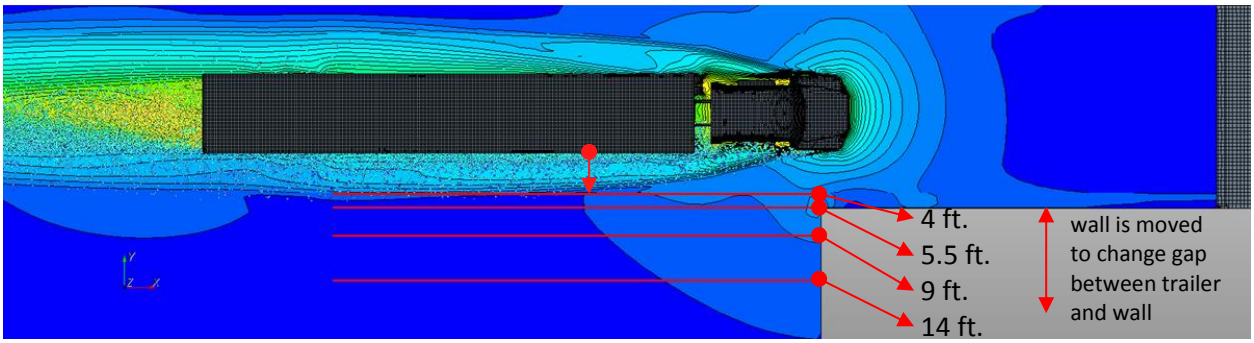

Figure 4.2: Location of the wall for abutment wall proximity effect studies

Figure 4.3 shows the cumulative plot for the basic cases together with the cases with different wall distances between the side of the truck and the wall. The cases with the abutment with a wing wall were more severe than the cases with the long wall.

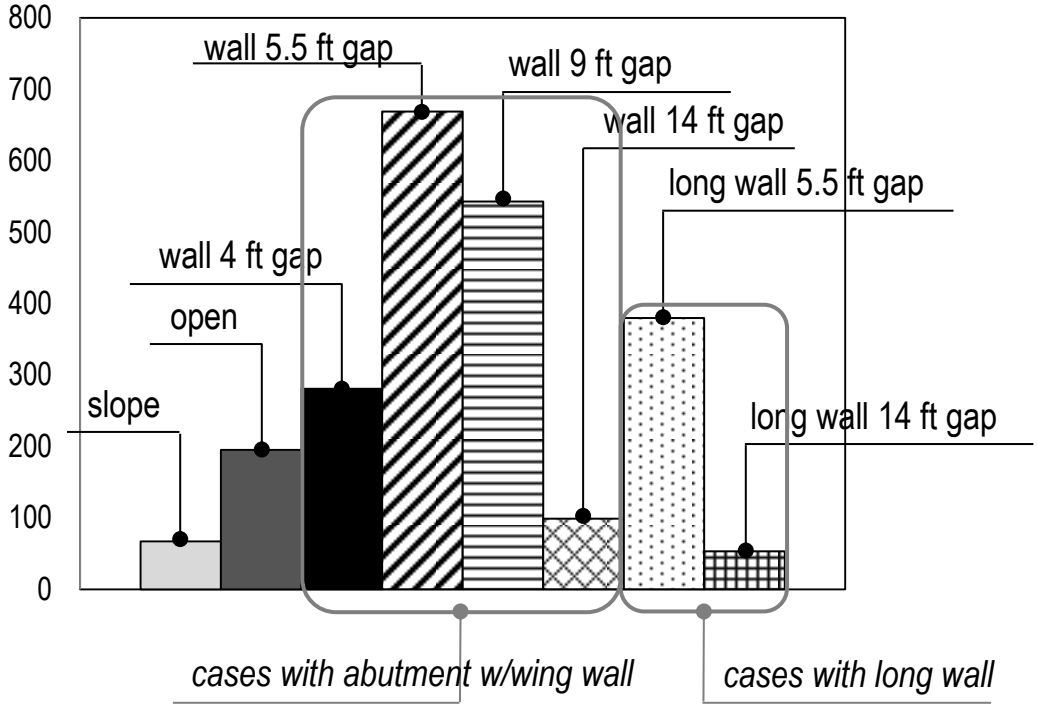

Figure 4.3: Cumulative plot presenting number of parcels at the bridge girder level for simulations with one truck and different geometry conditions

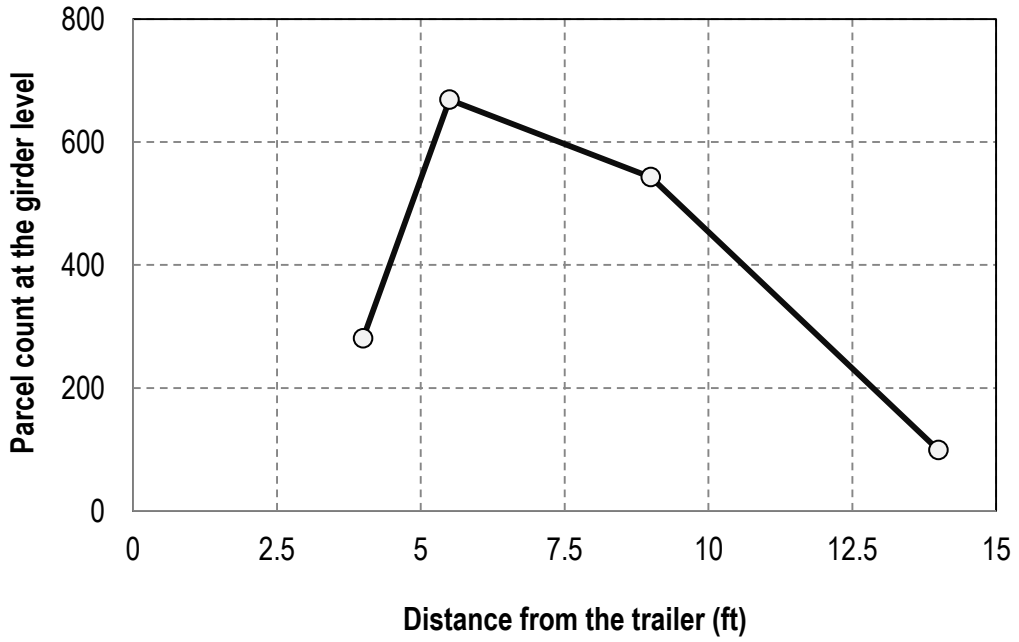

Figure 4.4: Parcel count at the bridge girder level in the models with different short vertical wall distance

For purposes of comparison, the results for the no wall and sloped embankment are also shown in Figure 4.3. The plot in Figure 4.4 indicates that the number of parcels reaching the girder level has its maximum when the gap between the wall and truck is between 5.5 ft. and 9 ft.

4.4 Particle Size Influence Study

Droplet size influence was also analyzed early on as one of possible factors in the count of parcels reaching the girder level. Simulations with different parcel size were performed for all the basic geometry cases with one and two trucks. As a general tendency from Figure 4.5, Figure 4.6, and Figure 4.7 it can be confirmed that the smaller the particle size, the more of them are reaching the girder level. Note that in Figure 4.6 the cases for one truck were analyzed for the wall located at 4 ft from the trailer and the cases with two trucks were analyzed for the wall at 5.5 ft from the trailer. This is a consequence of the fact that during the analysis of the cases with one truck it was discovered that the wall located at around 5.5 ft from the trailer was giving the worst case scenario for this type of geometry.

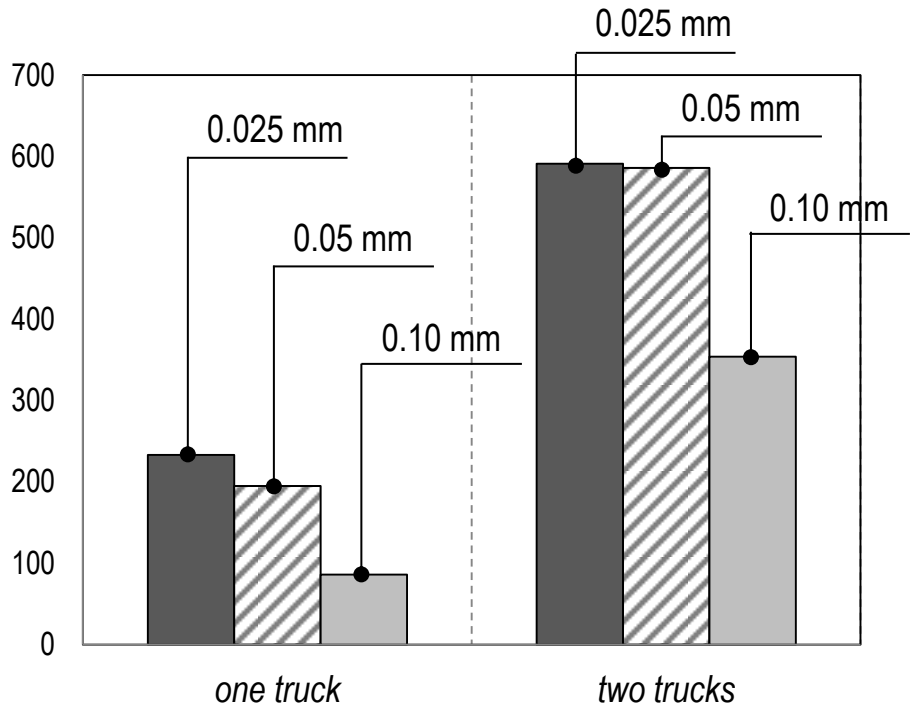

Figure 4.5: Cumulative plot presenting number of parcels at the bridge girder level for simulations with open boundary conditions and different particle size for cases with one and two trucks

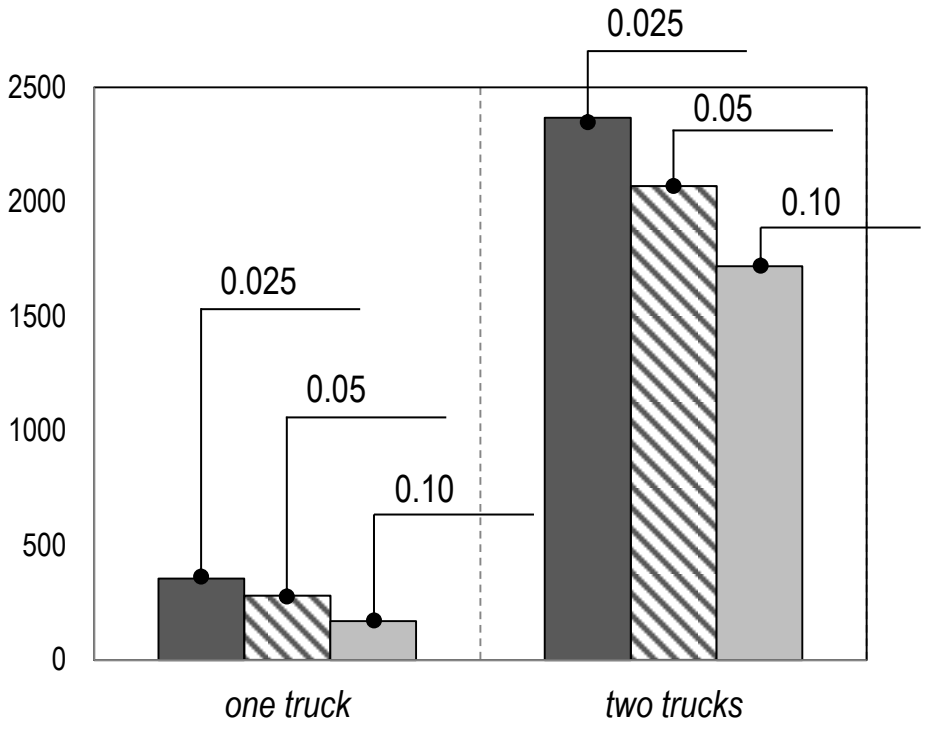

Figure 4.6: Cumulative plot presenting number of parcels at the bridge girder level for simulations with close wall embankment and different particle size for cases with one and two trucks

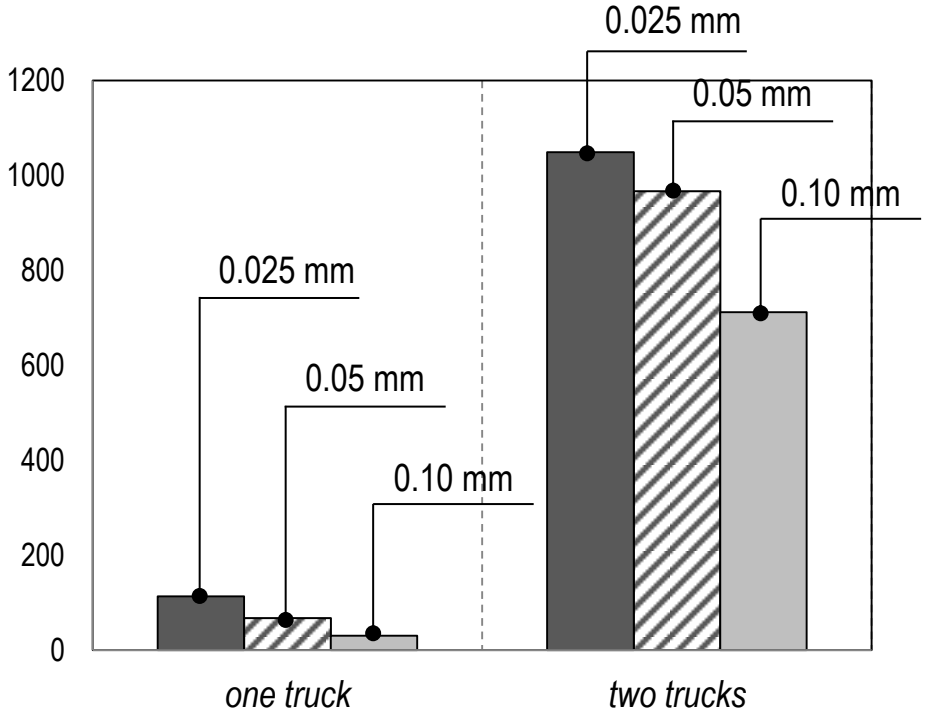

Figure 4.7: Cumulative plot presenting number of parcels at the bridge girder level for simulations with sloped embankment and different particle size for cases with one and two trucks

4.5 Wind Influence Study

Although the influence of wind was not in the initial plan of this study, several cases with different wind directions were included in the analysis to test the sensitivity of droplet transport to wind. Nearly all cases were run with a high wind velocity of 30 mph to determine a worst case scenario. Several cases were also run with a wind velocity of 10 mph to check response to wind speeds that are close to winter average in the mid-west and northeast U.S. The National Weather Service (Stokols, 2013) defines a blizzard as a snow storm with "sustained wind or frequent gusts to 35 miles an hour." The simulated velocity of 30 mph is near blizzard conditions. Average and maximum wind speeds by month are listed for a large number of cities over a long period time in the NOAA report: "Comparative Climate Data for the United States Through 2011" (National Climatic Data Center , 2011). In the Midwest and North Eastern states, average wind speeds vary around the approximate range of 10 to 14 mph for the winter months and maximum wind speeds are often four to five times higher. Results of simulations with wind appear to indicate that wind may have a very large influence on the fraction of droplets in a truck wake that reach bridge girder level. Noting that settling velocities for droplets are very low (about 1.4 mph for a 1 mm diameter droplet), only low upward wind speeds would be needed to lift droplets upward. In the simulations, wind enters the domain parallel to the ground with no upward component of velocity. Some of the results were unexpected and are discussed in the following sections. Additional analysis with more wind speeds and approach angles would be needed to investigate the results and wind effects in more detail.

4.5.1 Wind with Sloped Embankment Geometry

Four directions of the wind were simulated in the model with the sloped embankment: two from the front and two from the back, all with the wind entering at 45 degree angles to the road, shown schematically in Figure 4.8. Note that time and resources limited these simulations to the original half bridge geometry with the bridge abutment on one side only. To run the simulations with wind, the previously used symmetry condition down the centerline of the roadway on the left side as shown in Figure 4.8 was replaced with a specified velocity, air inlet condition. The inlet wind direction was parallel to the ground in all cases. Therefore, the only mechanisms to change the wind direction to give an upward, z-direction, component of velocity are obstacles in the domain that force the flow near the surface to follow the direction of the surface, such as the sloped embankment cases of the bridge abutment, the trucks, etc., and vortex structures that have an upward component generated in the flow field by flow past bluff bodies or other surfaces where flow separation may occur. The effect of wind action was also studied for the geometry of a vertical abutment with wing wall.

Figure 4.9 shows a cumulative plot presenting the number of parcels at the bridge girder level for the basic cases without wind in comparison to the cases for the sloped embankment with the wind. The counts were taken 8 seconds into the simulation after the truck has passed out of the domain. Even for the least severe case with the wind, a tail wind from the right, the number of parcels reaching girder level was nearly 20 times higher than the base case without the wind. For the most severe case the number of parcels transported to the girder level was over 8000, which is 120 times more than the base case. For a single truck passing, the cases with a head wind from the right and a tail wind from the left

produced the largest numbers of droplet parcels at girder level, more than a factor of two greater than the other cases. The reason for this result is not immediately obvious. Looking at the system geometry in Figure 4.8, the left tail wind direction would be expected to blow droplets in the truck wake up the embankment to bridge girder level, and it is not surprising that this case produced the largest parcel count at girder level. Figure 4.10 shows this result with a velocity vector plot in a cross section between the last girders of the bridge just behind the truck and droplet parcel distribution at two different times, when the truck exits from under the bridge, and at 8 seconds after it has left the domain.

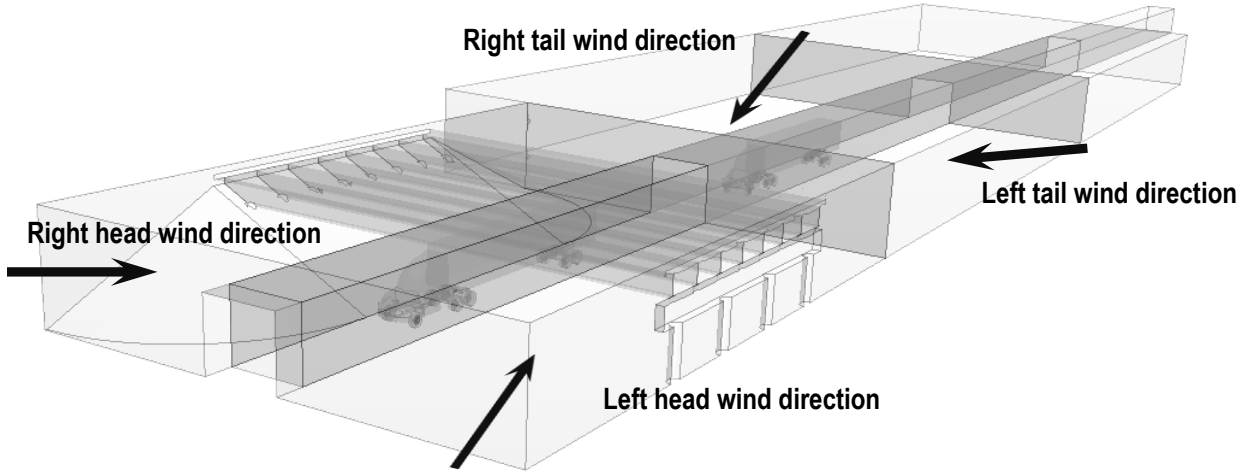

Figure 4.8: Geometry with inclined embankment showing wind directions for cases with wind

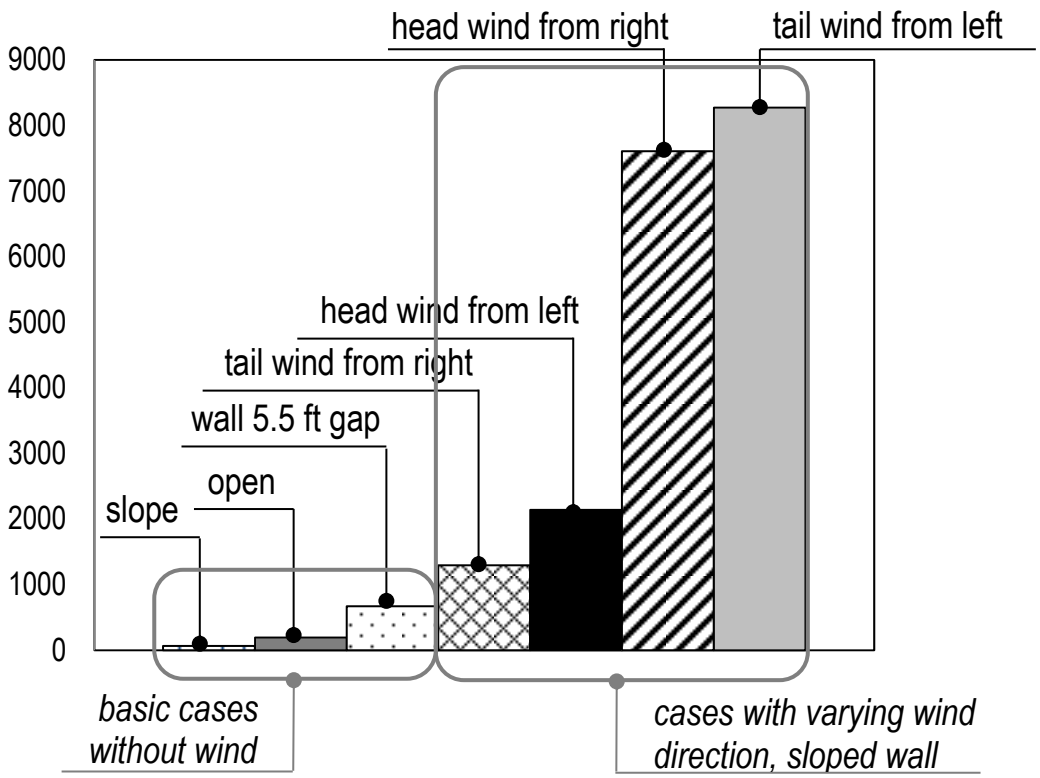

Figure 4.9: Cumulative plot presenting number of parcels at the bridge girder level for simulations with one truck and different wind conditions for the cases with sloped embankment

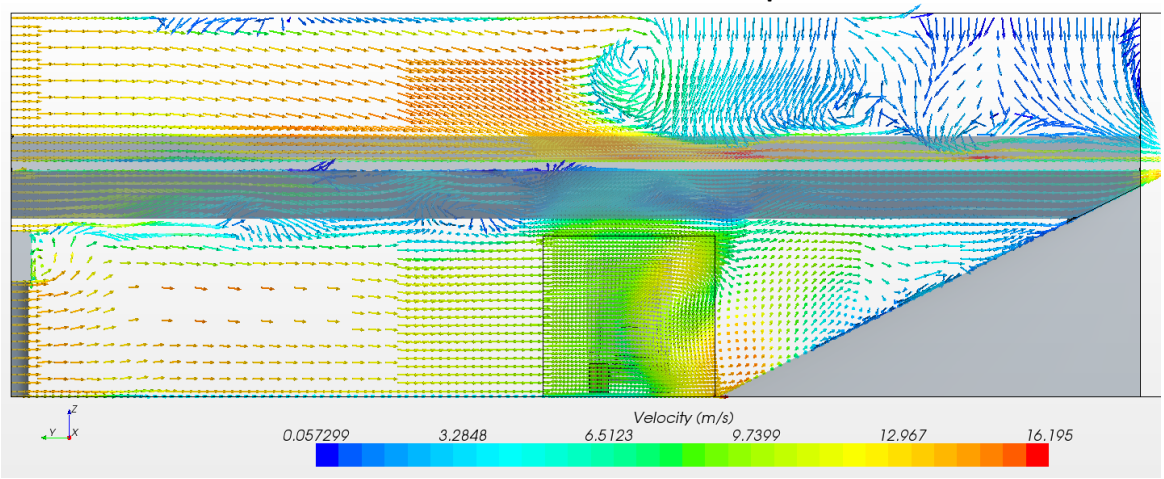

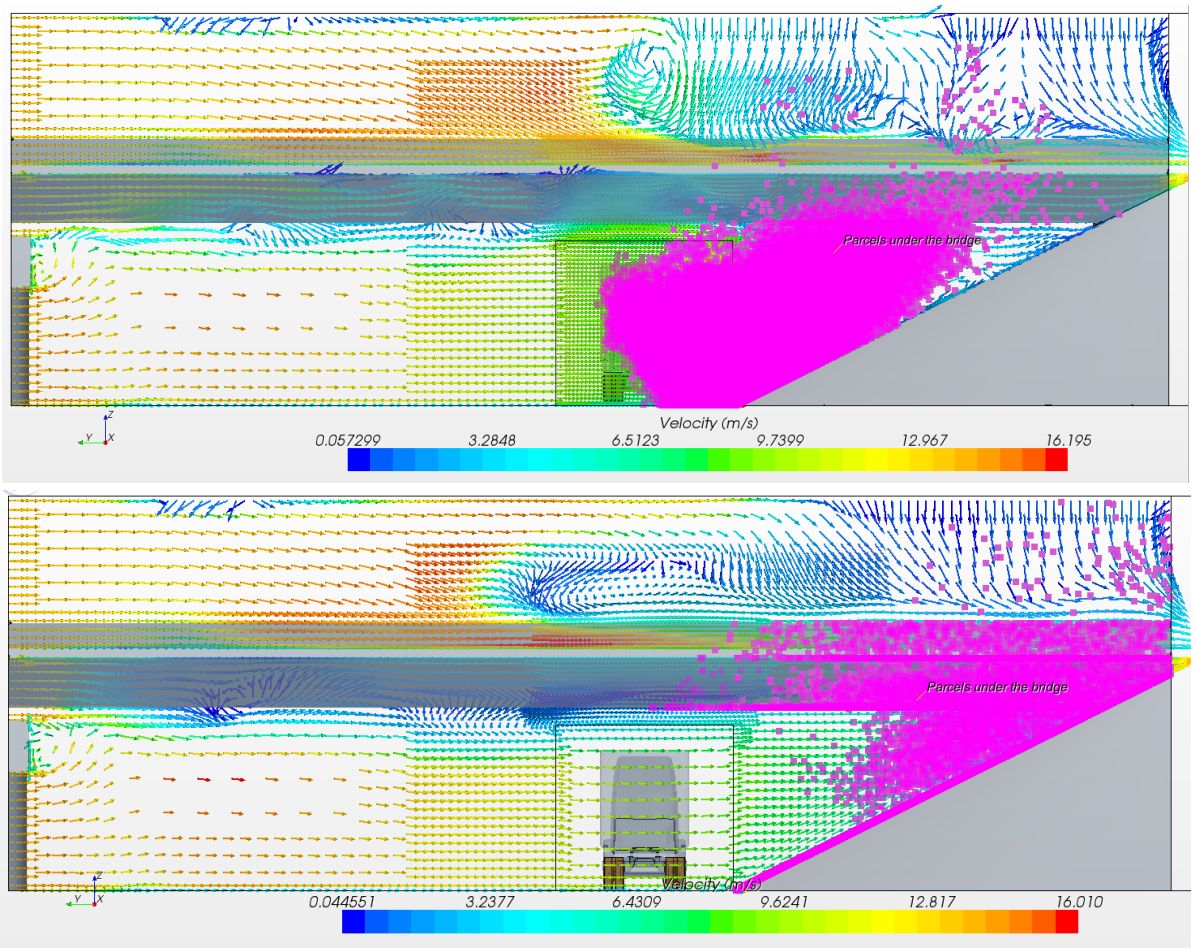

Figure 4.10: Velocity vector plot in the section between last two girders of the bridge for case with the left tail wind; (top) stage just after passage of the truck; (center) with droplet parcels residing at this moment under the bridge; (bottom) final stage of the simulation at 8 s

The left head wind direction might be expected to also blow droplets up the embankment and produce a girder level count close to the left tail wind case. However, it did not; its count was lower by close to a factor of four. Three possible reasons are: (1) Droplets were only injected from curbside tires to capture interaction with abutment geometry but keep computation time to about a week. The truck, therefore, appears to shield droplets on the curb side from the wind until they are exposed to the wind in the truck wake, Figure 4.11 top and middle frame. The velocity vector plots in cross section between the two last beams of the bridge are shown in Figure 4.11.

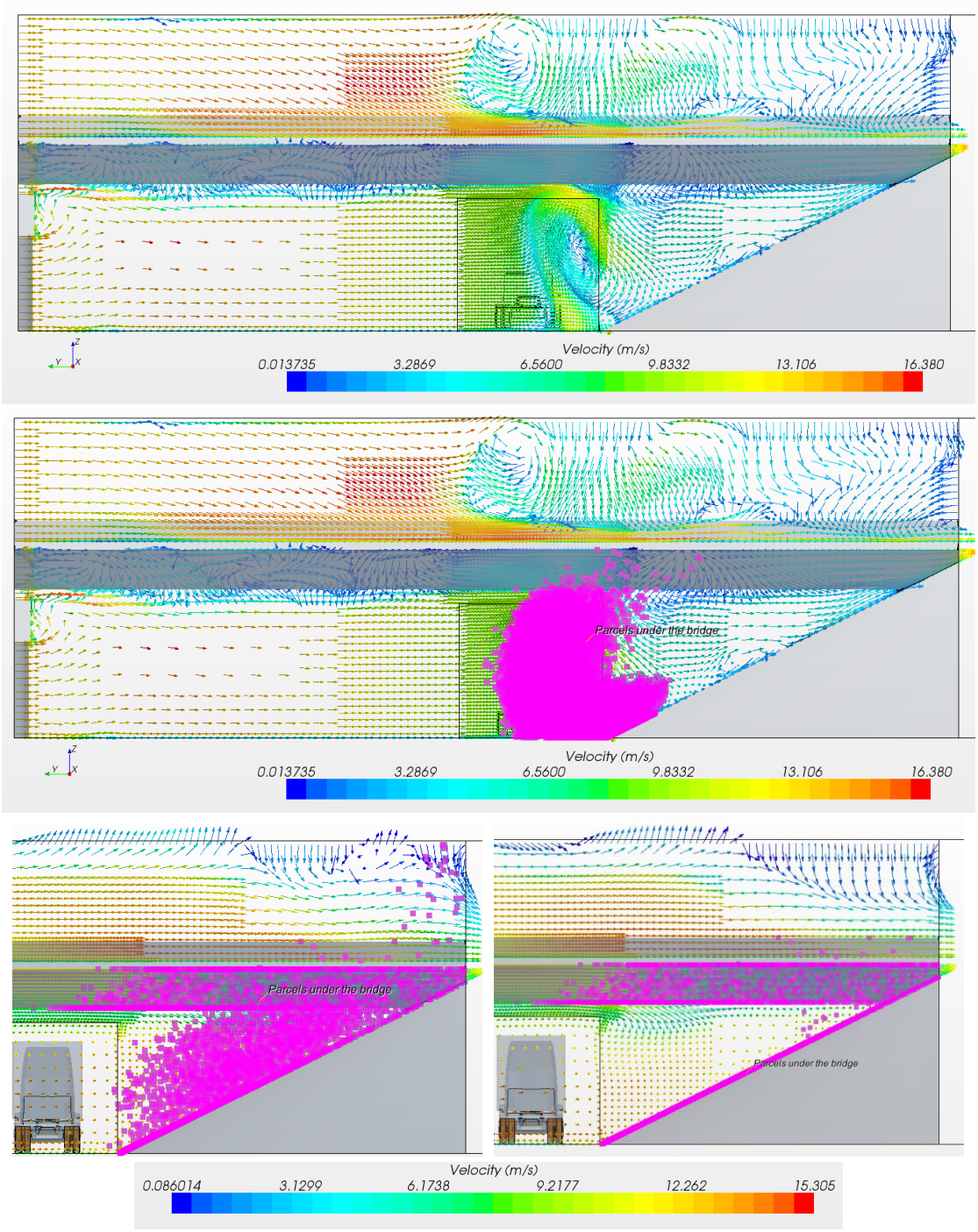

Figure 4.11: Velocity vector plot in the section between last two girders of the bridge for case with the left head wind; (top) stage just after passage of the truck (center) with droplet parcels residing at this moment under the bridge (bottom left) stage at 8 s (bottom right) stage at 10 s

(2) The left head wind may tend to blow more droplets out from under the bridge rather than up the embankment, once the passing of the truck exposes them to the wind, Figure 4.11, bottom frame, left snapshot at 8 seconds right snapshot at 10 seconds. At 8 seconds a large number of droplet parcels is seen in the embankment region. At 10 seconds most of the droplets have been blown out of the embankment zone without a noticeable increase in droplet parcels at the girder level. (3) The left head

wind also slows droplets through drag in the horizontal direction because it is in the opposite direction to the truck motion.

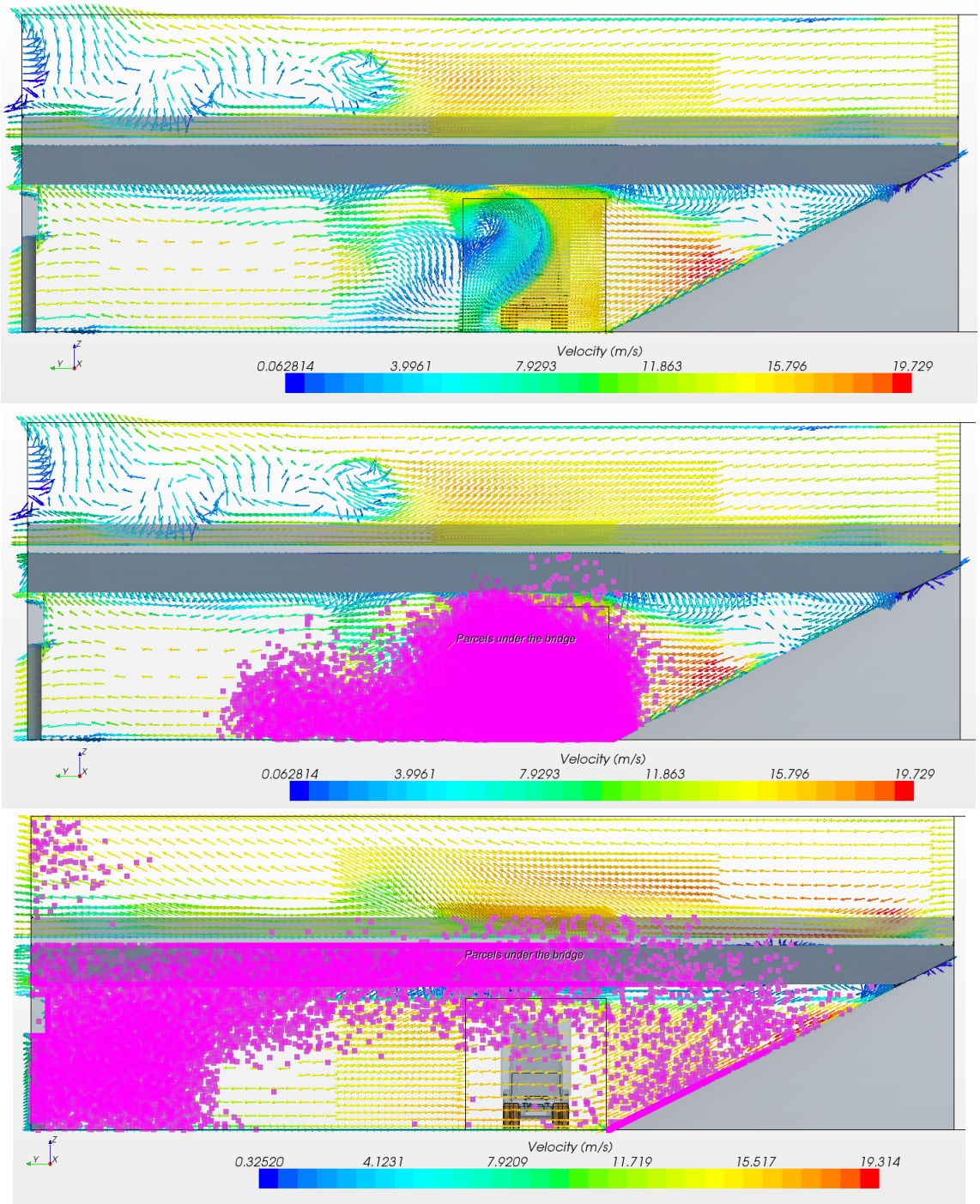

Figure 4.12: Velocity vector plot in the section between last two girders of the bridge for case with the right head wind; (top) stage just after passage of the truck (center) with droplet parcels residing at this moment under the bridge (bottom) final stage of the simulation at 8 sec

The right head wind case had a girder level parcel count at 8 seconds near that of the left tail wind, Figure 4.9, the worst case. Review of the parcel distribution at girder level at the end of simulation shows high parcel concentration on the left side of the domain at girder height, Figure 4.12 bottom frame. The right head wind enters, as previously noted, in the horizontal direction, however, the wind does follow embankment slope downward from right to left. This flow direction would move parcels downward away from girders on the left. When the wind enters the truck wake, at the time when the truck is exiting the underside of the bridge, and a vortex with upward flow is visible in the vector field, and appears to be the only mechanism that can carry parcels to girder level on the left. A snapshot of this behavior is presented in Figure 4.12.

The right tail wind case yields a parcel count at girder level, at 8 seconds time, that is twice the worst case without wind, Figure 4.9, but still lower by a factor more than four than the worst cases with wind. This result was expected because the wind direction, diagonal from right to left, is blowing droplets away from the embankment. It is not completely clear, however, why this case would be so different from right head wind case, except that apparently its interaction with the truck wake may not produce dynamic vortices with as strong an upward flow component in regions with high droplet parcel concentrations in the truck wakes. The vector plots of velocity in a cross section under the bridge between the two last girders are shown in Figure 4.13.

These cases have shown that of all mechanisms that may transport droplets from the low level part of the truck wake to the girder level, wind can have the greatest effect by a large margin, more than 120 times the base case sloped embankment geometry with no wind in the limited number of cases tested. These cases have also shown that addition of wind interacting with the trucks and bridge structures produces a very complex dynamic flow field that yields droplet transport and girder level counts with variations that are not always intuitively obvious. Additional simulations with wind that include the full bridge geometry on both the left and right, droplet parcel injection from all 18 tires on both sides of the truck, and more extensive collection and analysis of wind and droplet track development histories would provide a good follow up study of wind effects. The effects of wind speed should also be a part of that study. Such computations would require approximately double the computational resources, and the running time would also be double or more going from between one to two weeks to close to a month. Running time in more extensive wind studies might be brought down by reducing tire injection area to bring down the total droplet parcel count in the system to on the order of one to two hundred thousand parcels, the approximate count in the present study.

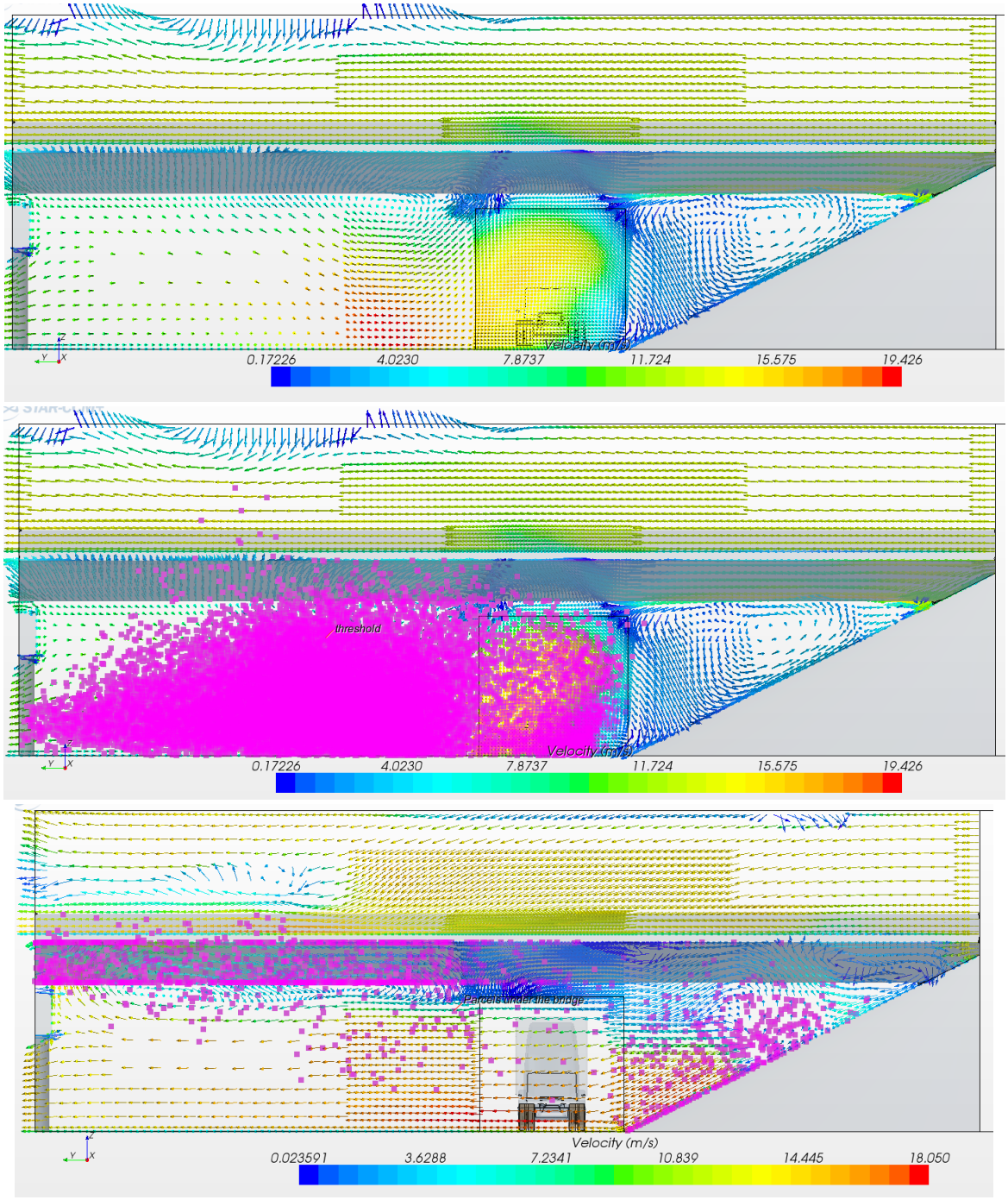

Figure 4.13: Velocity vector plot in the section between last two girders of the bridge for case with the right tail wind; (top) stage just after passage of the truck (center) with droplet parcels residing at this moment under the bridge (bottom) final stage of the simulation at 8 sec

4.5.2 Wind with Vertical Wall Abutment Geometry

Because time was not available to run a large number of wind cases, only the worst case wind direction from the study with the embankment geometry was tested for the vertical wall abutment geometry. The tests included one and two truck cases with 30 mph tail wind coming at a 45 degree angle from the

left, and a 10 mph one truck case also with tail wind from the left. These cases with vertical wall abutment under the bridge with wing wall geometry were not as severe as cases with an embankment. Figure 4.14 presents a cumulative plot with the number of parcels for the cases with wing wall at 5.5 ft distance from the trailer, with and without the tail wind blowing from the left side (toward the wall). For these cases many of the parcels hit the vertical wall because they have enough inertia to prevent them from making a sharp turn with the air flow as it approaches the wall obstacle. Once droplets hit the wall they are out of the system. If enough hit the wall they could form a water film that would flow back to road level on the wall under the influence of gravity. That water transport mechanism was not modeled because it would not add the amount transported to girder level. and influence of the wind was quite opposite than in the case with the sloped embankment. Note in Figure 4.14 that for the cases with the fairly high velocity 30 mph wind, enough droplet parcels are removed from the system by being blown into collision with the wall that the girder level parcel count is lower the case with no wind. For the case with wind at 10 mph, the number of parcels at girder level increased by 23 % (from 670 to 820), indicating that the lower velocity wind in this case results in more transport to bridge girders because far fewer are blown into the wall and the addition of the 10 mph wind to the wake flow of the truck may produce more of an up draft than in the no wind case.

These few vertical wall cases also illustrate that wind interaction with bridge structure geometry and truck wakes is a complex phenomenon and many more test cases would be needed to better characterize its effects.

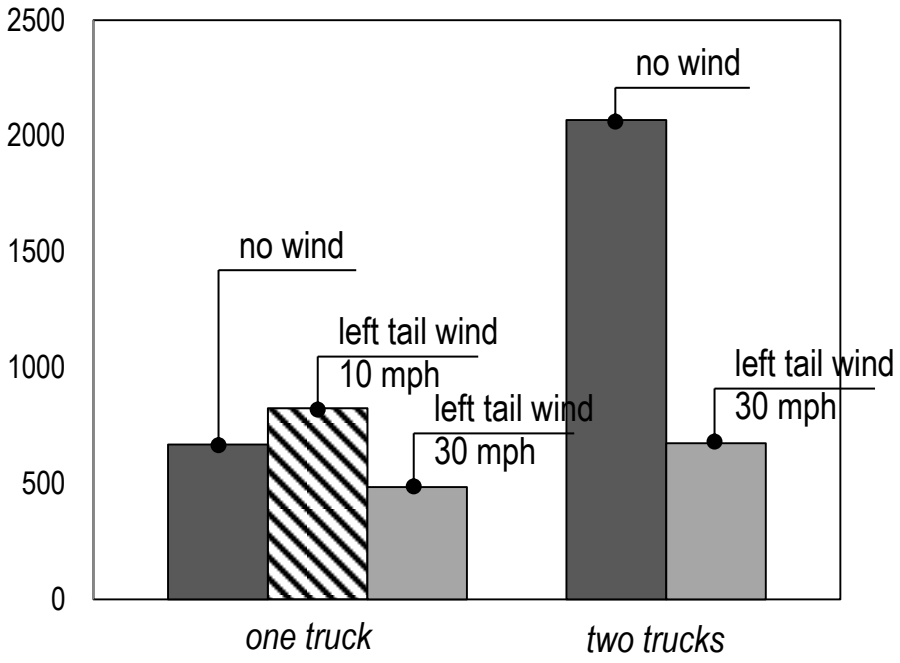

Figure 4.14: Cumulative plot presenting number of parcels at the bridge girder level for simulations with one truck and different wind conditions for the cases with vertical abutment with wing wall

4.6 Depressed Grade Approach Effect Study

Bridges with depressed grade approaches with vertical abutments or very steep berm approaches may prevent transport of droplet plumes created by trucks and other vehicle traffic from being transported laterally away from the road and bridge structure.

Figure 4.15: Depressed grade bridge approach with vertical abutments

Figure 4.16: An example of a long depressed grade approach to a bridge with vertical walls

An additional model has been built to represent an extreme case of depressed approach with long vertical walls near the roadway on both sides. An extended domain above the bridge level has been built as shown in Figure 4.17. The vertical side boundaries of the lower part were set as walls. The vertical side boundaries in the upper region were set as velocity inlet and pressure outlet on the opposite side to

include wind action. Three cases were analyzed: case without the wind, with 10 mph wind and 30 mph head right wind.

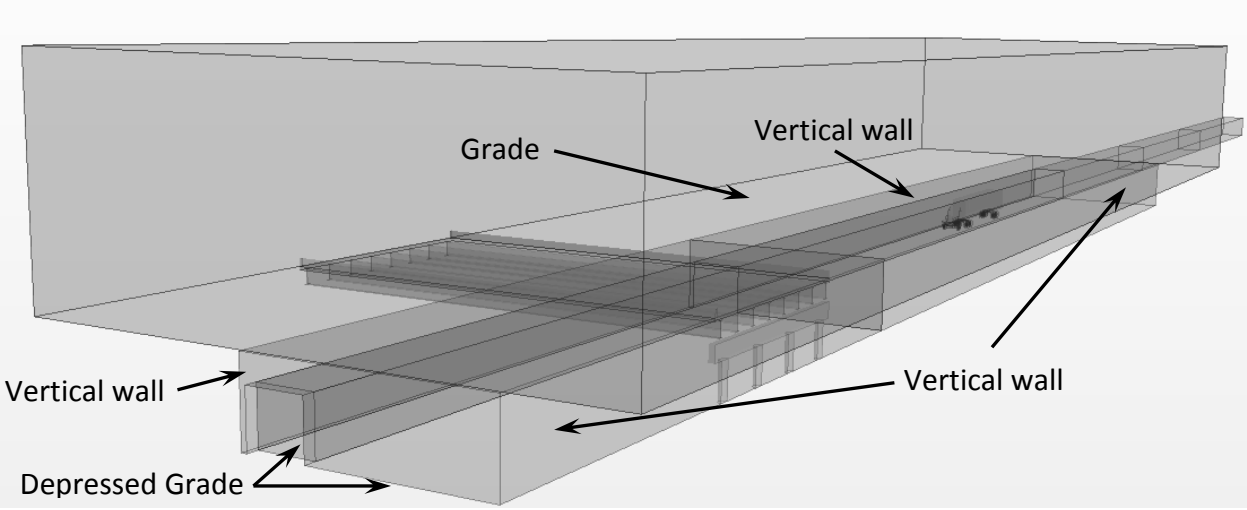

Figure 4.17: Geometry of the bridge with extreme depressed approach with vertical walls on both sides of the roadway creating a cavity in the terrain near the bridge

The case without the wind was similar to the case where close long wall was placed underneath the bridge. The main difference between these two cases was the size and extent of the domain above the bridge. For the case with the tunnel the space was open above the bridge deck. For the case with the wall the vertical boundary was extended higher. Nevertheless, the results for these two cases were expected to be qualitatively the same if there is no tunnel effect. For the case with the vertical wall around 380 parcels were counted at the end of simulation near the bridge girders. For the case with the tunnel without the wind there were 200 parcels near the girders and no change in the behavior of the parcels was noticed. The cases with the wind increased significantly the number of the parcels transported to the girder level. Figure 4.18 shows the plot comparing the number of parcels at the bridge girder level for these cases. The case with 30 mph wind brought a very high number, about 11,000, of parcels to the bridge girders. This behavior can be explained based on vector plots post-processed from the simulations as shown schematically in Figure 4.19. Secondary flow in the depressed grade cavity approaching the bridge induced by the wind was moving the particles up to the girders. In summary for this part of analysis it can be it appears that a tunnel effect may be significant in conditions where a depressed grade approach to the bridge forms a cavity with respect to the surrounding terrain and there is wind blowing across the cavity.

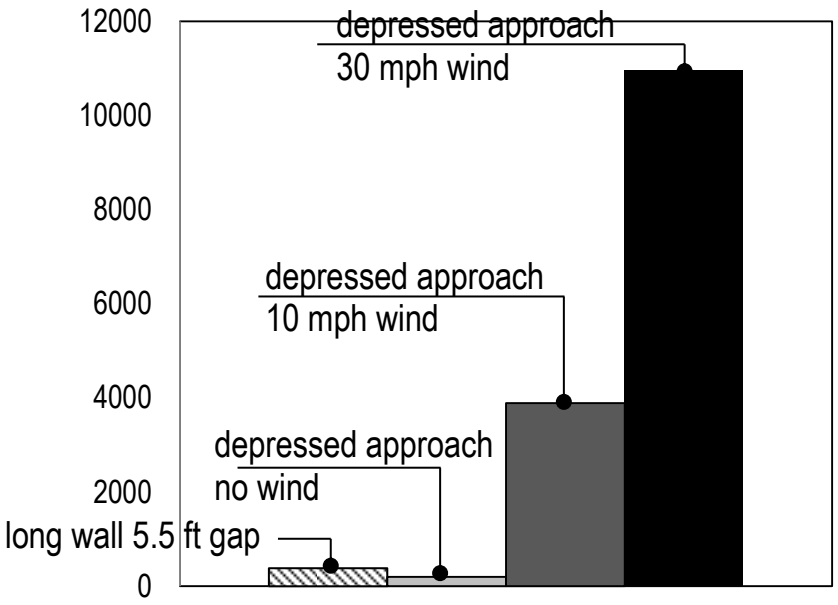

Figure 4.18: Cumulative plot presenting number of parcels at the bridge girder level for simulations with tunnel conditions

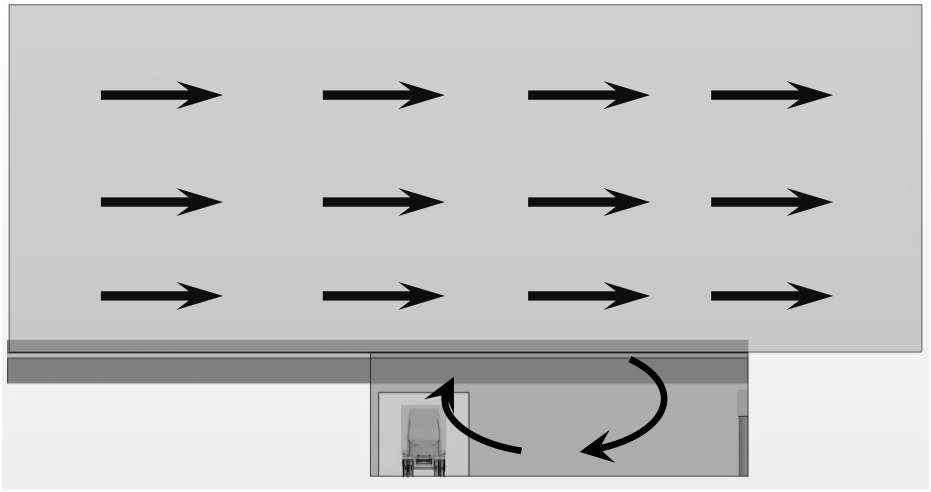

Figure 4.19: Flow induced in the tunnel causing transport of increased number of salt spray parcels to the bridge girder level

4.7 Aerosol Studies

Neither funding nor time were available to do an extensive study of the possible contribution to salt deposition on bridge girders of dry salt on the road re-suspended as an aerosol by traffic for days or weeks after snow storms. However, a few computations were run because they were easy to set up by modeling the aerosol as one component of a multicomponent mixture and they provide insight into the processes that can transport salt from the road surface to the bridge girders. Dry salt particles or

droplets re-suspended from the roadway by traffic can be considered an aerosol if the settling time is very long compared to other time scales of phenomenon near the bridge and the time for drag to reduce a slip velocity between particles and air is very small. Referring to Figure 3.14, particles in a size range less than about 10 μm in diameter stay suspended for hours to days and can be considered aerosols. Particles in the aerosol size range follow the motion of the air very closely and can be treated as component of a multi-species mixture in the gas when modeling the transport of the aerosol particles.

It was assumed that the important factors in aerosol transport would be similar to those of small droplet transport without limitations imposed by settling times that could be a short as a few minutes or less. For this reason cases with a following truck, no wind, head and tail winds at a forty-five degree angle, and a couple of cases with a close vertical wall were run. In the absence of good data on re-entrainment rates of dry salt films on roads from heavy vehicle traffic, assumptions based on the study by Williams (Williams, et al., 2000) were used to obtain an estimate of salt aerosol mass flux from tires as boundary conditions. A dry salt film of 10 μm height was estimated to be on the road surface. This corresponds to 2×10^2 kg/mile (467 lb/mile) on a 6.1 m (20 ft.) wide road, and is within the range of reported salting rates NCHRP Report 577 (Brent T. Mussato, 2007). Assuming that a heavy vehicle aerosolizes one percent of the dry salt film mass beneath a tire as it passes leads to an aerosol re-entrainment rate of 0.065 g/s or mass flux of 1×10^{-4} kg/(s m^2) coming from a tire. Williams notes that at this rate a thin salt film eroded by the passage of hundreds of vehicles would not generate a visible plume in the wake and could therefore be possible, even though dust plumes are generally not observed. While the assumed percent re-entrainment rate of 1 percent may be off by a significant factor, it lies in a plausible range, and that is sufficient for the results related to aerosol transport mechanisms reported here.

There is some evidence that dry entrainment and deposition on the land surrounding roadways in the days following a snow event may be the dominate process that determines the deposition pattern. Regardless of whether wet or dry entrainment and deposition dominates in the process of salt deposition on weathering steel girders, the simulations reported here were intended to test the relative importance of several of the possible transport mechanisms.

Table 4.2 lists the set of aerosol cases that were analyzed. The computations used less computer resources because they did not have to track droplets through the flow field. A case using the same computational grid as the droplet transport cases reached completion in between 1 and 2 days running on eight cores.

The cases were chosen to test the basic effects that were shown to have an impact in the truck droplet spray studies: traffic modeled with a trailing truck, sloped embankment versus vertical abutment, and wind from several directions versus no wind. In each case aerosol injection from the tires was done for the lead truck only. This configuration for the test isolates the aerodynamic effects of the second truck representing large vehicle traffic from the effects of additional salt entrainment. The wind was considered to have two possible significant effects: increasing transport when diverted upward by a trailing truck and diversion upward when approaching a slopped abutment. To keep the number of cases within a number that could be run in the available time, the wind direction was set at a 45 degree

angle to the road, which would give both a component in the direction of truck motion and a component in the direction of the slopped abutment. For the vertical abutment wall cases there is also a possible significant effect of flow turning in all directions including upward as it approaches a stagnation point on the wall.

Table 4.2: Analyzed cases for aerosol transport study. All included two trucks, a lead and trailing truck. The gap is the distance from truck trailer wall to vertical abutment wall.

Geometry	Wind direction and velocity
sloped abutment	no wind
sloped abutment	30 mph, 45 degree tail wind
sloped abutment	30 mph, 45 degree head wind
vertical wall with wing wall (4 ft gap)	no wind
vertical wall with wing wall (4 ft gap)	30 mph, 45 degree head wind

To obtain a single data point for comparison of the cases, the maximum salt aerosol mass concentration in parts per million (PPM) at the bridge girder level was monitored and in plotted in Figure 4.20 for the cases analyzed.

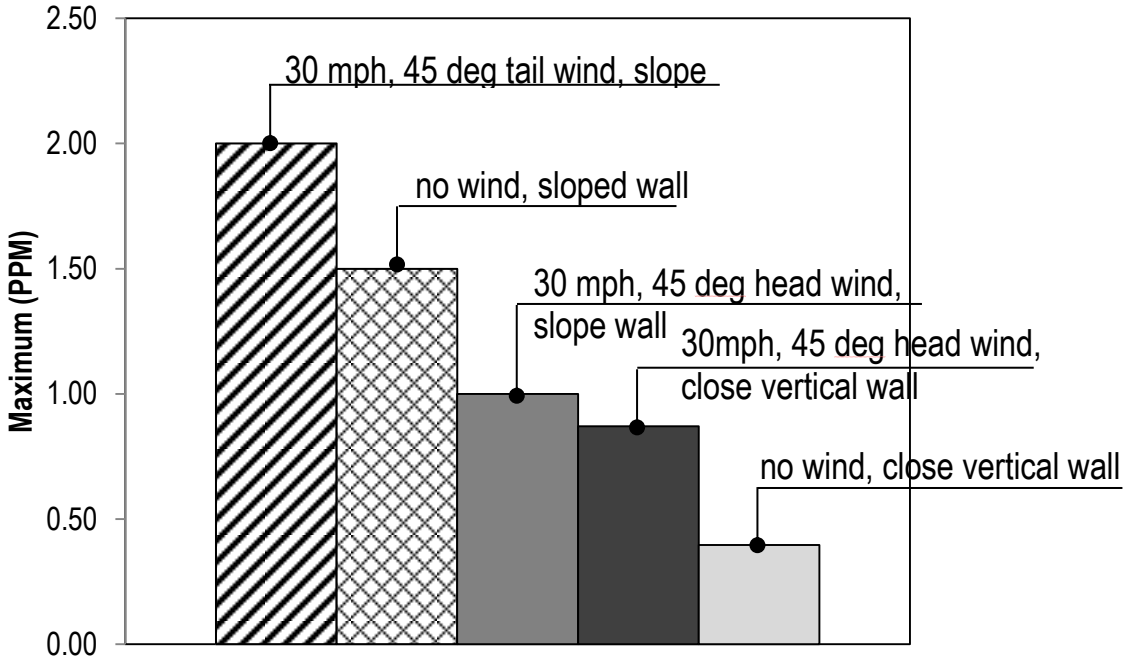

Figure 4.20: Dry particle aerosol transport to the girder zone for several cases with wind and no wind with two trucks where the aerosol is resuspended by the first truck only

The maximum concentration rather than the volume mean concentration was monitored because the potential for accelerated corrosion at local sites among the girders is of concern. While most of the volume between the girders may have very low salt concentrations, the high concentrations along the path of the salt aerosol plume if it reaches the girder level is more relevant to local corrosion risk on the

girders. The maximum concentration case with a 45 degree tail wind with a slopped abutment was not expected, but was apparently a consequence of wind transport to an outer corner of the bridge deck and abutment, as seen in Figure 4.27.

In the comparison of girder level salt concentration maximums in Figure 4.20, the reasons for the values are not immediately obvious and depend in part on the combination of the traffic effect in a truck following directly behind with a wind that is at a 45 degree angle across the road. In the cases with wind, the salt plume formed in the wake of the first truck can be blown partly out of the path of the following truck, reducing the traffic effect. A look at the salt concentration profiles for several cases can help to illustrate the complexity that arises when there are multiple salt transport mechanisms active in an analysis. The geometry for the cases discussed in the following paragraphs is that of the bridge with slopped embankment as shown in Figure 3.7b. As previously noted all cases included two trucks.

The first case in Table 4.2, that of a pair of trucks with a sloped abutment and no wind traveling under the bridge, is shown at three different times in Figure 4.21 through Figure 4.23. Figure 4.21 shows a color density plot of salt mass fraction on a vertical slice cut through the centerline of the path of the trucks as the first truck exits the bridge. The salt plume from the first truck is seen to have a maximum height equal to the trailer height in the immediate wake of the first truck. This is the only source of salt re-suspension from the tire treads of the first truck, and air with no salt aerosol from the upstream is diverted up and over the cab and trailer body of the first truck. When this salt free air reaches the end of the trailer, it mixes with salt aerosol in the wake and dilutes it causing high concentration areas to be reduced toward the road level.

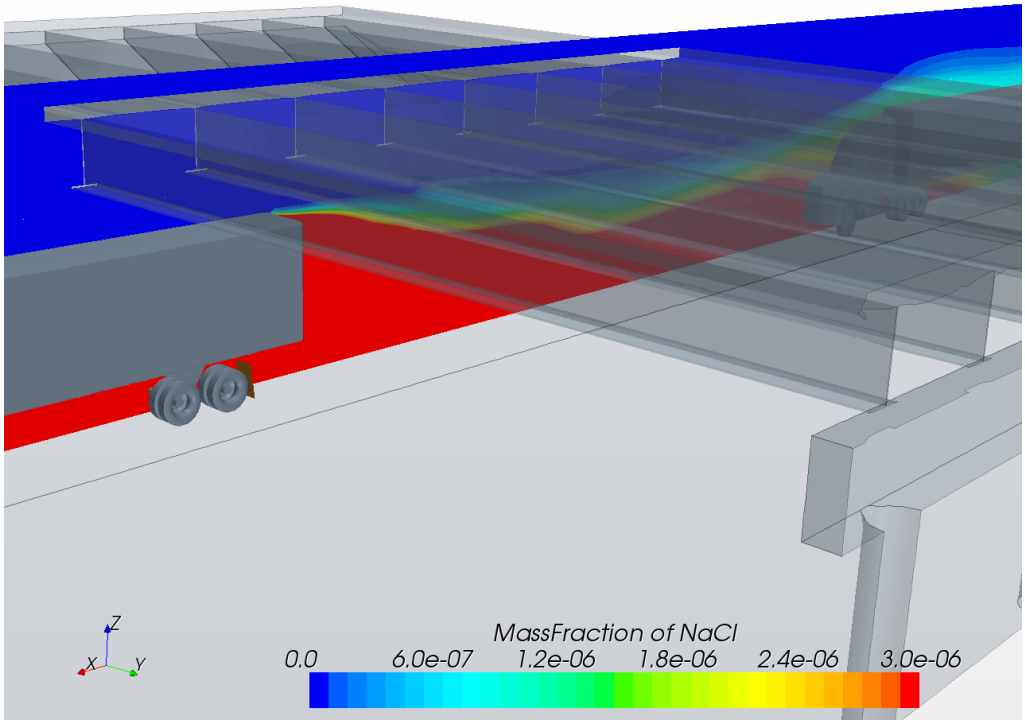

Figure 4.21: Salt aerosol plume from first truck does not reach significantly above the trailer height

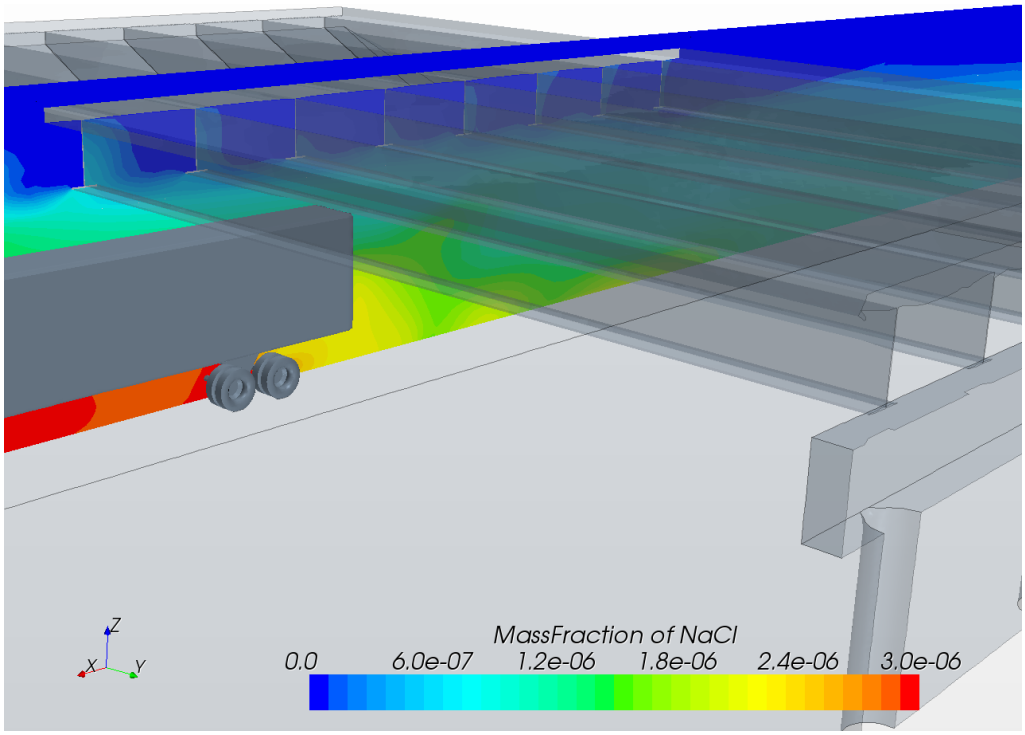

Figure 4.22: Salt aerosol in from first truck wake reaching girder level when flowing up over the second following truck and entering cavities between the girders

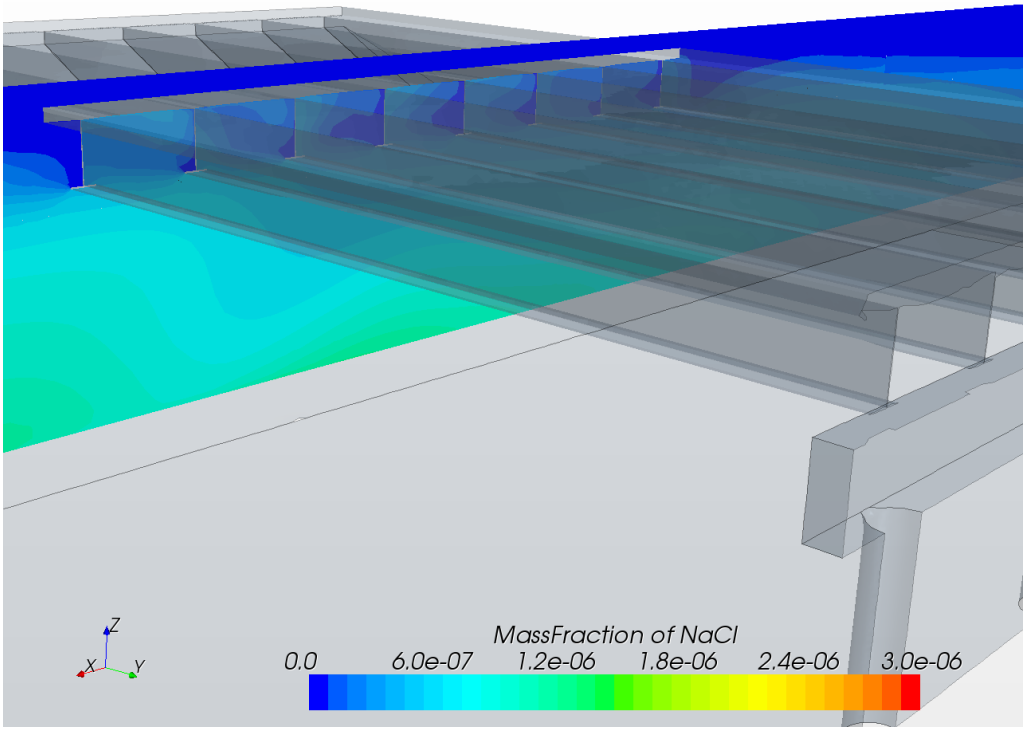

Figure 4.23: Recirculation induced in the cavities between girders by passing truck rolling the salt aerosol around to fill the cavity

The 45 degree tail wind case effectively reduced the relative velocity of the salt plume from the first truck in the direction of the second following truck. Its cross road component also contributed to diverting the plume partly out of the path of the following truck and shortened the downstream extent of the plume in the vertical plane of the truck path as shown in Figure 4.24. As a consequence, less of the plume is deflected up to girder level directly over the second truck.

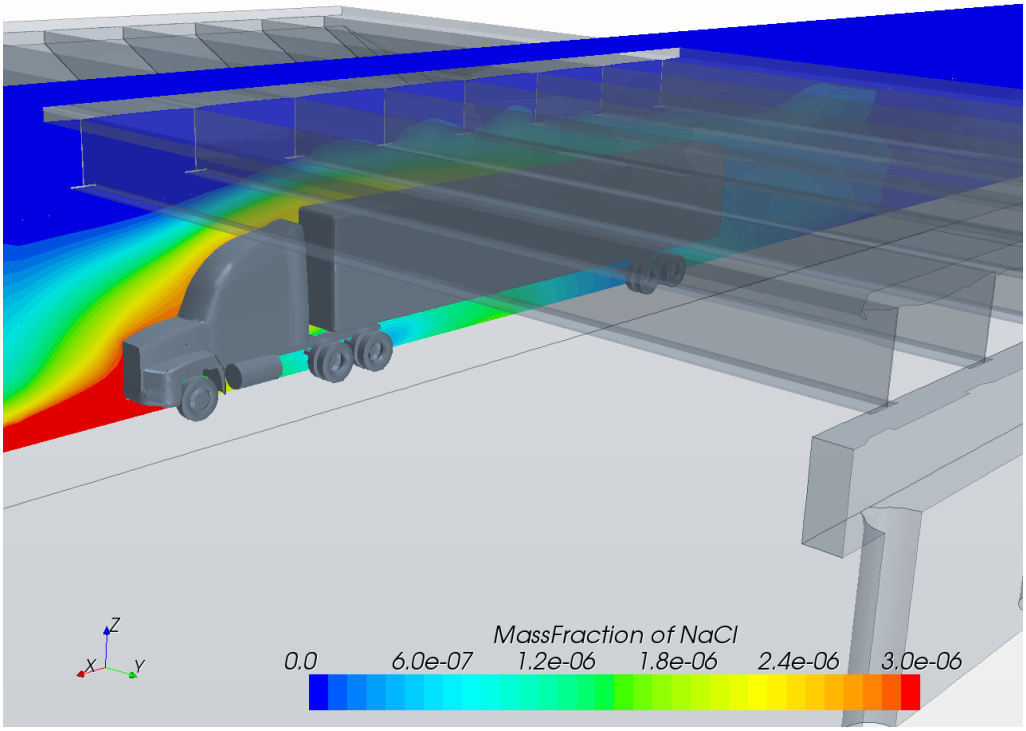

Figure 4.24: Second truck passing for case with a tail wind showing less salt aerosol from first truck reaching girder level when passing over following truck

Another view of what happens when the salt plume from the first truck is diverted up to girder level by the following truck can be visualized by color plotting salt concentrations on a horizontal plane cut through the bridge girders. This view shows the distribution of salt aerosol in a plane between the girders in relation to paths of the trucks. In the case with no wind, as shown in Figure 4.25, the region of higher salt concentration is very close to the straight line path of the trucks. The path line of the trucks is indicated by the thin black line running across the plot through the lighter blue and green salt concentration contours. The time of the plot is after both trucks have passed under the bridge.

The salt concentration plot in Figure 4.26 is for the case with a head wind at a 45 degree angle toward the bridge abutment. The wind direction entering the domain is from the upper boundary of the horizontal plane of the plot moving from right to left on diagonal until diverted by blocking objects. The time of the plot is when the following truck in under the bridge, and its outline is shown in white. As shown in the plot, one of the effects of the wind is to move the plume toward the bridge abutment away from the path line of the trucks.

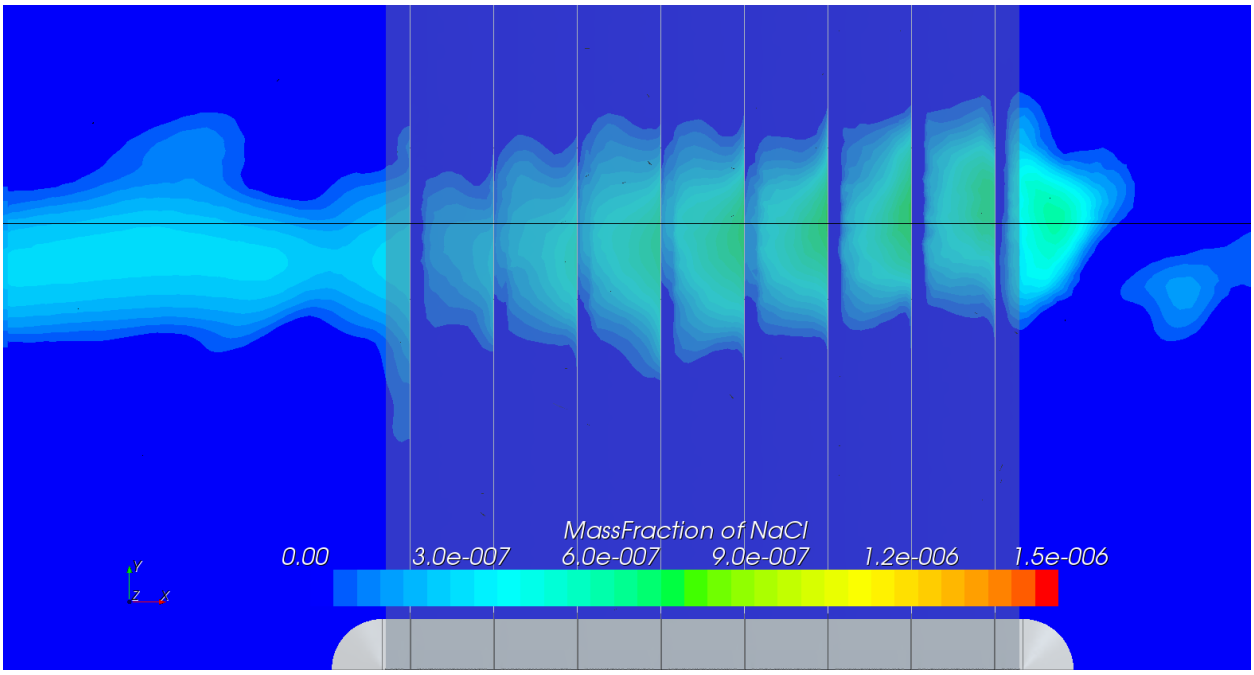

Figure 4.25: Aerosol concentration above lip of girders after second truck has past, no wind

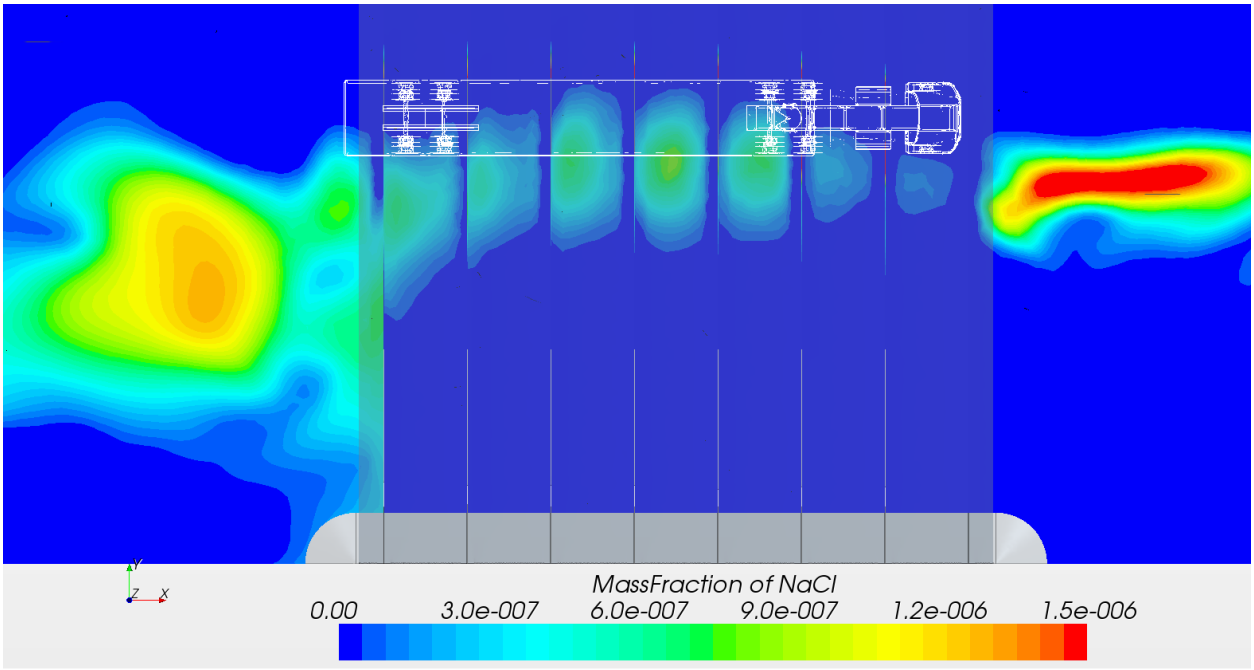

Figure 4.26: Aerosol concentration above lower girder flange with 30 mph wind from upper right

In the case with the tail wind, the wind direction was also at a 45 degree angle toward the bridge abutment next to the truck path lane. As previously noted, less of the leading truck's salt plume appears to be diverted upward into the girders by the second truck in this case, and that lower concentration is visible in Figure 4.27. However, outside of the bridge zone, enough of the salt plume is diverted up to bridge girder height to allow the wind moving diagonally from top to bottom and left to right in Figure 4.27 to stagnate the plume and create a small zone of high salt concentration at the entry corner of the

abutment and on the entry side of the first girder. This result demonstrates how wind, which may be much more variable than the steady speed and direction used in these test cases, in combination with large vehicle traffic and the geometry of the bridge structure and abutments may lead to localized spots where high relative salt concentrations are possible.

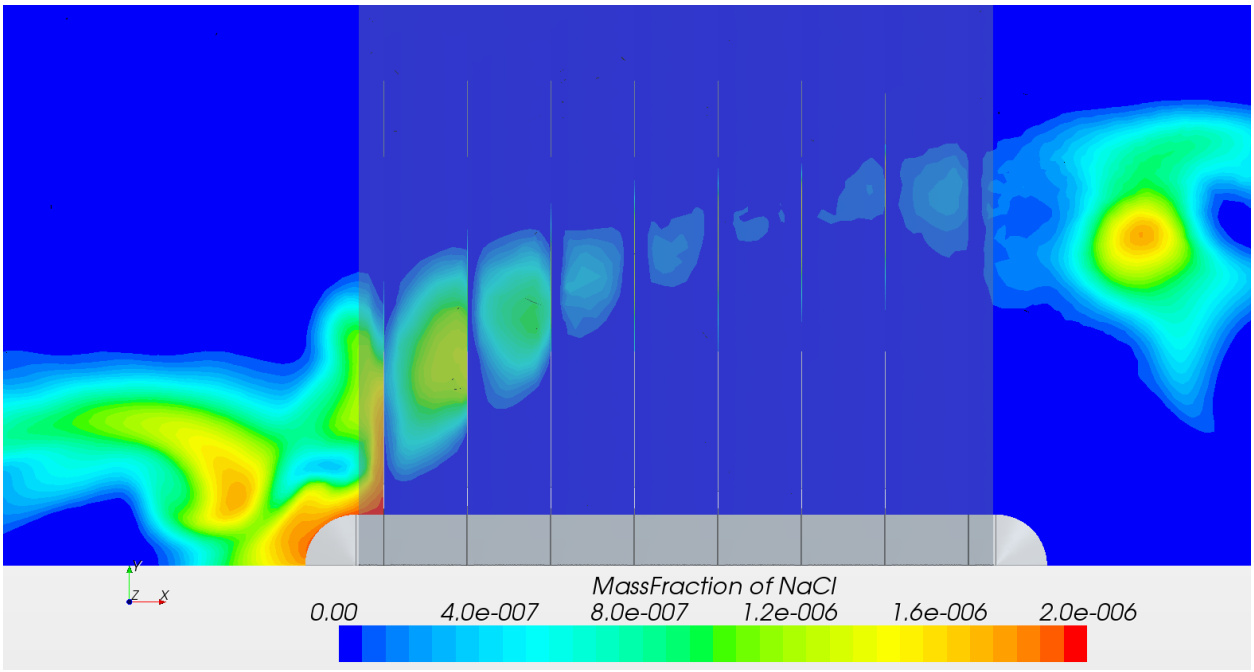

Figure 4.27: Aerosol Concentration above lower girder flange with 30 mph wind from upper left

5. Summary and Conclusions

While truck tires may throw off a lot of water, most of this impinges on walls in wheel wells, mud flaps, and structures on the underside of the truck tractor or trailer. A few study cases analyzed droplet interaction with walls in a wheel well using rebound and droplet break-up models available in the CFD software. These computations required too much computing resources and time to run for a full moving truck case interacting with bridges. Wall impingement can yield rebound and break-up, or the formation of a film on surfaces that flows under action of gravity downward and drips back onto the roadway. To emerge into the truck wake, either along the sides of the vehicle or in the rear, droplets need to be turned around blocking structures of the truck by air flowing out from wheel wells and the truck undercarriage. Smaller droplets require less air drag force, proportional to diameter squared, to turn, and the mean of the size range that emerge into the wake is on the order of 100 µm. The settling time for droplets much larger than 100 µm is seconds or less, indicating that while large droplets may end up in the splash zone along the road side and a couple of meters high on retaining and bridge abutment walls, it is unlikely that a significant number of large droplets (1 mm or greater) could be carried up to bridge girder level from below in the absence of strong updrafts or wind. The droplet size range considered for analysis in this study was therefore in the range up to 200 µm.

Study cases found that on an open flat road nearly all droplets in the wake are below the trailer mid height. However, when passing beneath the bridge, there was an observed influence of the geometry. While only a limited number of analysis runs were conducted, the following were observed, but are not to be considered firm conclusions:

1) The embankment or abutment shape does have a minor influence on the number of droplets that can migrate to the elevation of the girders, albeit a small influence compared to the other factors studied. It was found that distant geometrical obstacles along the side of the roadway (for example a wall more than 15 ft from the truck) have virtually no influence. The close sloped embankment has the next most influence, then followed by the close vertical abutment with a wing wall or a long continuous wall.
2) The next largest influence on the number of droplets migrating to the girder elevation was traveling truck trains. It was observed in the few cases studied, that a second, trailing truck would increase the number of droplets transported to the girder elevation by 3-15 times that of an equivalent simulation with just a single truck passage. That is, the first truck would suspend the droplets at about the mid-height of the truck, then the second truck would push the droplets up to the girder elevation. This would speak to the ADTT influence on the tunnel effect, though the study did not get to modeling cars with trucks, nor investigate the spacing between trucks, so a much more complete characterization of ADTT effect could not be established, only that higher ADTTs would be expected to have higher corrosion rates.

3) The proximity of the geometric barrier did have an influence. The spacing between curb side walls and the truck was varied from 4-14 ft. It was found that the number of droplets reaching the girder elevation was maximized with the simulations using a 5.5 ft. gap. Interestingly, the number of droplets decreased either side of 5.5 ft, indicating there is an optimal spacing that maximizes the effect. However, the number of droplets decreased by a factor of about 7 between a spacing of 5.5 ft to 14 ft. The concentration at 14 ft spacing had a droplet concentration very near that of an open structure (with no geometric obstacles). This would indicate that walls at a distance of about 15 ft from the truck have no influence on the number of droplets migrating to the girders.
4) Wind had the largest influence of all the variables. It was observed that winds could increase the number of droplets at the girder level by 20-120 times that of an equivalent simulation without the wind. This was true for the sloped embankment case. A similar conclusion could be drawn for the cases with a severe depressed grade approach with wind blowing across the cavity formed by the depressed grade. In the cases with a close wall and wind approaching at truck road level the quite opposite was true for high wind velocity – the wind was causing less parcels to reach the girder level because they were blown into the wall. Time was not available to run a large number of wind cases needed to better understand wind effects. The primary conclusion from the wind test cases is that wind move droplets in the size range of truck spray very easily, and therefore may play a major role in droplet transport.
5) The migration of salt laden spray does not have to be in a liquid phase; it was shown that a dry aerosol is also a viable transport mechanism. This could take place many days after a snow event, and would be subject to the same influences of ADTT, wind, and proximity of geometric obstacles.

6. Future Work and Verification

6.1 Future Work

A significant portion of the work in conducting this study involved identifying the droplet size range of interest, setting up and testing the advanced sliding mesh models for moving a truck or trucks under the bridge, determining the level of detail in truck geometry that is sufficient to capture the physics of flow past the truck and yields numerically stable results, testing droplet injection methods, etc. Now that a functioning model has been built that will converge for a variety of conditions and geometry changes, follow on studies with the model can be conducted with much less setup work. The following areas are among many that are good candidates for future study.

- Effect of clearance between bottom of the girders and the top of the truck in both calm air and wind conditions
- Effects of the width of the bridge (number of lanes)
- Effects of wind velocity with full bridge geometry modeled, in particular average and very low velocities
- Injectors of parcels for the cases with the wind located on both sides of the truck
- Effects of smaller vehicle traffic such as a car following a truck or a car following a car
- Effect of a non-aerodynamic truck cab
- Additional study of dry aerosol size particulate erosion from road surface and transport
- Other minor geometry effects such as girder spacing and girder depth
- Modeling of one or two real bridges that have known issues with accelerated corrosion
- Verification of trends observed in CFD simulation with field measurements

6.2 Model Verification

This study relied on the use of well benchmarked commercial CFD software that is routinely used by a variety of industries in the analysis of flow in and around vehicles and other obstacles in the design of their products to obtain qualitatively accurate results. There is limited data on the rate at which tires pick up and shed water spray from wet road surfaces and this rate is known to vary significantly with tire and tread design. Much of the tire spray ends up on surfaces in wheel wells and surfaces under truck trailers. There is also very limited data on how much water thrown off by tires makes into a truck wake

after undergoing the complex droplet surface collisions, rebounds, breakup, and eventual transport by air exiting the wheel wells and underside of the vehicle into the wake. Under these circumstances, the important relations determined in the study were the relative importance of droplet transport mechanisms and geometry effects on the fraction of droplets reaching bridge girder level for cases that have the same amount of droplet spray mass leaving the tires in truck passing under bridge events.

The k-epsilon turbulence model was used in the analysis because eddy resolving techniques such as large eddy simulation (LES) are about an order of magnitude more expensive to run and also require considerably more time to complete.

Field measurements that could verify that the accuracy of the results using the k-epsilon or other variants of two equation turbulence models are adequate for engineering application in improving evaluation of weathering steel bridge corrosion risk due to salt spray from trucks and other traffic after winter road salting would be beneficial.

Optical measurements of spray distribution patterns for several of the modeled cases could provide an additional level of confidence in the CFD model results. Such measurements would need to include measurement of wind speeds in the vicinity of the bridge, the complete bridge geometry, the terrain elevations around the bridge, and the geometry of any large obstacles near the bridge such as trees, signs, etc.

7. Bibliography

AISI, 1982. *AISI Phase 1 Report, Performance of Weathering Steel in Highway Bridges,* Washington, D.C.: American Iron and Steel Institute.

Bai, C., Rusche, H. & A.D., G., 2002. Modeling of Gasoline Spray Impingment. *Technology and Medicine,* 12(1-3).

Brent T. Mussato, e. a., 2007. *NCHRP Report 577, Guidelines for the Selection of Snow and Ice Control Materials to Mitigate Environmental Impacts,* Washington, D.C.: Transportation Research Board.

CD-adapco, 2012. *User Guide STAR-CCM+ Version 7.04.011,* s.l.: s.n.

FHWA, 1989. *Uncoated Weathering Steel in Structures, TA 5140.22,* s.l.: U.S. Department of Transportation.

Gertler, A. et al., 2006. A case study of the impact of Winter road sand/salt and street sweeping on road dust re-entrainment. *Atmospheric Environment,* pp. 5976-5985.

McCallen, R. et al., 2005. *DOE Project on Heavy Vehicle Aerodynamic Drag FY 2005 Annual Report,* s.l.: Lawrence Livermore National Laboratory.

McCallen, R. et al., 2007. *DOE Project on Heavy Vehicle Aerodynamic Drag,* s.l.: Lawrence Livermore National Laboratory.

McDad, B., Laffrey, D., Dammann, M. & Medlock, R., 2000. *Performance of Weathering Steel in TxDOT Bridges,* s.l.: Texas Department of Transportation.

National Climatic Data Center , 2011. *Comparative Climate Data,* Asheville, North Carolina: National Oceanic and Atmospheric Administration, National Climatic Data Center.

Paschkewitz, J., 2006. *A comparison of dispersion calculations in bluff body wakes using LES and unsteady RANS,* Livermore, CA: Lawrence Livermore National Laboratory.

Paschkewitz, J., 2006. *A computational study of tandem dual wheel areodyanmics and the effect of fenders and fairings on spray dispersion,* Livermore, CA: Lawrence Livermore National Laboratory.

Paschkewitz, J., 2006. *Simulation of spray dispersion in a simplified heavy wehicle wake,* Livermore, CA: Lawrence Livermore National Laboratory.

Radovich, C., 2010. Los Angeles(CA): Univeristy of Southern California.

Schmitt, R., 1989. *Selection of Weathering Steel for a Given Location, FHWA-TS-89-016,* s.l.: Federal Highway Administration.

Stokols, P., 2013. *National Weather Service Instruction 10-513 WFO Winter Weather Products Specification,* Washington, D.C.: National Oceanic & Atmospheric Administration.

Williams, A. L. & Stensland, G. J., 2004. *Atmospheric Emission and Deposition of Deicing Salt Applied to*

Highways in the Chicago Area. Sewickley, PA, Air & Waste Management Association.

Williams, A. L. & Stensland, G. J., 2006. *Atmospheric Dispersion Study of Deicing Salt Applied to Roads,* Springfield, Illinois: Illinois Department of Transportation.

Williams, A. L., Stensland, G. J., Peters, C. R. & Osborne, J., 2000. *Atmospheric Dispersion Study of Deicing Salt Applied to Roads: First Progress Report,* Champaign, Illinois: Illinois Department of Natural Resources.

8. Acknowledgements

The funding for this project came from the 2005 SAFETEA-LU Transportation Bill under Title V, Section 5202C, “High Performing Steel Bridge Research”, through Interagency Agreement Number DTFH61-10-X-30040 between DOT and DOE, and the work was performed under DOE’s contract with UChicago Argonne, LLC, Contract No. DE-AC02-06-CH11357. The authors would like to thank our FHWA sponsors, Dr. Justin Ocel Structural Steel Research Program Manager and Dr. Kornel Kerenyi Hydraulics Research Program and Laboratory Manager at the FHWA Turner-Fairbank Highway Research Center. We thank Dr. Ocel for much appreciated guidance during the project and review and for helpful commentary in preparing this report. The authors also wish to thank Dr. Brian Kozy, FHWA Office of Bridge Technology, for his review of the draft report and helpful comments.

9. Appendix A. Histograms from simulations at their final stage

The histograms in this appendix show the droplet parcel height distribution in the space under the bridge. The counts were taken at 8 seconds into the simulation. At this time the truck or both trucks, if two trucks were included in the test have passed under the bridge and left the domain. The first or only truck exits from under the bridge at approximately 5 seconds. The additional 3 seconds allow time for the wake flow to transport most of the droplets to their peak height that results from the truck passing event. The bottom of the girders is at 5.5 m. Droplet parcels are considered to be at girder level when they are at a height of 5.5 m or greater. The histograms show parcel counts between 5 and 5.5 m in orange and parcel counts above the bottom of the girders in red.

Parcel counts above the bottom flange include parcels on the girders, bottom of the bridge deck and in the air between the girders. The turbulence model with the Lagrangian parcel tracking was judged to insufficient to obtain an accurate count to parcels that hit the girders or underside of the bridge deck. The primary recognized mechanisms for small particle or droplet deposition on surfaces are Brownian diffusion, interception, impaction, and sedimentation. The software models sedimentation, which is gravitational settling and impaction, which is a collision with the surface when particle inertia is too large for it to follow the flow approaching a surface that turns to become parallel with the surface. It does not model Brownian diffusion or impaction. Such models could be added with a substantial amount of effort, and would then require experimental verification. In the absence of complete surface deposition models and computer resources to compute the long time history of particles suspended in the air between girders to determine the eventual total deposition on surfaces under the bridge, droplet parcels suspended in the air between girders are assumed to contribute a substantial corrosion risk.

Note that the quantities of interest are the tails of the distributions on the right side, which in most cases contain a small fraction of the total number of droplet parcels suspended in the air under the bridge. The scale of the droplet count frequency on the ordinate varies from plot to provide a better view of the shape of the distribution. The shapes of the distributions also carry some information of interest. The peaks of the distributions vary in their positions for various geometries and conditions. When the distribution has higher counts near the girder level other events, such as wind gusts not modeled in this study, could move more of these near girder suspended droplets to girder levels.

A number of histograms have spikes at the level of the lower flange of the girders and at the level of the underside of the bridge deck, which is at 7 m. These spikes primarily occur in cases with wind and reflect the action of wind blowing a relatively large number of droplet parcels onto the surfaces through the impaction mechanism of deposition. Some cases also show counts above the bridge deck level that primarily occur when wind carries droplets up and over the bridge.

9.1 Histograms from simulations with one truck, open boundaries

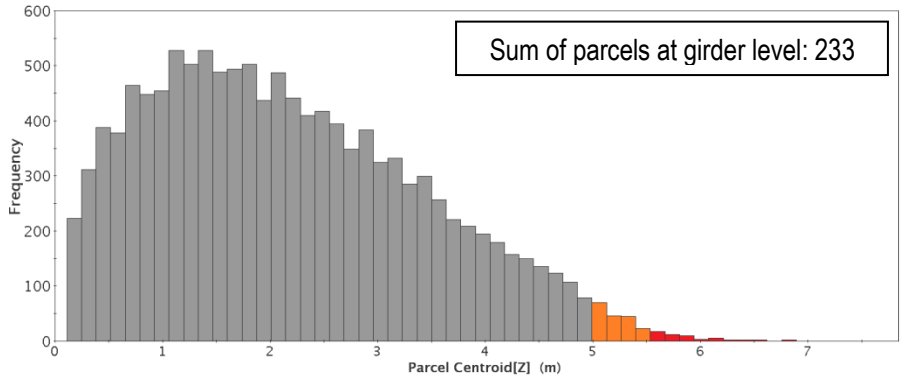

Figure A.1: Parcel droplet distribution; case with one truck, open boundaries, no wind, particle size 25 µm

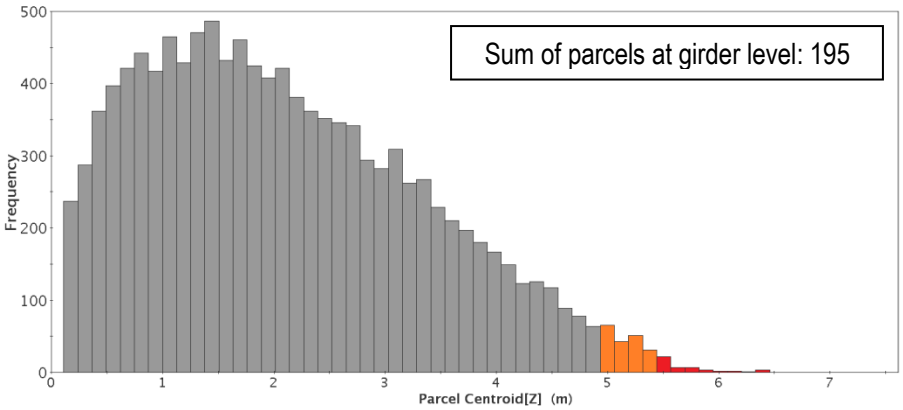

Figure A.2: Parcel droplet distribution; case with one truck, open boundaries, no wind, particle size 50 µm

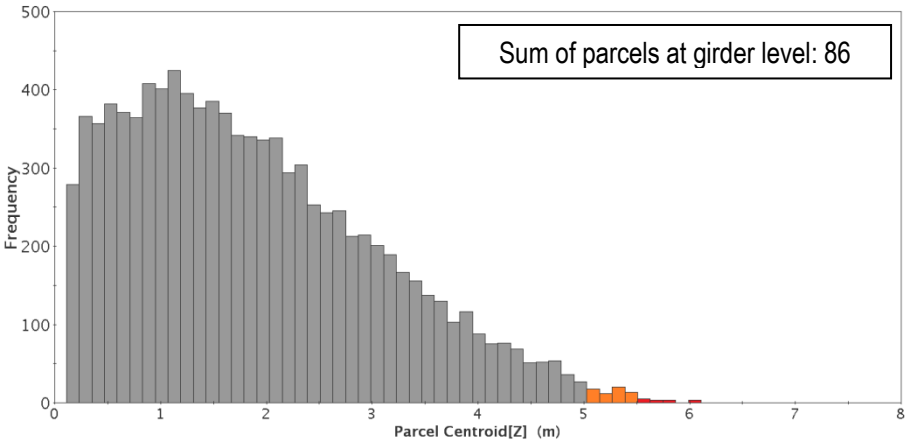

Figure A.3: Parcel droplet distribution; case with one truck, open boundaries, no wind, particle size 100 µm

9.2 Histograms from simulations with one truck, wall boundary

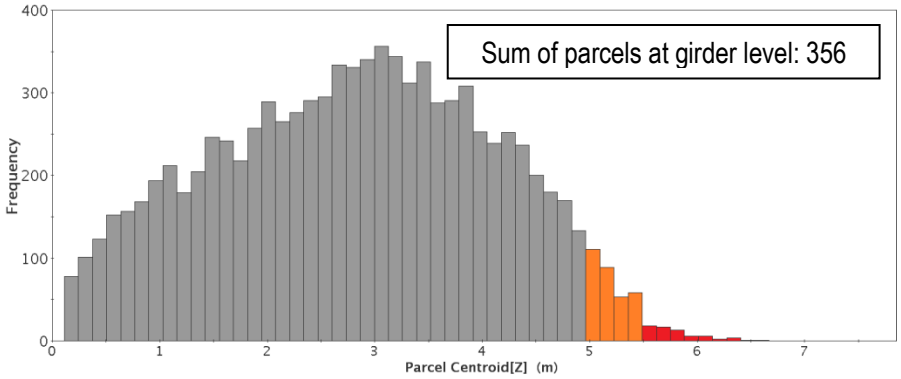

Figure A.4: Parcel droplet distribution; case with one truck, wall boundary at 4 ft, no wind, particle size 25 µm

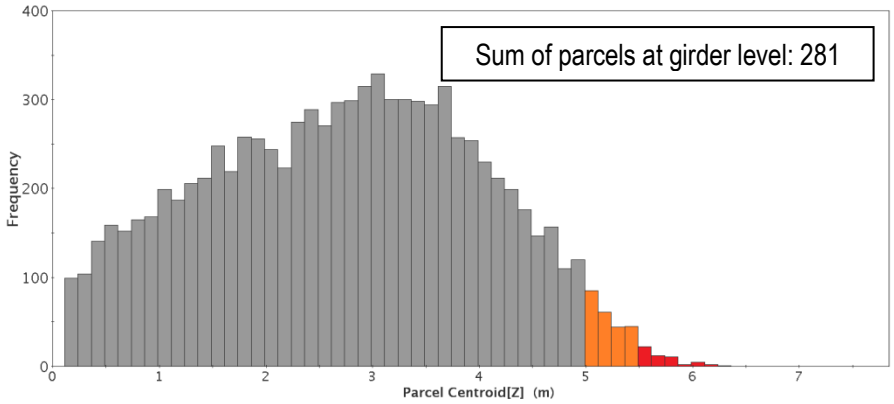

Figure A.5: Parcel droplet distribution; case with one truck, wall boundary at 4 ft, no wind, particle size 50 µm

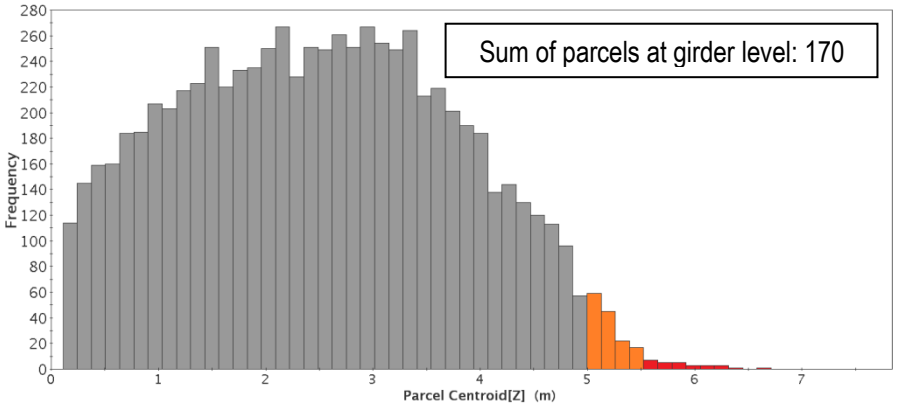

Figure A.6: Parcel droplet distribution; case with one truck, wall boundary at 4 ft, no wind, particle size 100 µm

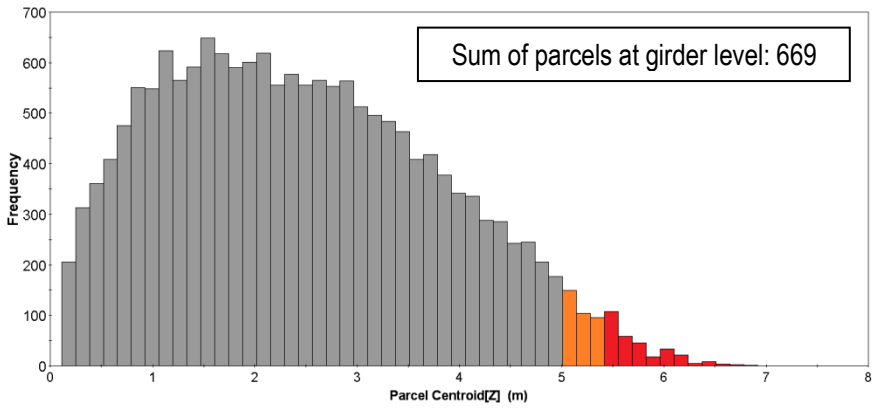

Figure A.7: Parcel droplet distribution; case with one truck, wall boundary at 5.5 ft, no wind, particle size 50 µm

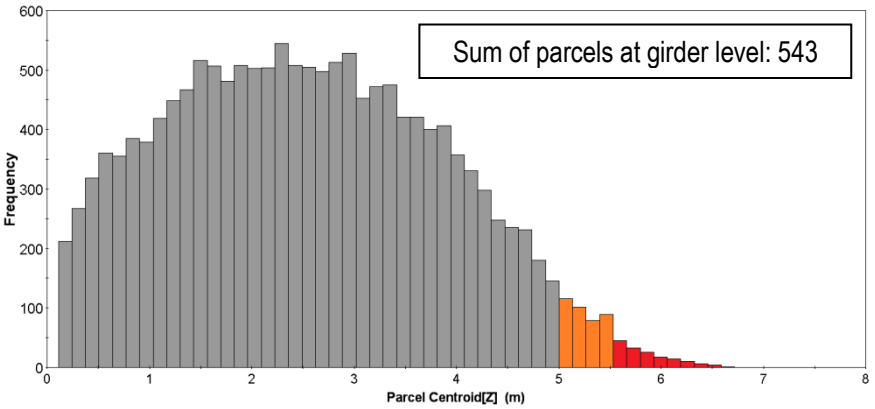

Figure A.8: Parcel droplet distribution; case with one truck, wall boundary at 9 ft, no wind, particle size 50 µm

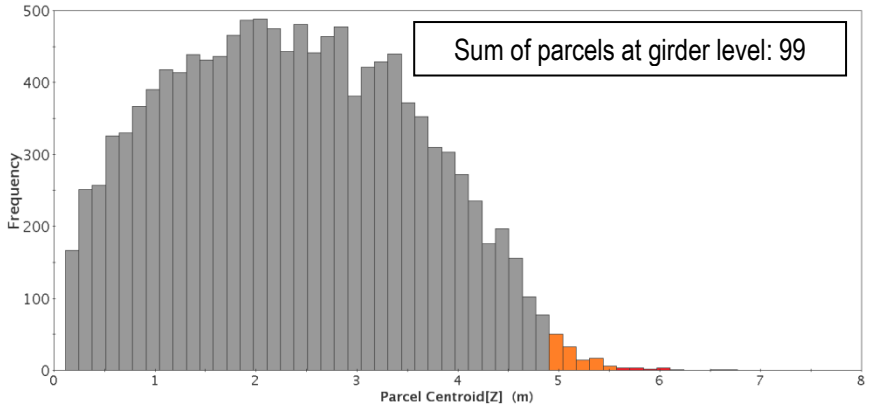

Figure A.9: Parcel droplet distribution; case with one truck, wall boundary at 14 ft, no wind, particle size 50 µm

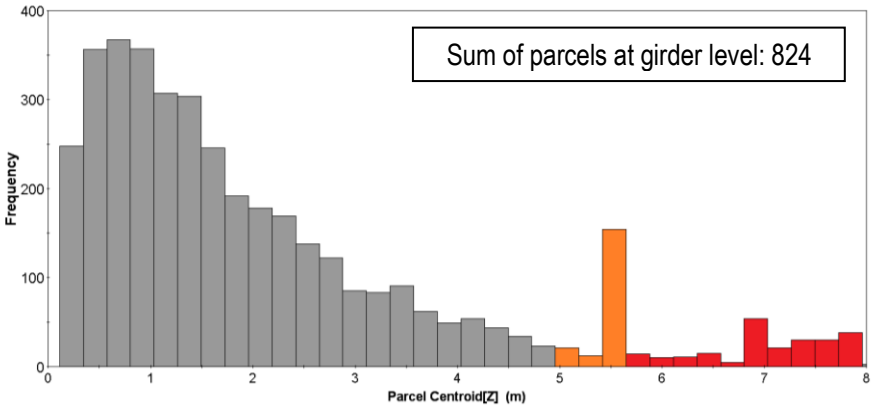

Figure A.10: Parcel droplet distribution; case with one truck, wall boundary at 5.5 ft, left tail 10 mph wind, particle size 50 µm

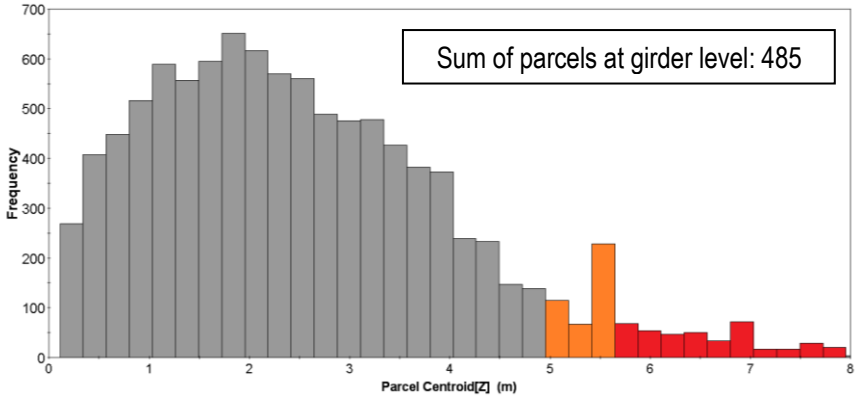

Figure A.11: Parcel droplet distribution; case with one truck, wall boundary at 5.5 ft, left tail 30 mph wind, particle size 50 µm

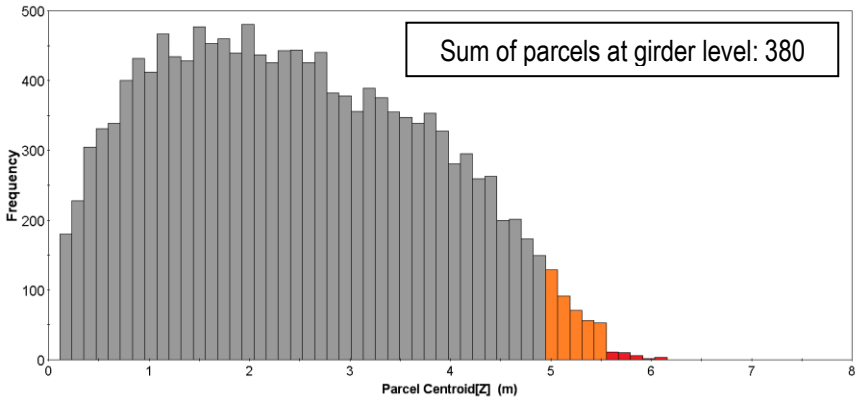

Figure A.12: Parcel droplet distribution; case with one truck, continuous abutment at 5.5 ft, no wind, particle size 50 µm

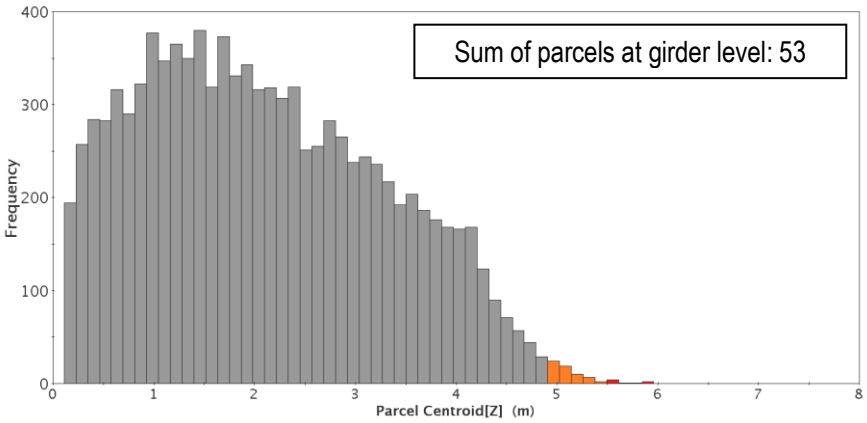

Figure A.13: Parcel droplet distribution; case with one truck, continuous abutment at 14 ft, no wind, particle size 50 µm

9.3 Histograms from simulations with one truck, sloped embankment

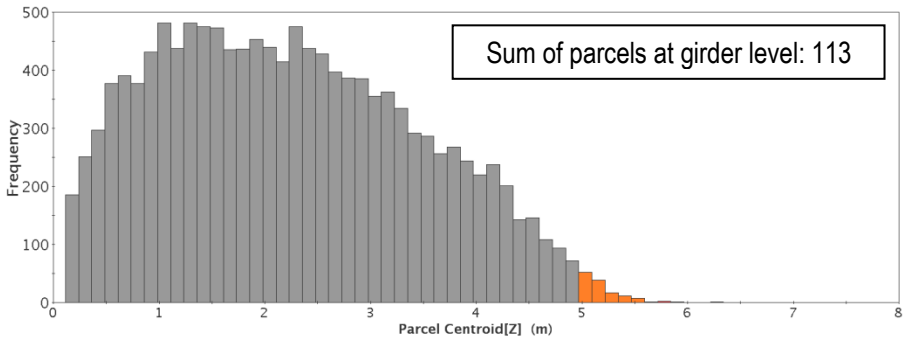

Figure A.14: Parcel droplet distribution; case with one truck, sloped embankment, no wind, particle size 25 µm

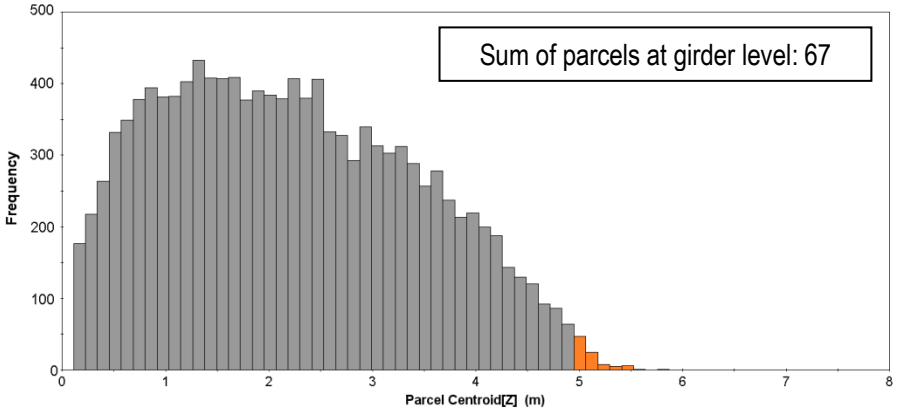

Figure A.15: Parcel droplet distribution; case with one truck, sloped embankment, no wind, particle size 50 µm

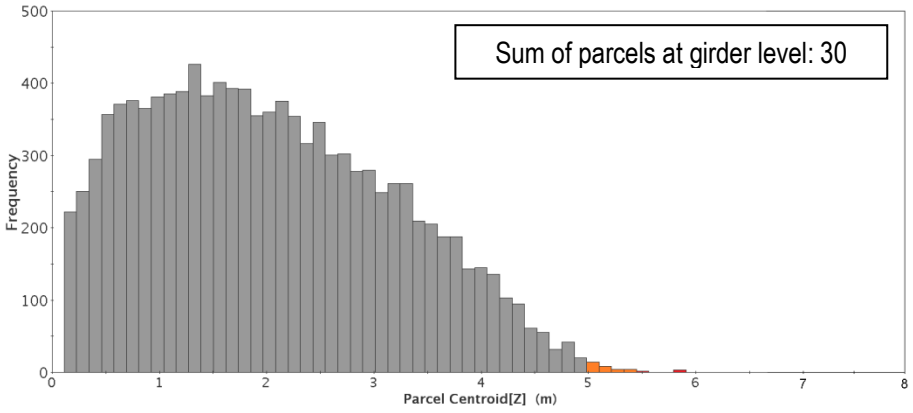

Figure A.16: Parcel droplet distribution; case with one truck, sloped embankment, no wind, particle size 100 µm

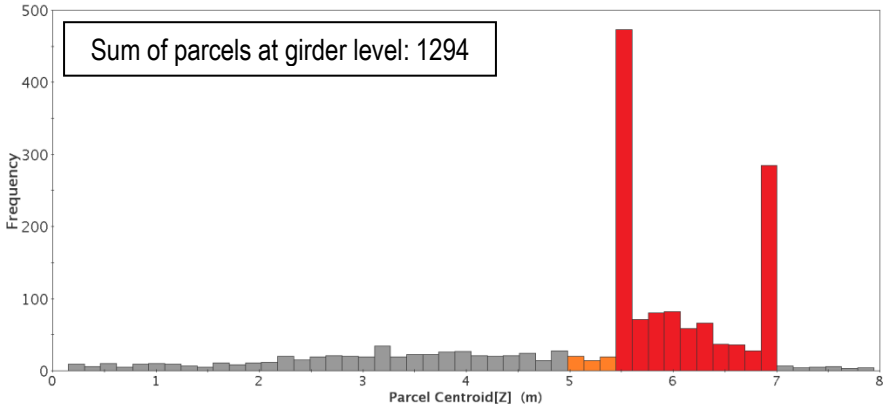

Figure A.17: Parcel droplet distribution; case with one truck, sloped embankment, 30 mph right tail wind, particle size 50 µm

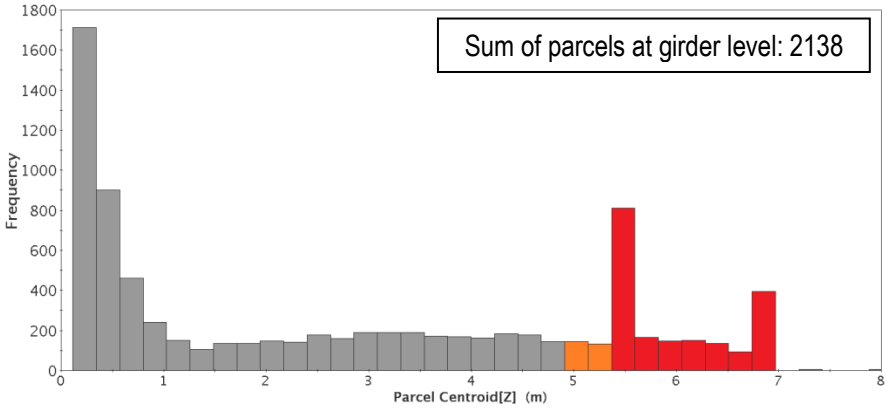

Figure A.18: Parcel droplet distribution; case with one truck, sloped embankment, 30 mph left head wind, particle size 50 µm

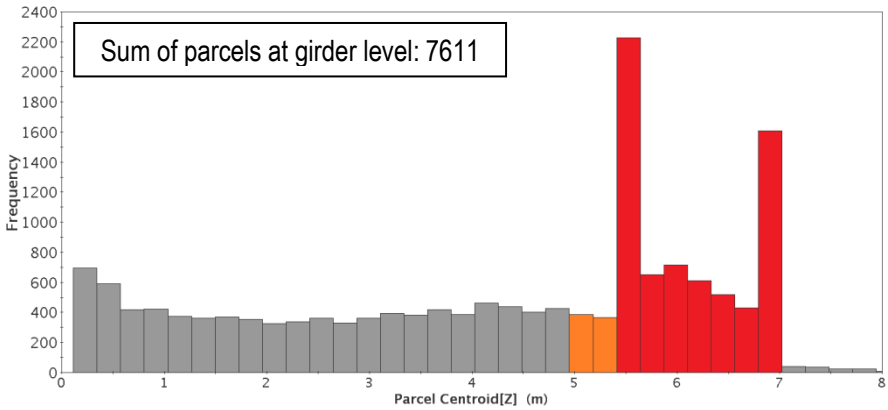

Figure A.19: Parcel droplet distribution; case with one truck, sloped embankment, 30 mph right head wind, particle size 50 µm

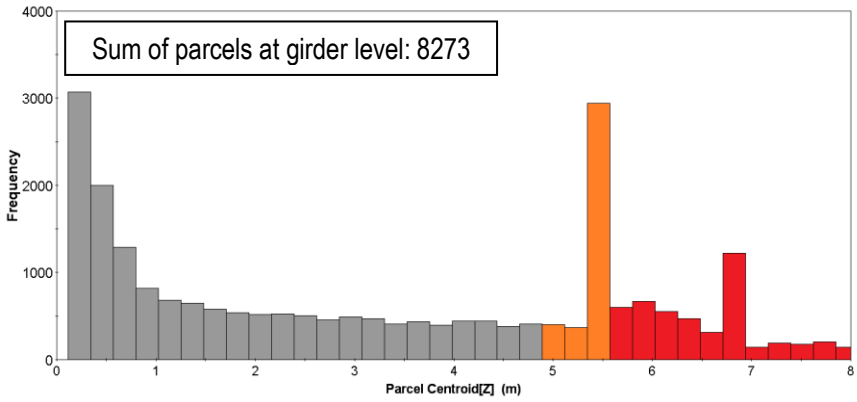

Figure A.20: Parcel droplet distribution; case with one truck, sloped embankment, 30 mph left tail wind, particle size 50 µm

9.4 Histograms from simulations with one truck, depressed grade boundary

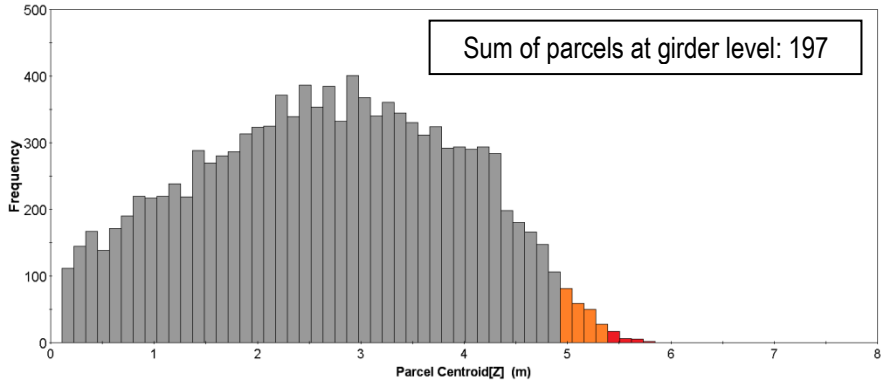

Figure A.21: Parcel droplet distribution; case with one truck, depressed grade boundary at 5.5 ft, no wind, particle size 50 µm

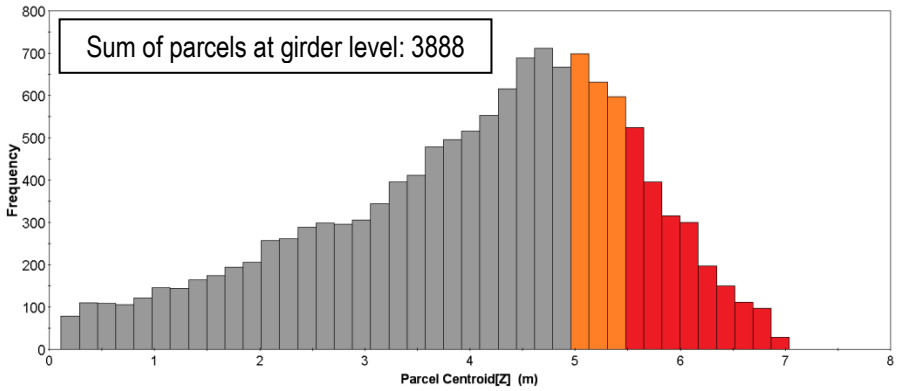

Figure A.22: Parcel droplet distribution; case with one truck, depressed grade at 5.5 ft, wind 10 mph head right, particle size 50 µm

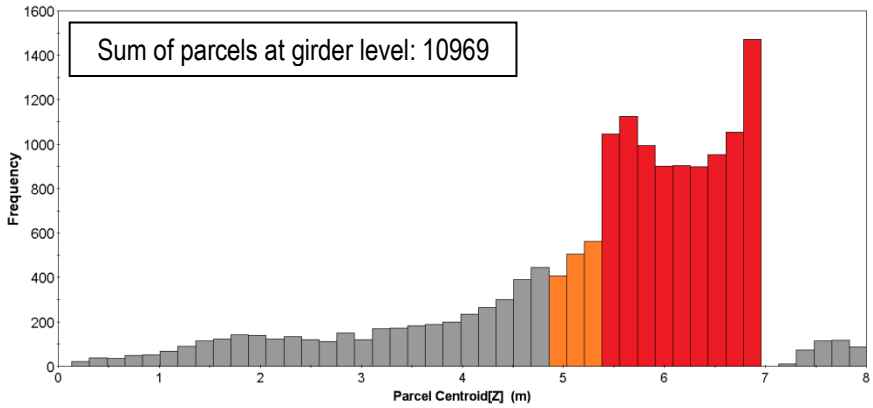

Figure A.23: Parcel droplet distribution; case with one truck, depressed grade at 5.5 ft, wind 30 mph head right, particle size 50 µm

9.5 Histograms from simulations with two trucks, open boundaries

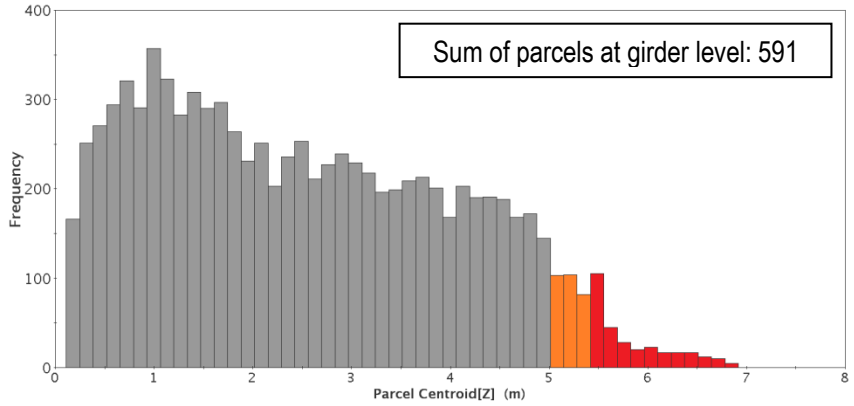

Figure A.24: Parcel droplet distribution; case with two trucks, open boundaries, no wind, particle size 25 µm

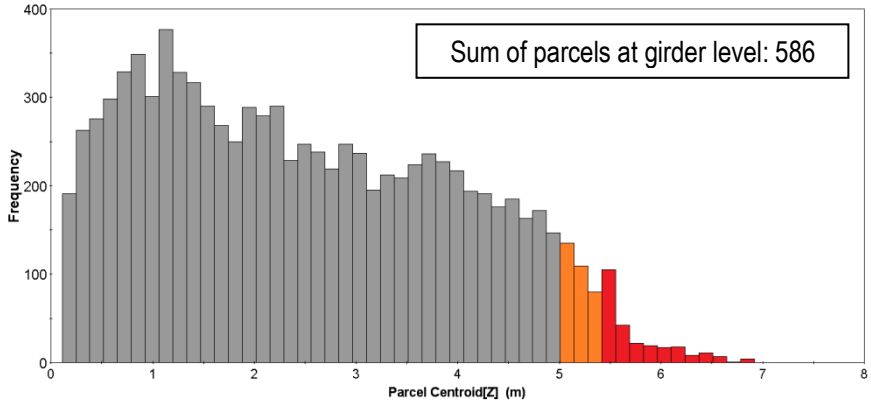

Figure A.25: Parcel droplet distribution; case with two trucks, open boundaries, no wind, particle size 50 µm

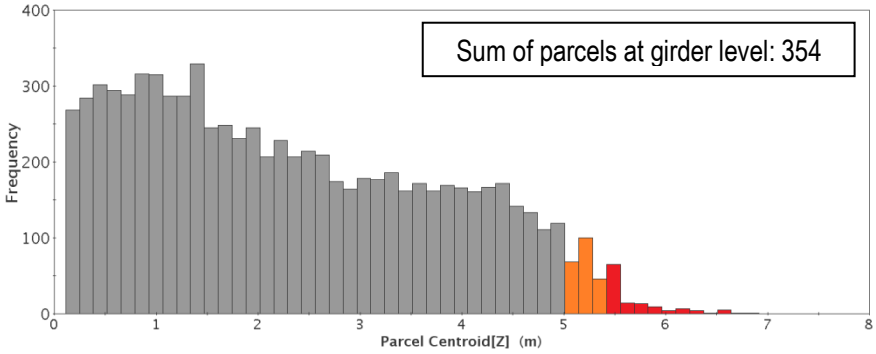

Figure A.26: Parcel droplet distribution; case with two trucks, open boundaries, no wind, particle size 100 µm

9.6 Histograms from simulations with two trucks, sloped embankment

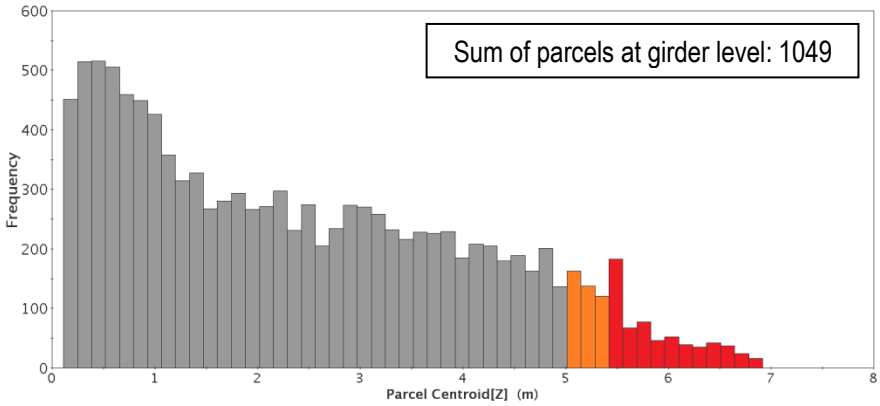

Figure A.27: Parcel droplet distribution; case with two trucks, sloped embankment, no wind, particle size 25 µm

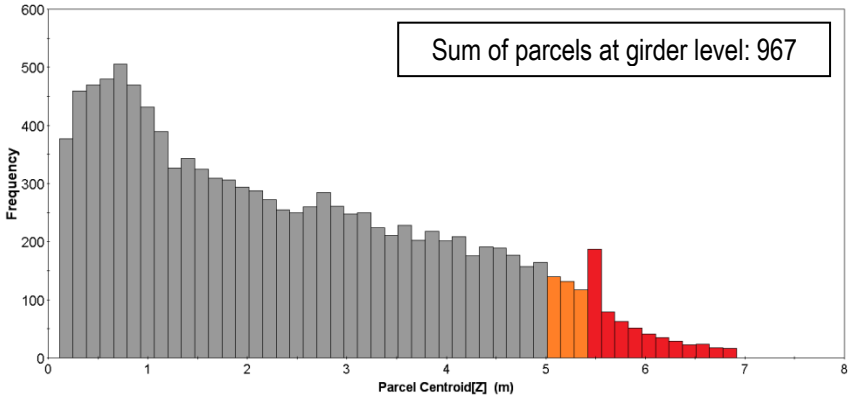

Figure A.28: Parcel droplet distribution; case with two trucks, sloped embankment, no wind, particle size 50 µm

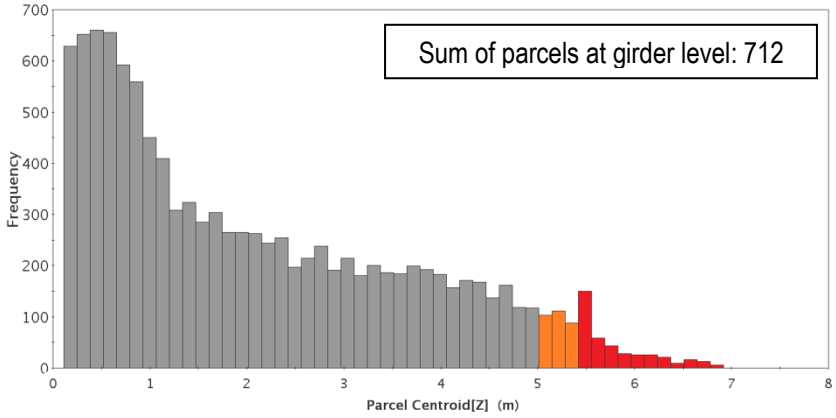

Figure A.29: Parcel droplet distribution; case with two trucks, sloped embankment, no wind, particle size 100 µm

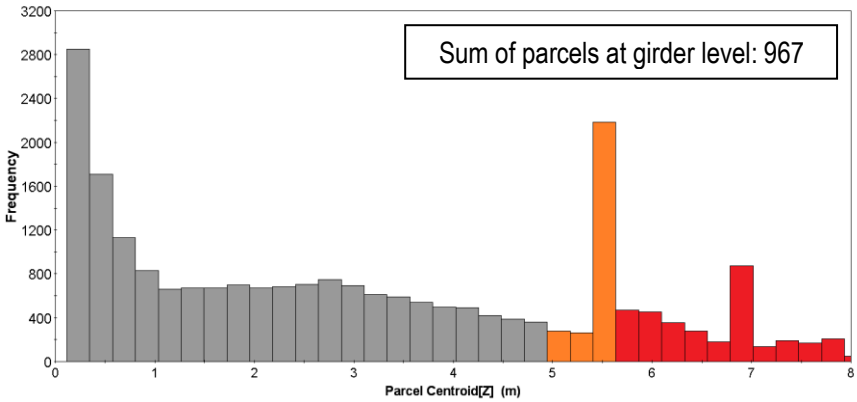

Figure A.30: Parcel droplet distribution; case with two trucks, sloped embankment, tail left 30 mph wind, particle size 50 µm

9.7 Histograms from simulations with two trucks, wall boundary

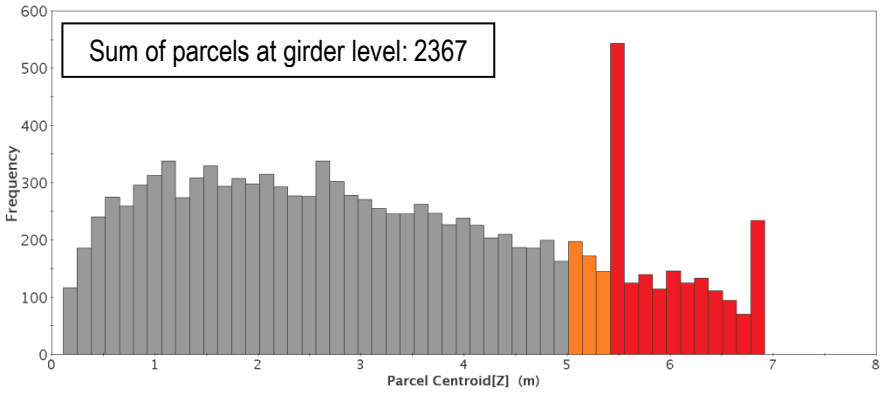

Figure A.31: Parcel droplet distribution; case with two trucks, wall boundary at 5.5 ft, no wind, particle size 25 µm

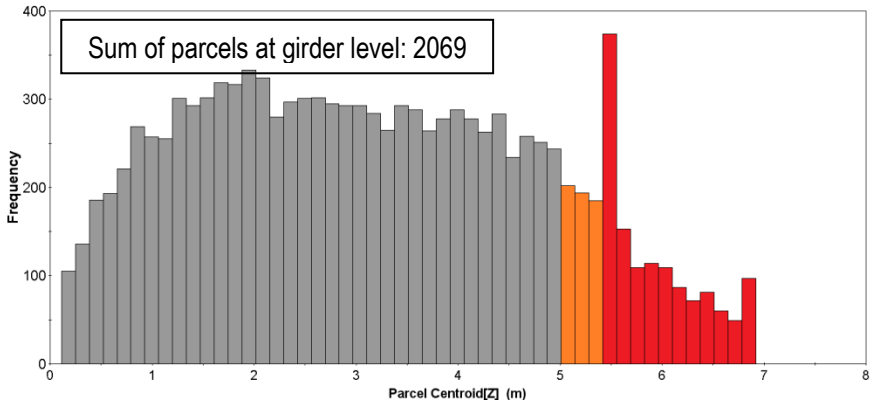

Figure A.32: Parcel droplet distribution; case with two trucks, wall boundary at 5.5 ft, no wind, particle size 50 µm

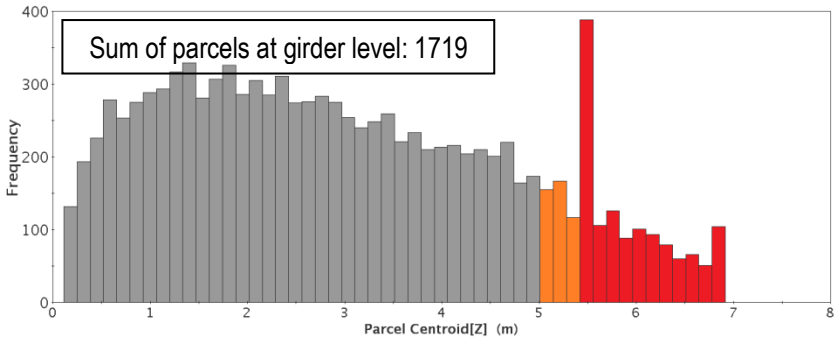

Figure A.33: Parcel droplet distribution; case with two trucks, wall boundary at 5.5 ft, no wind, particle size 100 µm

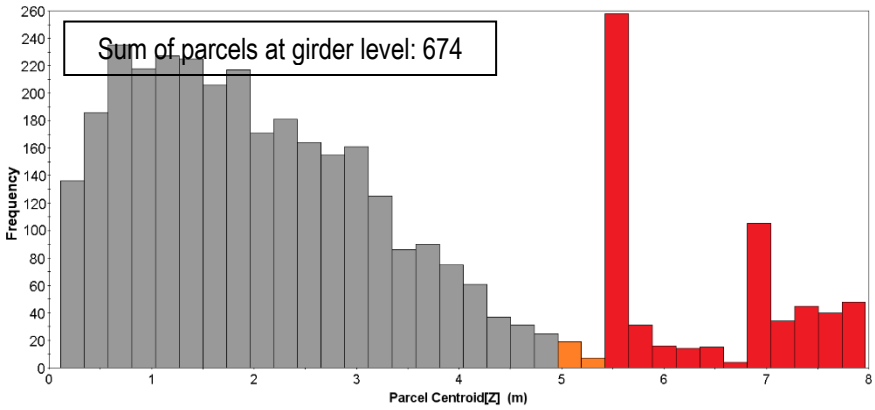

Figure A.34: Parcel droplet distribution; case with two trucks, wall boundary at 5.5 ft, left tail 30 mph wind, particle size 50 µm

10. Appendix B. Snapshots from simulations

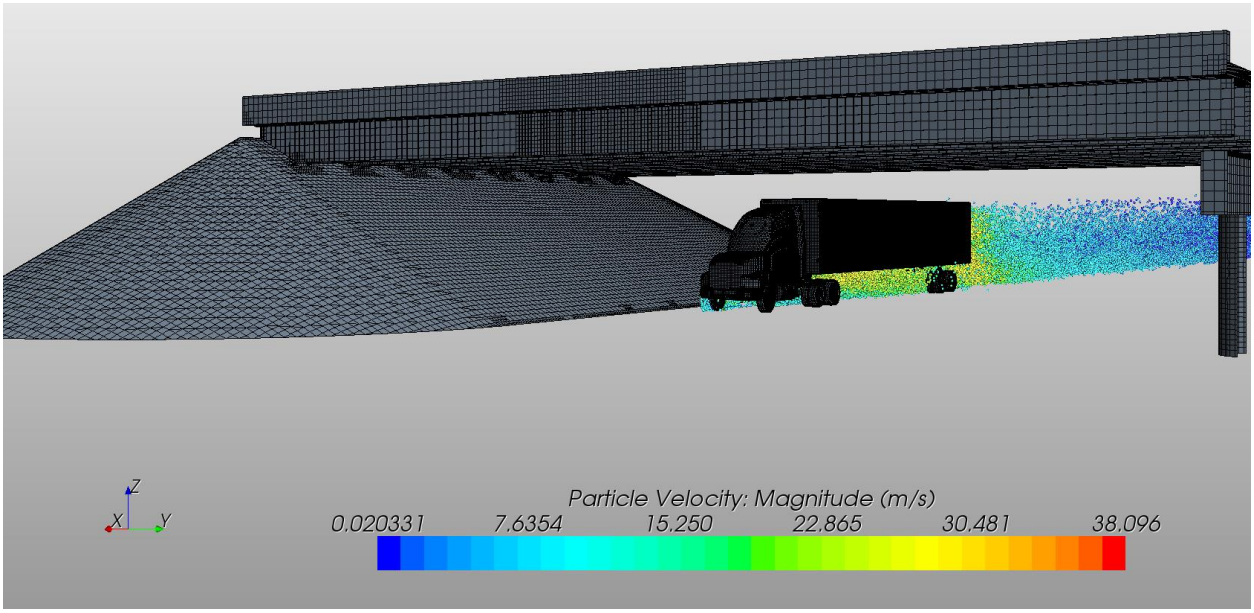

Figure B.1: Snapshot from simulation; with one truck, sloped embankment, no wind, particle size 50 µm, intermediate state 1

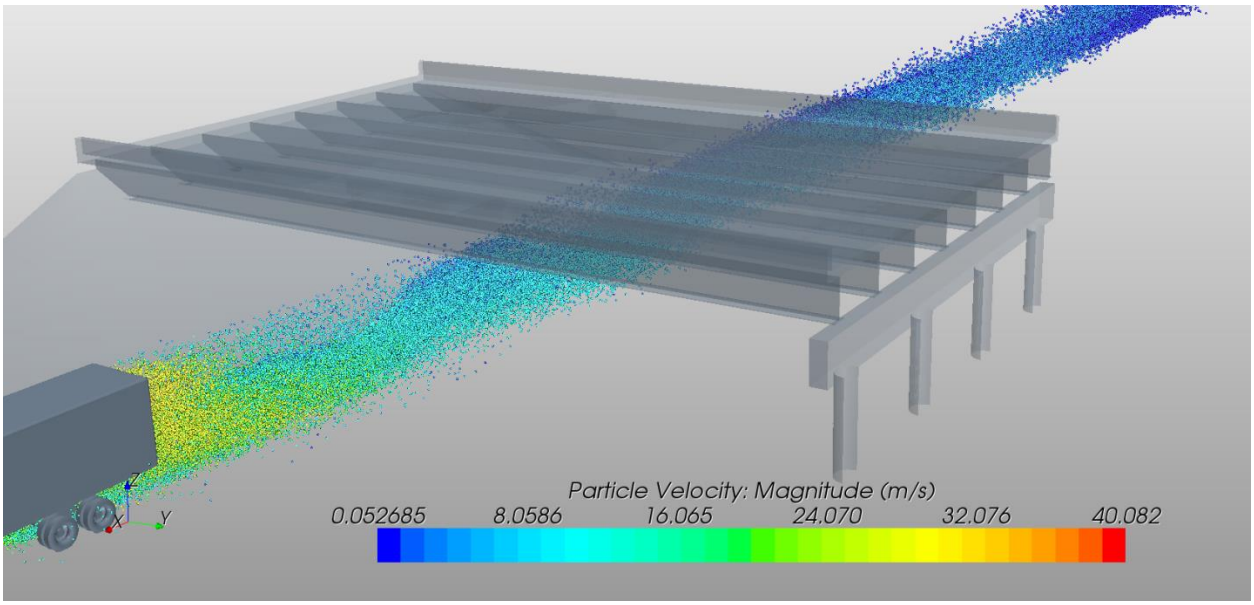

Figure B.2: Snapshot from simulation; with one truck, sloped embankment, no wind, particle size 50 µm, intermediate state 2

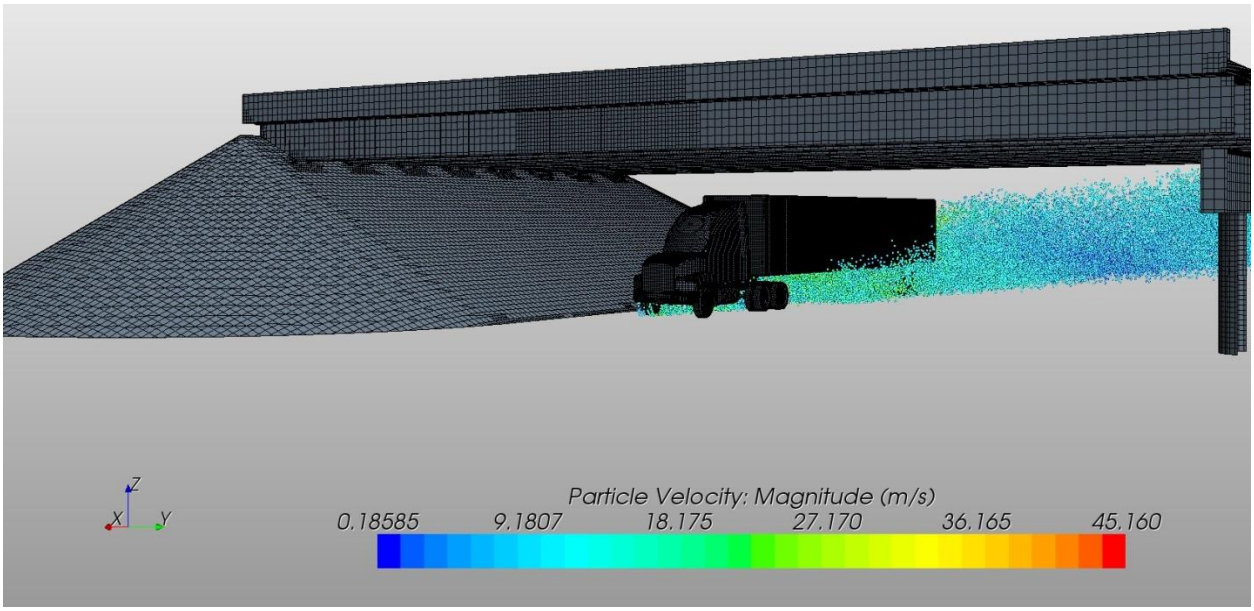

Figure B.3: Snapshot from simulation; with one truck, sloped embankment, right head wind, particle size 50 µm, intermediate state 1

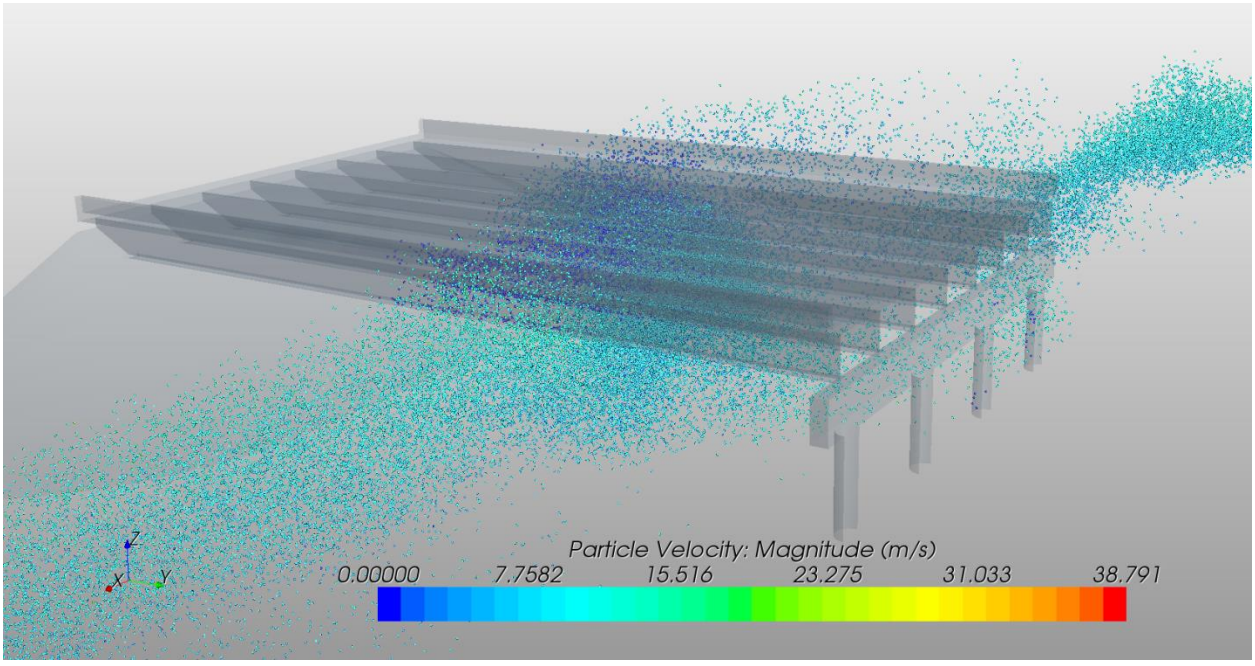

Figure B.4: Snapshot from simulation; with one truck, sloped embankment, right head wind, particle size 50 µm, intermediate state 2

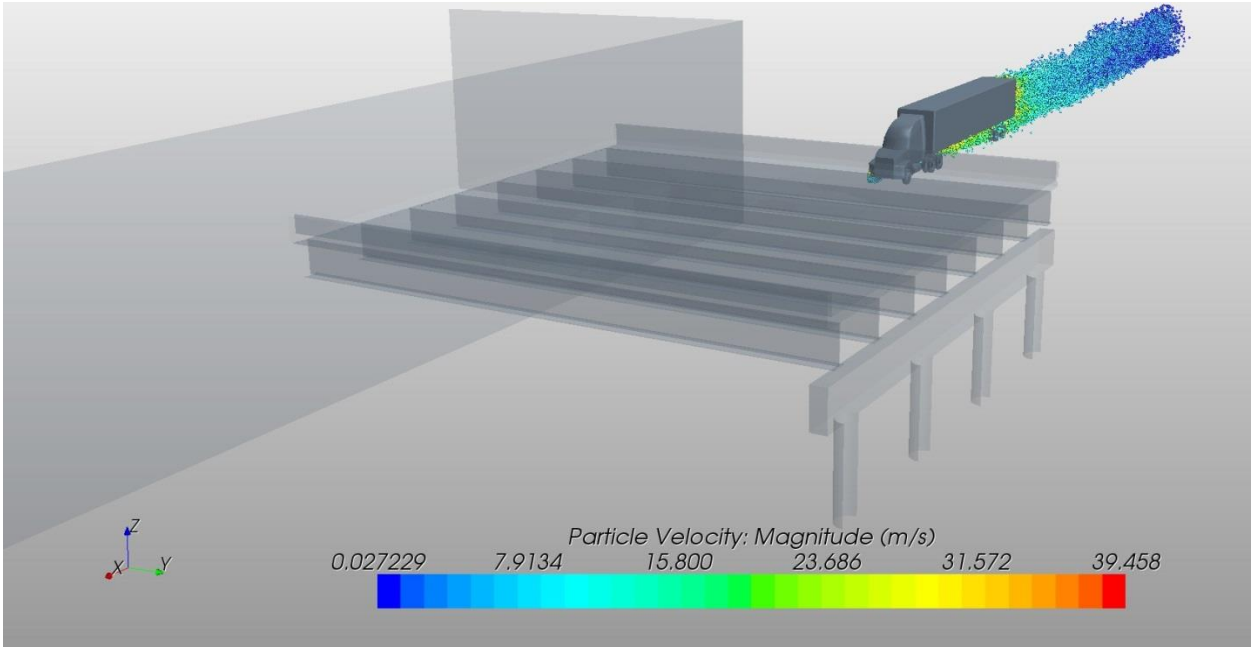

Figure B.5: Snapshot from simulation; with one truck, close vertical wall, no wind, particle size 50 µm, intermediate state 1

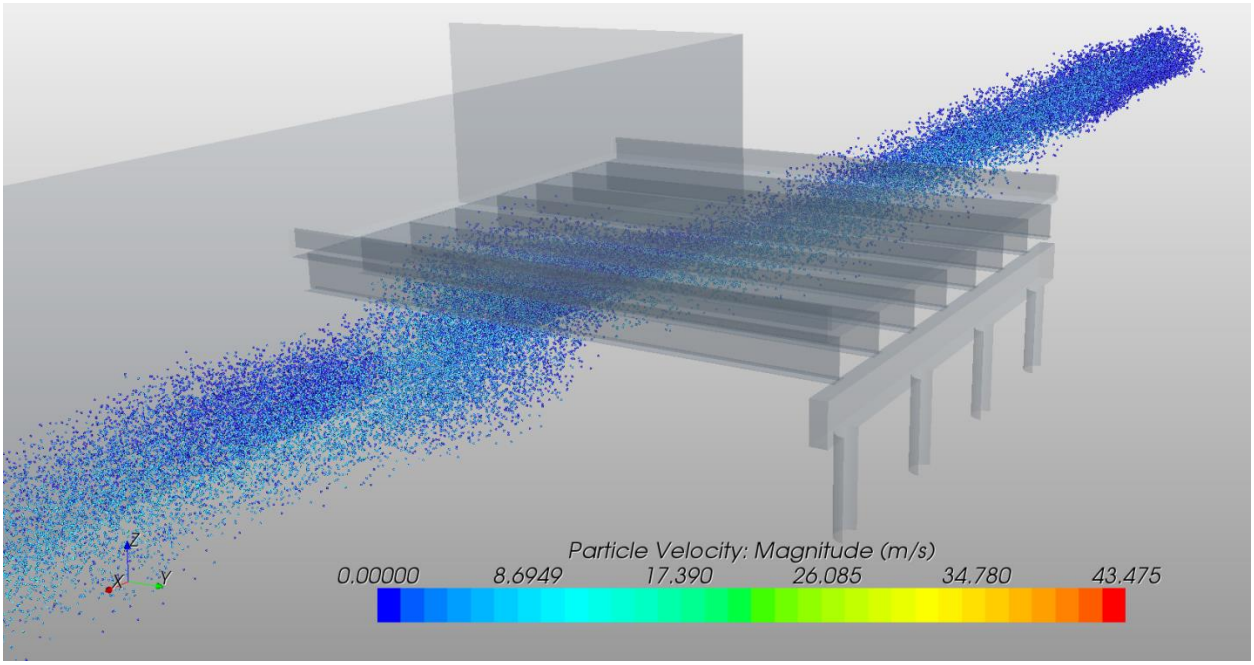

Figure B.6: Snapshot from simulation; with one truck, close vertical wall, no wind, particle size 50 µm, intermediate state 2

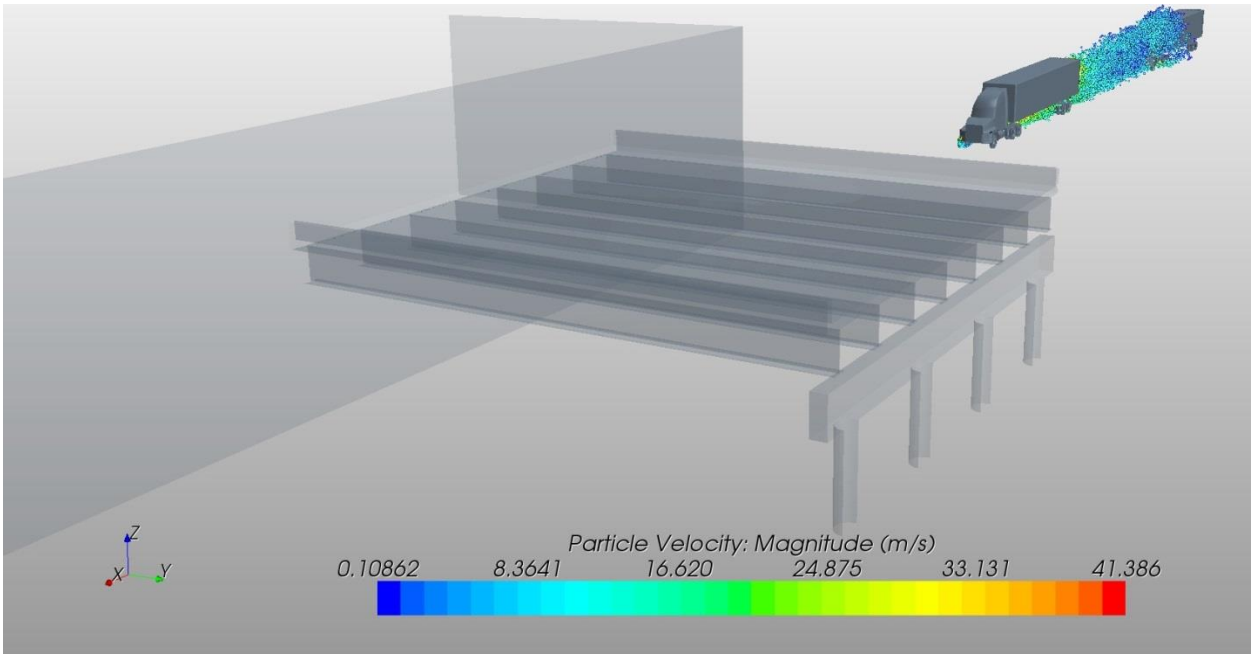

Figure B.7: Snapshot from simulation; with two trucks, close vertical wall, no wind, particle size 50 µm, intermediate state 1

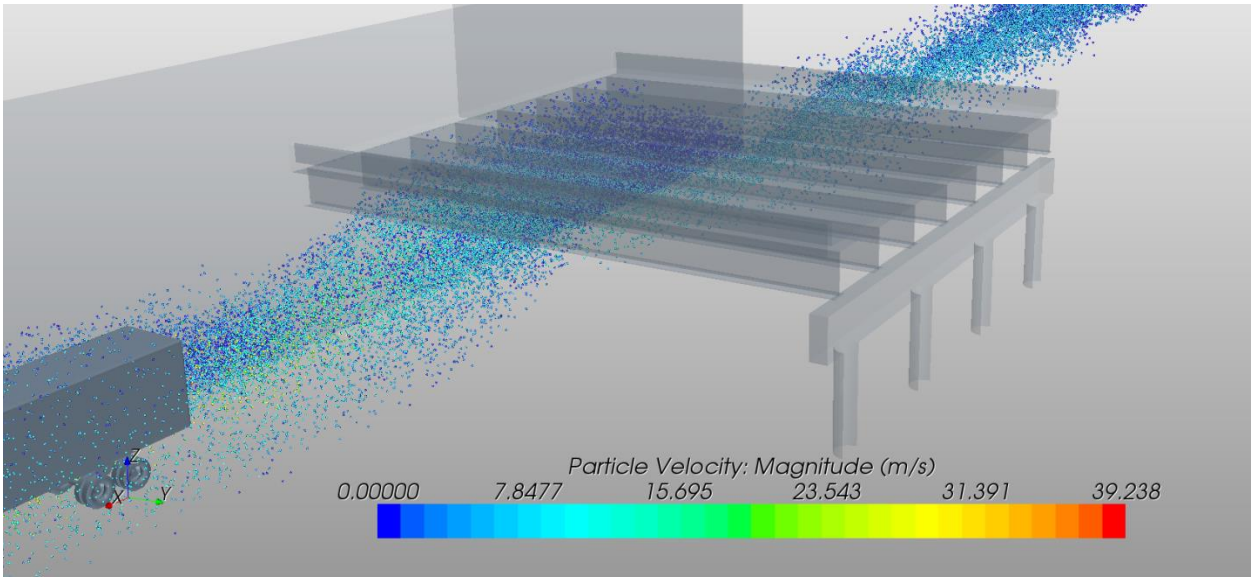

Figure B.8: Snapshot from simulation; with two trucks, close vertical wall, no wind, particle size 50 µm, intermediate state 2

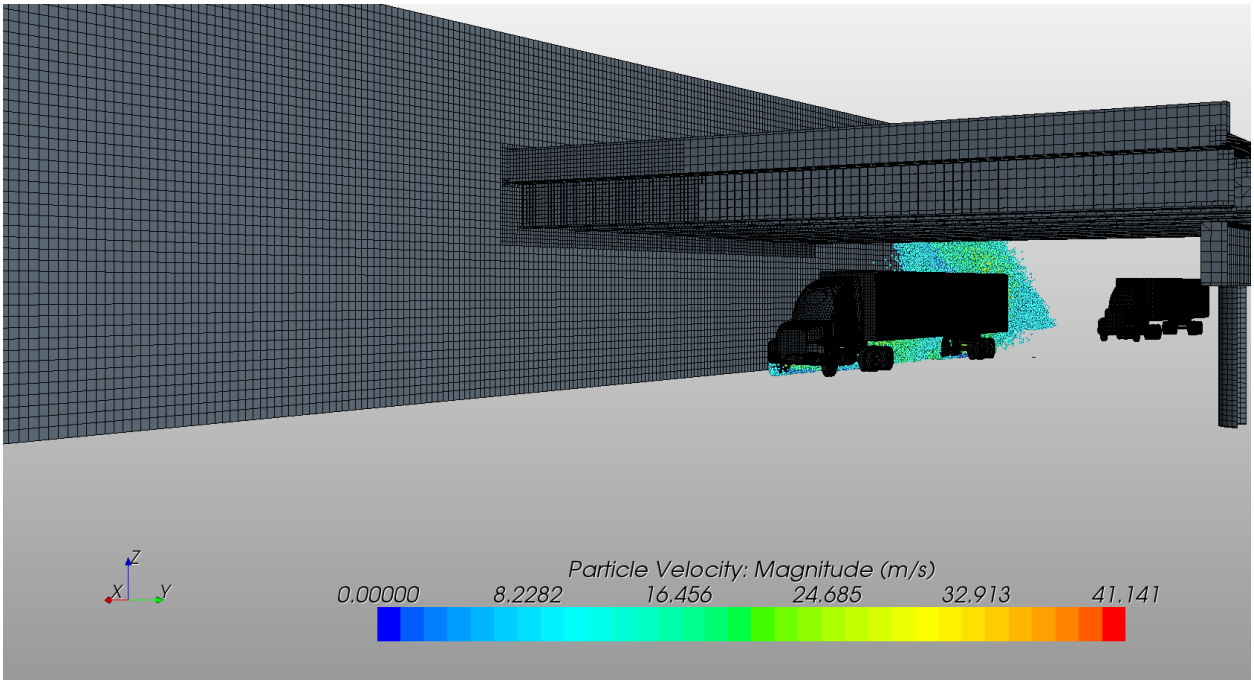

Figure B.9: Snapshot from simulation; with two trucks, close vertical wall, left tail wind, particle size 50 µm, intermediate state 1

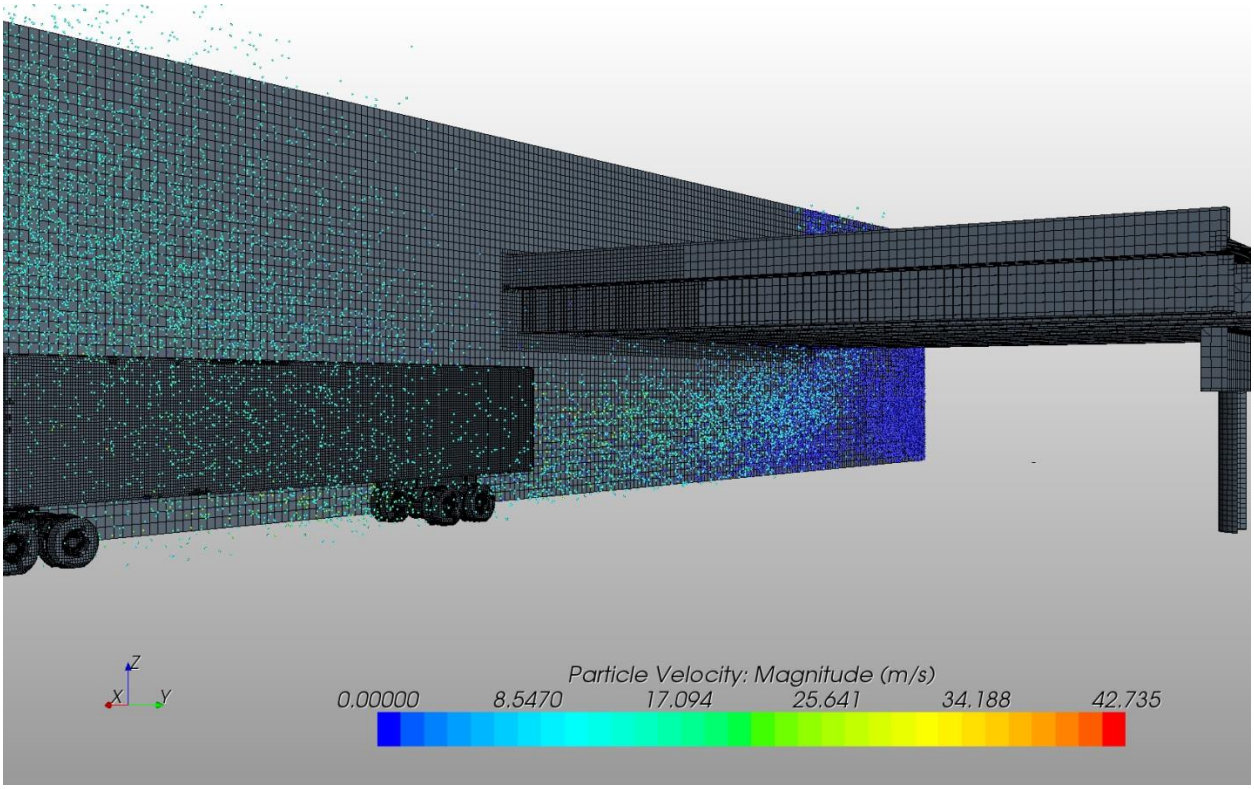

Figure B.10: Snapshot from simulation; with two trucks, close vertical wall, left tail wind, particle size 50 µm, intermediate state

Energy Systems Division
Argonne National Laboratory
9700 South Cass Avenue, Bldg. 362
Argonne, IL 60439-4815

www.anl.gov